Ultramacrocyclization in water via External Templation

Supporting Information

Table of Contents

1. General Methods

All reagents and solvents were purchased from commercial sources and used without further purification. Compounds **3**[1] were prepared according to a reported procedure. Manipulations were performed under a normal laboratory atmosphere unless otherwise noted. Nuclear magnetic resonance (NMR) spectra were recorded at ambient temperature using Bruker AVANCE III 400, Bruker AVANCE III 500, or Agilent DD2 600 spectrometers, with working frequencies of 400/500/600 and 100/125/150 MHz for ^{1}H and ^{13}C, respectively. Chemical shifts are reported in ppm relative to the residual internal non deuterated solvent signals (D_2O: δ = 4.79 ppm, DMSO-d_6: δ = 2.50 ppm, CD_3CN: δ = 1.94 ppm). High-resolution mass spectra (HRMS) were measured by using a SHIMADZU liquid chromatograph mass spectrometry ion trap time of flight (LCMS-IT-TOF) instrument. X-ray crystallographic data were collected on a Bruker D8 Venture. UV/Vis spectra were recorded on a Agilent Cary 5000 instrument.

2. Synthetic Procedures

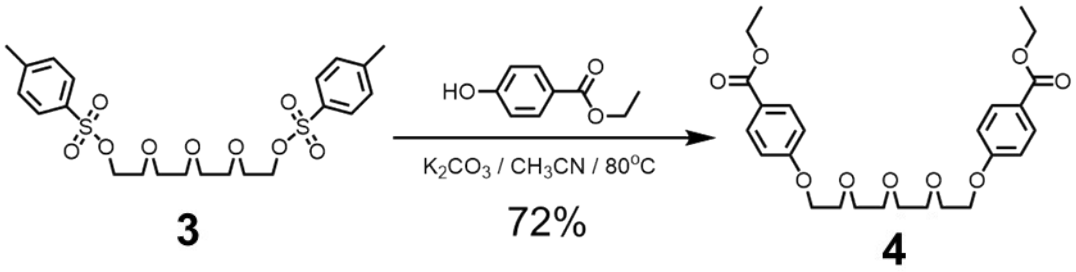

Scheme S1. Synthesis of **4**.

4: **3** (2mmol, 1.0g) and ethylparaben (4.4mmol, 731.1mg) were dissolved in 40ml anhydrous acetonitrile placed in a 100 ml round bottom flask. In a nitrogen atmosphere, K_2CO_3 (8.8mmol, 1.2g) was then added into the flask. The mixture was heated at 80 °C for 12 h. After completion of reaction, the solution was cooled to room temperature. The precipitates were removed by filtration. The filtrate was collected and most of the solvent was removed under vacuum. The residue was poured into water, which was then extracted with ethyl acetate. The resulting organic layer was combined, and washed with water (3 x 50 mL), dried over anhydrous Na_2SO_4, and then concentrated to give the crude product. Purification by flash column chromatography (petroleum ether/ethyl acetate (4:1); silica gel, 200-300 mesh) yielded the white solid-state product **4** (686.2 mg, 70 %). **^{1}H NMR** (400 MHz, $CDCl_3$): δ = 7.99 (d, J=8.0Hz, 4H), 6.93 (d, J=8Hz, 4H), 4.35 (q, J=8.0Hz, 4H), 4.17 (t, J=4.0Hz, 4H), 3.88 (t, J=4.0Hz, 4H), 3.72(m, 8H), 1.39 (t, J=8.0Hz, 6H). **^{13}C NMR** (400 MHz, $CDCl_3$): δ = 166.3, 162.5, 131.5, 123.1, 114.1, 70.9, 70.7, 69.6, 67.5, 60.6, 14.4. **HRMS**: *m/z* calculated for $C_{24}H_{30}O_8Na^+$ ($[M + Na]^+$): 469.1817; found: 469.1833.

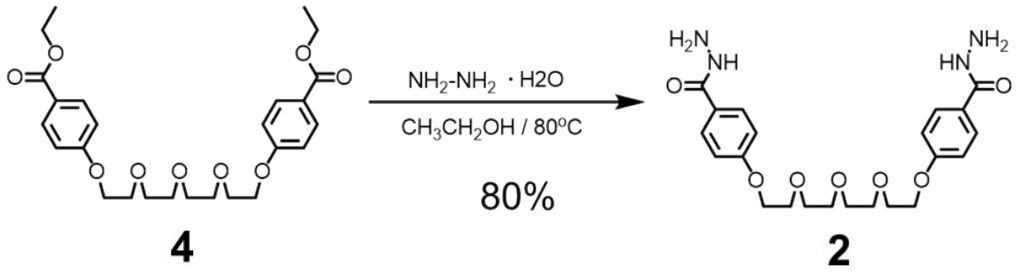

Scheme S2. Synthesis of **2**.

2: In a 50mL round bottom flask, **4** (490.2mg, 1mmol) was dissolved in 15ml ethyl alcohol. Hydrazine hydrate (1.0g, 200mmol) was then added into the flask. The mixture was refluxed for 12 h at 80 °C. After completion of reaction, the solution was cooled to room temperature. The solvent was removed under vacuum to give the crude product. In order to remove residual hydrazine hydrate, the crude product was washed with ethanol for several times, yielding the orange-red solid-state product **2c** (369.6 mg, 80 %). **^{1}H NMR** (400 MHz, D_2O): δ = 7.45 (d, J=8.0Hz, 4H), 6.80 (d, J=8.0Hz, 4H), 4.00 (t, J=4.0Hz, 4H), 3.74 (t, J=4.0Hz, 4H), 3.61(m, 8H), 3.25 (s, 6H). **^{13}C NMR** (400 MHz, D_2O): δ = 169.0, 160.9, 128.8, 124.3, 114.3, 69.7, 69.6, 68.8, 67.1. **HRMS**: *m/z* calculated for $C_{22}H_{30}N_4O_7Na^+$ ($[M + Na]^+$): 485.2012; found: 485.2000.

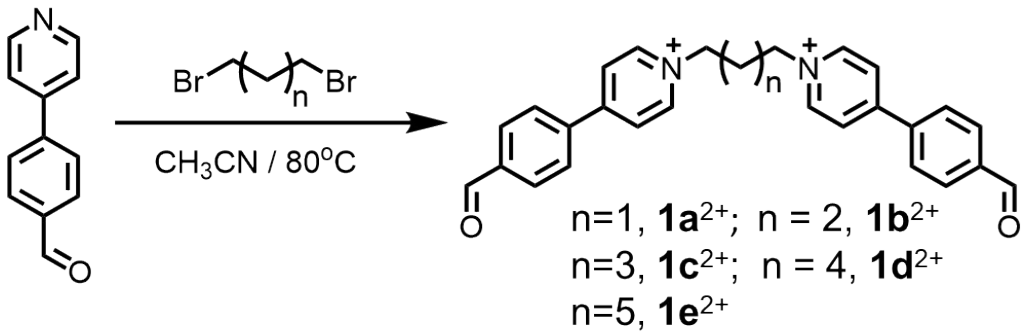

Scheme S3. Synthesis of $\mathbf{1a}^{2+}$, $\mathbf{1b}^{2+}$, $\mathbf{1c}^{2+}$, $\mathbf{1d}^{2+}$and $\mathbf{1e}^{2+}$. Charges are balanced by bromide counteranions, which are omitted here for the sake of clarity.

$\mathbf{1a}^{2+}\cdot 2Br^-$: 1,3-Dibromopropane (202.0 mg, 1.0 mmol) and 4-(4-formylphenyl)pyridine (457.5 mg, 2.5 mmol) were dissolved in 15 ml dry MeCN placed in a 50ml round bottom flask. The reaction mixture was stirred at 80°C for 24 h, during which a white precipitate was formed. After cooling to room temperature, the precipitate was collected via filtration, which was washed with ethyl acetate to give a white solid $\mathbf{1a}^{2+}\cdot 2Br^-$ (537.7 mg, 95%). **^{1}H NMR** (600 MHz, D_2O): δ = 9.97 (s, 2H), 8.90 (d, J=6.0Hz, 4H), 8.32 (d, J=6.0Hz, 4H), 8.00 (d, J=6.0Hz, 4H), 7.95 (d, J=6.0Hz, 4H), 4.87 (t, J=6.0Hz, 4H), 2.90 (m, 2H). **^{13}C NMR** (400 MHz, D_2O): δ = 195.3, 155.7, 144.5, 139.1, 137.6, 130.7, 128.7, 126.1, 58.1, 31.0. **HRMS**: *m/z* calculated for $C_{27}H_{24}N_2O_2^{2+}$ ($[M - 2Br]^{2+}$): 204.0913; found: 204.0925.

$\mathbf{1b}^{2+}\cdot 2Br^-$,$\mathbf{1c}^{2+}\cdot 2Br^-$,$\mathbf{1d}^{2+}\cdot 2Br^-$, and $\mathbf{1e}^{2+}\cdot 2Br^-$ were synthesized via similar procedures, using different dibromo precursors.

$\mathbf{1b}^{2+}\cdot 2Br^-$: The yield of a white solid $\mathbf{1b}^{2+}\cdot 2Br^-$ is 98 %. **^{1}H NMR** (500 MHz, D_2O): δ = 9.95 (s, 2H), 8.80 (d, J=10.0Hz, 4H), 8.27 (d, J=10.0Hz, 4H), 8.01 (d, J=8.0Hz, 4H), 7.96 (d, J=8.0Hz, 4H), 4.61 (m, 4H), 2.10 (m, 4H). **^{13}C NMR** (400 MHz, D_2O): δ = 195.4, 155.5, 144.3, 139.5, 137.5, 130.7, 128.7, 125.9, 60.2, 27.2. **HRMS**: *m/z* calculated for $C_{28}H_{26}N_2O_2^{2+}$ ($[M - 2Br]^{2+}$): 211.0992; found: 211.0994.

$\mathbf{1c}^{2+}\cdot 2Br^-$: The yield of a light yellow solid $\mathbf{1c}^{2+}\cdot 2Br^-$ is 85 %. **^{1}H NMR** (500 MHz, D_2O): δ = 9.88 (s, 2H), 8.74 (d, J=10.0Hz, 4H), 8.19 (d, J=10.0Hz, 4H), 7.85 (d, J=8.0Hz, 4H),

7.81 (d, J=8.0Hz, 4H), 4.57 (t, J=6.5Hz, 4H), 2.03 (m, 4H), 1.01 (m, 2H). **^{13}C NMR** (400 MHz, D_2O): δ = 195.3, 154.8, 144.4, 138.9, 137.3, 130.6, 128.4, 125.4, 60.6, 29.0, 20.9. **HRMS**: *m/z* calculated for $C_{29}H_{28}N_2O_2^{2+}$ ([M – 2Br]$^{2+}$): 218.1070; found: 218.1077.

1d^{2+}·2Br$^-$: The yield of a white solid is **1d**$^{2+}$·2Br$^-$ is 88 %. **^{1}H NMR** (400 MHz, D_2O): δ = 9.88 (s, 2H), 8.73 (d, J=8.0Hz, 4H), 8.16 (d, J=8.0Hz, 4H), 7.92 (d, J=8.0Hz, 4H), 7.86 (d, J=8.0Hz, 4H), 4.48 (t, J=6.8Hz, 4H), 1.92 (m, 4H), 1.21 (m, 4H). **^{13}C NMR** (400 MHz, D_2O): δ = 195.4, 155.1, 144.3, 139.4, 137.5, 130.7, 128.6, 125.6, 61.3, 29.8, 25.0. **HRMS**: *m/z* calculated for $C_{30}H_{30}N_2O_2^{2+}$ ([M – 2Br]$^{2+}$): 225.1148; found: 225.1159.

1e^{2+}·2Br$^-$: The yield of a white solid **1e**$^{2+}$·2Br$^-$ is 86 %. **^{1}H NMR** (400 MHz, D_2O): δ = 9.88 (s, 2H), 8.74 (d, J=8.0Hz, 4H), 8.17 (d, 4H), 7.88 (d, J=8.0Hz, 8H), 7.84 (d, J=8.0Hz, 8H), 4.48 (t, J=7.2Hz, 4H), 1.86 (m, 4H), 1.30 (m, 2H), 1.23 (m, 4H). **^{13}C NMR** (400 MHz, D_2O): δ = 195.1, 154.6, 144.3, 139.2, 137.3, 130.6, 128.5, 125.5, 61.2, 30.0, 27.2, 24.6. **HRMS**: *m/z* calculated for $C_{31}H_{32}N_2O_2^{2+}$ ([M – 2Br]$^{2+}$): 232.1226; found: 232.1226.

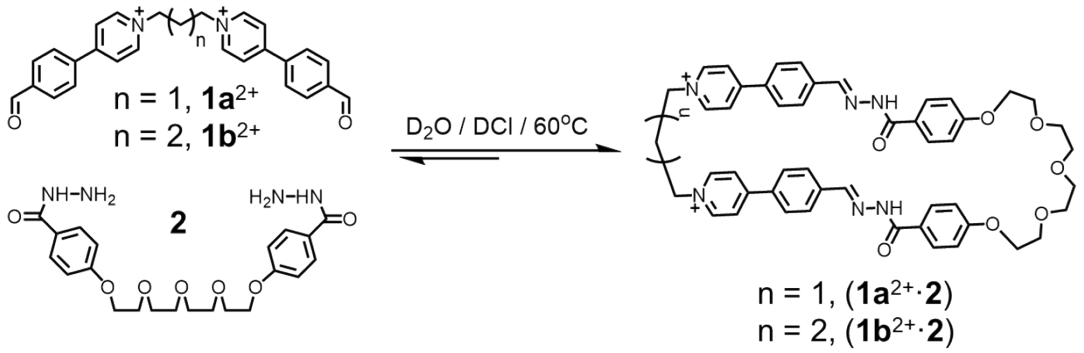

Scheme S5. Self-assembly of (**1a**$^{2+}$·**2**) and (**1b**$^{2+}$·**2**) (counteranions could be either Cl^- or Br^-).

We combined **2** (4.62 mg, 0.01 mmol) with each of the dialdehyde compounds either **1a**$^{2+}$·2Br^- or **1b**$^{2+}$·2Br^- (0.01 mmol), in D_2O (4 mL) in the presence of catalytic amount of DCl (10 μL). After heating the corresponding solutions at 60 °C for 8 h, the ^{1}H NMR and mass spectra of the corresponding solutions were recorded. It was demonstrated that the macrocycles (**1a**$^{2+}$·**2**) and (**1b**$^{2+}$·**2**), whose counteranions could be either Cl^- or Br^-, were produced as the major products, which were fully characterized in D_2O by ^{1}H NMR spectroscopy, 2D NMR spectroscopy , as well as mass spectrometry (see Figure S1-5, S10-14).

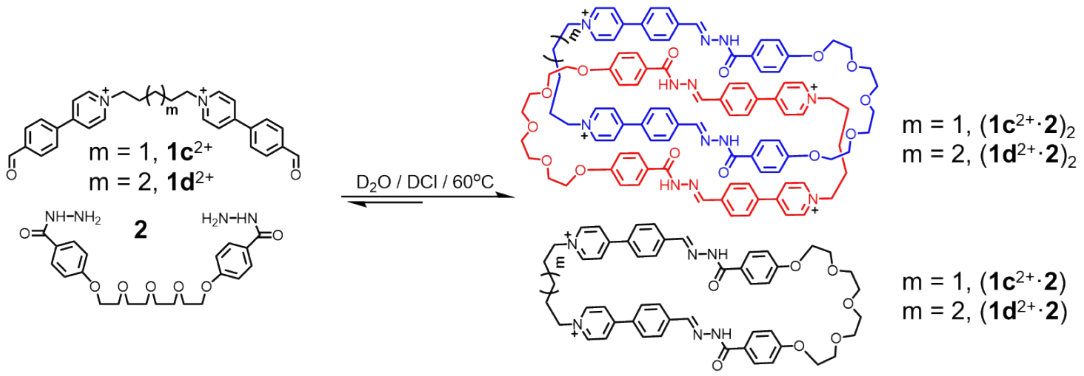

Scheme S6. Self-assembly of ($\mathbf{1c}^{2+}\cdot\mathbf{2}$), $(\mathbf{1c}^{2+}\cdot\mathbf{2})_2$, ($\mathbf{1d}^{2+}\cdot\mathbf{2}$) and $(\mathbf{1d}^{2+}\cdot\mathbf{2})_2$ (counteranions could be either Cl^- or Br^-).

We combined **2** (4.62 mg, 0.01 mmol) with each of the dialdehyde compounds either $\mathbf{1c}^{2+}\cdot 2Br^-$ or $\mathbf{1d}^{2+}\cdot 2Br^-$ (0.01 mmol) in a 1:1 ratio, in D_2O (4 mL) in the presence of catalytic amount of DCl (10 μL). After heating the corresponding solutions at 60 °C for 8 h, the ^1H NMR and mass spectra of the corresponding solutions were recorded. It was demonstrated that [2]catenanes $(\mathbf{1c}^{2+}\cdot\mathbf{2})_2$, $(\mathbf{1d}^{2+}\cdot\mathbf{2})_2$ and macrocycles ($\mathbf{1c}^{2+}\cdot\mathbf{2}$), ($\mathbf{1d}^{2+}\cdot\mathbf{2}$) (counteranions could be either Cl^- or Br^-) were produced at the same time, which were fully characterized in D_2O by ^1H NMR spectroscopy, 2D NMR spectroscopy , as well as mass spectrometry (see Figure S19-24, S29-32).

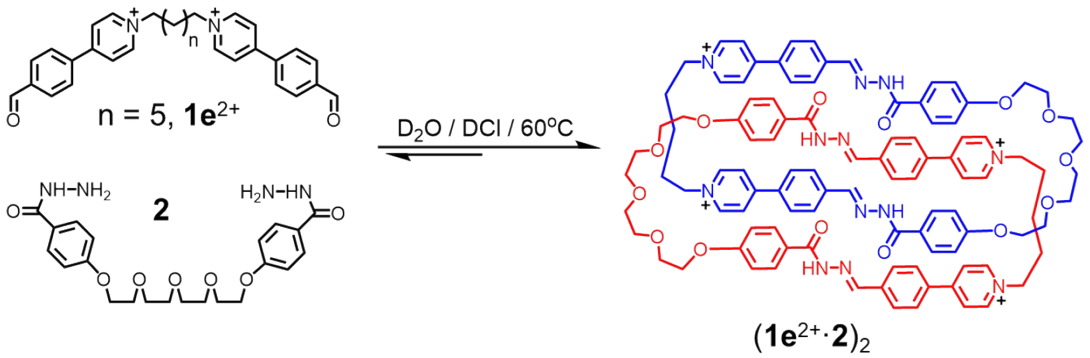

Scheme S7. Self-assembly of $(\mathbf{1e}^{2+}\cdot\mathbf{2})_2$ (counteranions could be either Cl^- or Br^-).

We combined **2** (4.62 mg, 0.01 mmol) with the dialdehyde compound $\mathbf{1e}^{2+}\cdot 2Br^-$ (0.01 mmol) in a 1:1 ratio, in D_2O (4 mL) in the presence of catalytic amount of DCl (10 μL). After heating the corresponding solution at 60 °C for 8 h, the ^1H NMR and mass spectra of the corresponding solution was recorded. It was demonstrated that the [2]catenane $(\mathbf{1e}^{2+}\cdot\mathbf{2})_2$ (counteranions could be either Cl^- or Br^-) were produced as the major product, which were fully characterized in D_2O by ^1H NMR spectroscopy, 2D NMR spectroscopy , as well as mass spectrometry (see Figure S37-41).

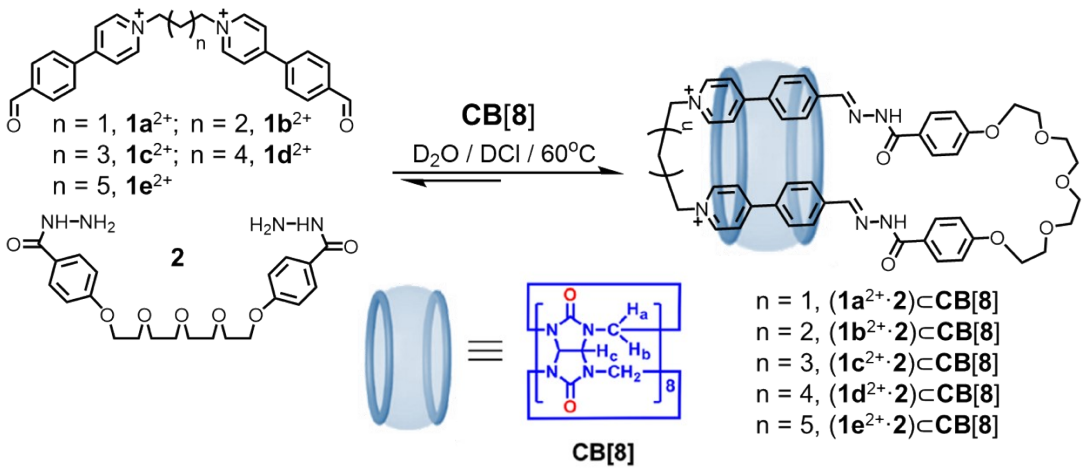

Scheme S8. Self-assembly of (**1x**$^{2+}$·**2c**)⊂**CB**[**8**] (**x** = **a**, **b**, **c**, **d** and **e**) (counteranions could be either Cl^- or Br^-).

A 1:1:1 mixture of **2** (4.62 mg, 0.01 mmol), each of the dialdehyde compounds **1x**$^{2+}$·2Br^- (**x** = **a**, **b**, **c**, **d** and **e**) (0.01 mmol) and **CB**[**8**] (0.01 mmol) were combined and dissolved in D_2O (4 mL) in the presence of catalytic amount of DCl (10 μL). After heating the corresponding solutions at 60 °C for 8 h, the ^{1}H NMR and mass spectra of the corresponding solutions were recorded. It was demonstrated that the [2]pseudorotaxanes (**1x**$^{2+}$·**2c**)⊂**CB**[**8**] (counteranions could be either Cl^- or Br^-) were produced as the major products, which were fully characterized in D_2O by ^{1}H NMR spectroscopy, 2D NMR spectroscopy , as well as mass spectrometry (see Figure S6-9, S15-18, S25-28, S33-36, S42-45).

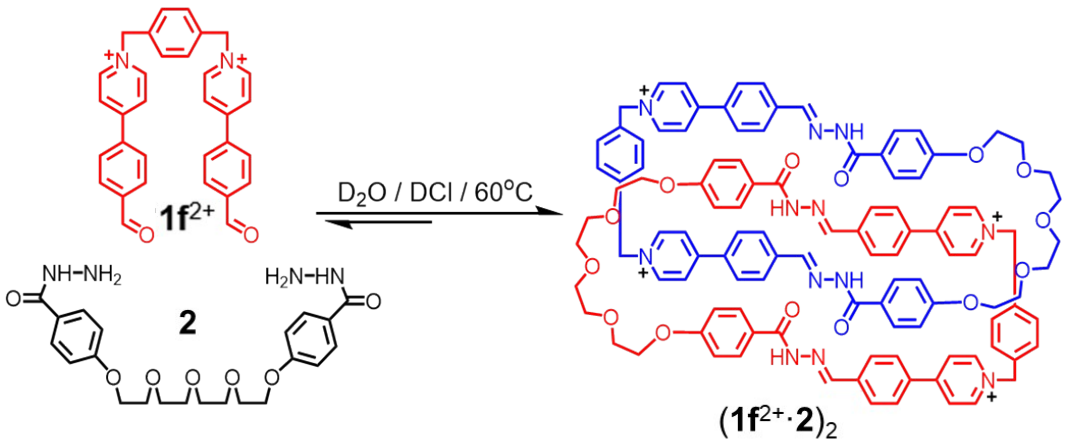

Scheme S9. Self-assembly of $(\mathbf{1f}^{2+}\cdot\mathbf{2})_2$. Charges are balanced by chloride counteranions, which are omitted here for the sake of clarity.

A 1:1 mixture of the dialdehyde compound $\mathbf{1f}^{2+}\cdot 2Cl^-$ (5.40 mg, 0.01 mmol) and the dihydrazine linker **2** (0.01 mmol) were combined in D_2O (4 mL) in the presence of catalytic amount of DCl (10 μL). After heating the corresponding solutions at 60 °C for 8 h, the ^1H NMR (Figure S47) and mass spectra (Figure S46) of the corresponding solution were recorded. To our delight, the corresponding ^1H NMR spectrum indicated the formation of a thermodynamically stable product, a homo [2]catenanes $(\mathbf{1f}^{2+}\cdot\mathbf{2})_2\cdot 4Cl^-$. The structure of $(\mathbf{1f}^{2+}\cdot\mathbf{2})_2\cdot 4Cl^-$ was further convinced by $^1H-^1H$ COSY spectrum (Figure S49), $^1H-^1H$ NOESY spectrum (Figure S50) and DOSY spectrum (Figure S51).

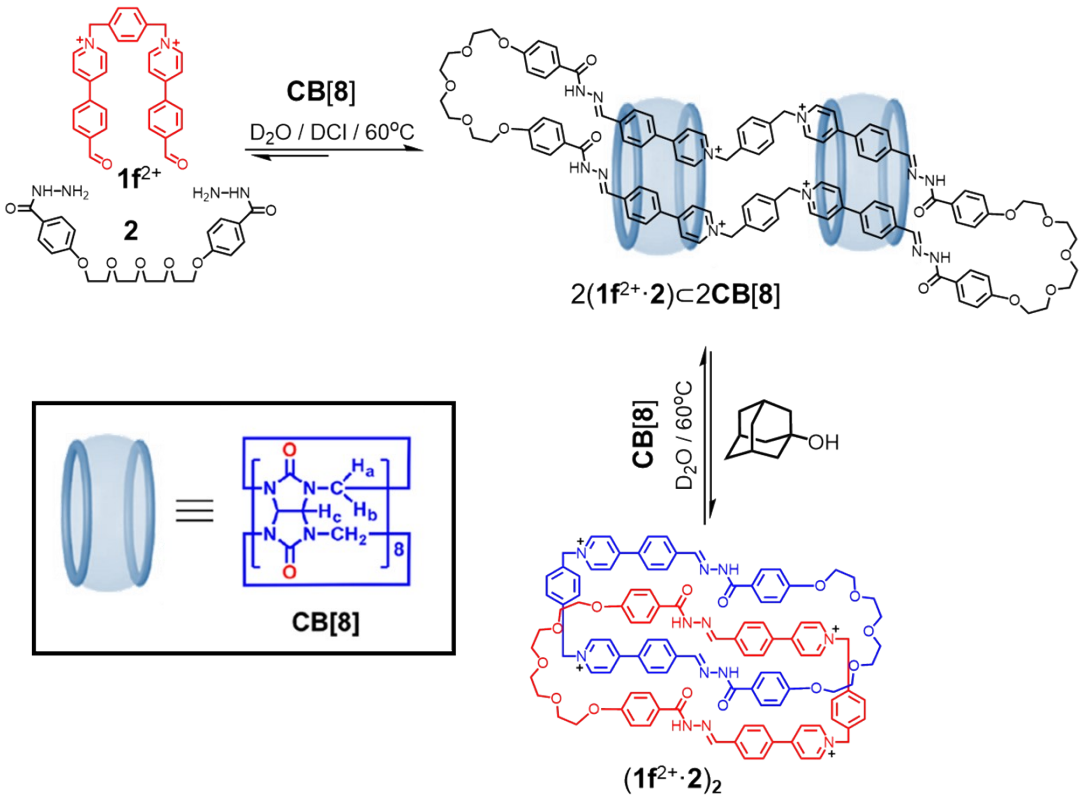

Scheme S10. Self-assembly of (**1f**$^{2+}$·**2**·**1f**$^{2+}$·**2**) ⊂2**CB**[**8**]. Charges are balanced by chloride counteranions.

A 1:1:1 mixture of the dihydrazine **2** (4.62 mg, 0.01 mmol), the dialdehyde compound **1f**$^{2+}$·2Cl^{-} (5.40 mg, 0.01 mmol) and **CB**[**8**] (0.01 mmol) were combined and dissolved in water (4 mL) in the presence of catalytic amount of DCl (10 μL). After heating the corresponding solutions at 60 °C for 8 h, the ^{1}H NMR and mass spectra of the corresponding solutions were recorded. It was demonstrated that the [3]pseudorotaxane (**1f**$^{2+}$·**2**·**1f**$^{2+}$·**2**) ⊂2**CB**[**8**] was produced as the major product, which were fully characterized in D_2O by ^{1}H NMR spectroscopy, 2D NMR spectroscopy , as well as mass spectrometry (see Figure S52-55).

Upon removal of **CB**[**8**] by adding excess amount of adamantan-1-ol, the [3]pseudorotaxane (**1f**$^{2+}$·**2**·**1f**$^{2+}$·**2**) ⊂2**CB**[**8**] could be transformed back to the [2]catenane (**1f**$^{2+}$·**2**)$_2$, accompanied with a complex namely adamantan-1-ol ⊂**CB**[**8**].

3. Characterization of the macrocycles, catenanes and pseudorotaxanes

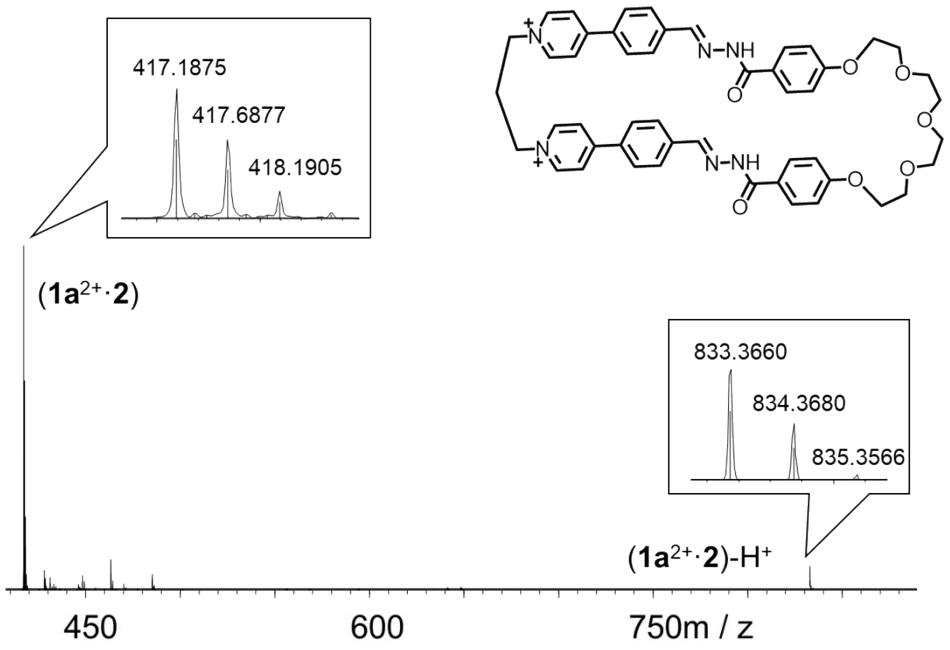

Figure S1. High-resolution LCMS-IT-TOF of (**1a**$^{2+}$·**2**). Counteranions could be either Cl^- or Br^-. The signals labeled in the spectrum correspond to molecular cations that contain two and one positive charges, respectively. *m/z* [(**1a**$^{2+}$·**2**)]$^{2+}$ calculated for $C_{49}H_{50}N_6O_7^{2+}$: 417.1865; found: 417.1875. [(**1a**$^{2+}$·**2**) − H^+]$^+$ calculated for $C_{49}H_{49}N_6O_7^+$: 833.3657; found: 833.3660.

;

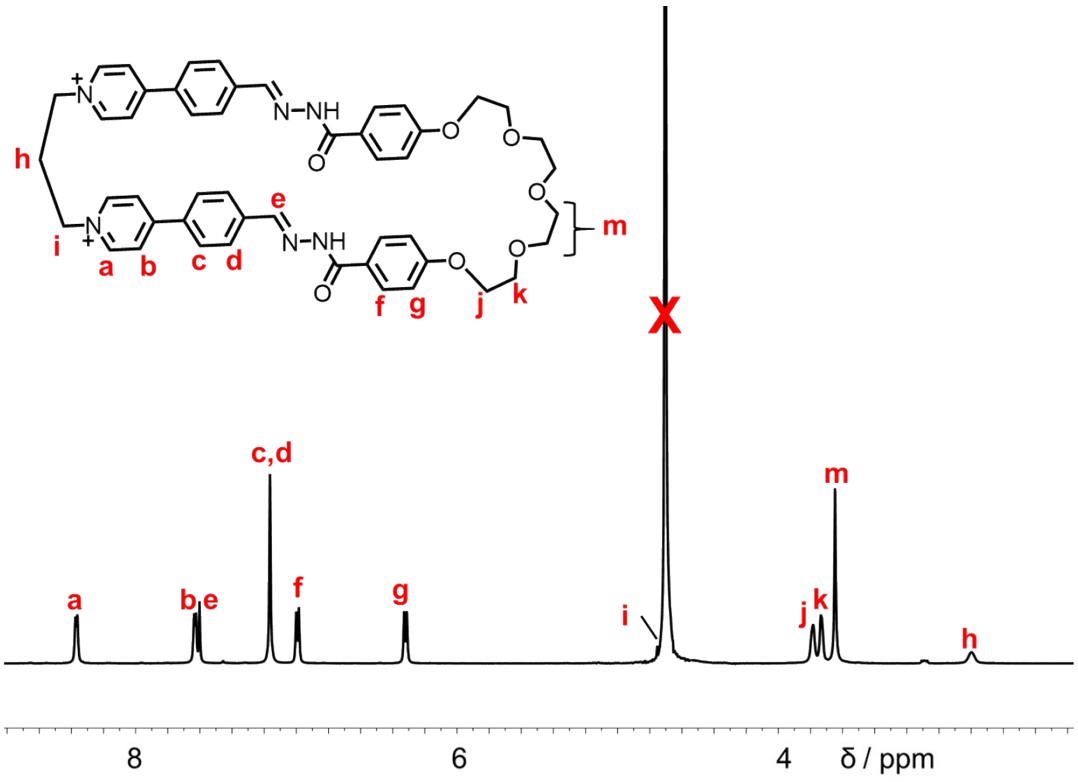

Figure S2. Partial ^{1}H NMR spectrum of (**1a**$^{2+}$·**2**) (500 MHz, D_2O, 298 K). Counteranions could be either Cl^- or Br^-.

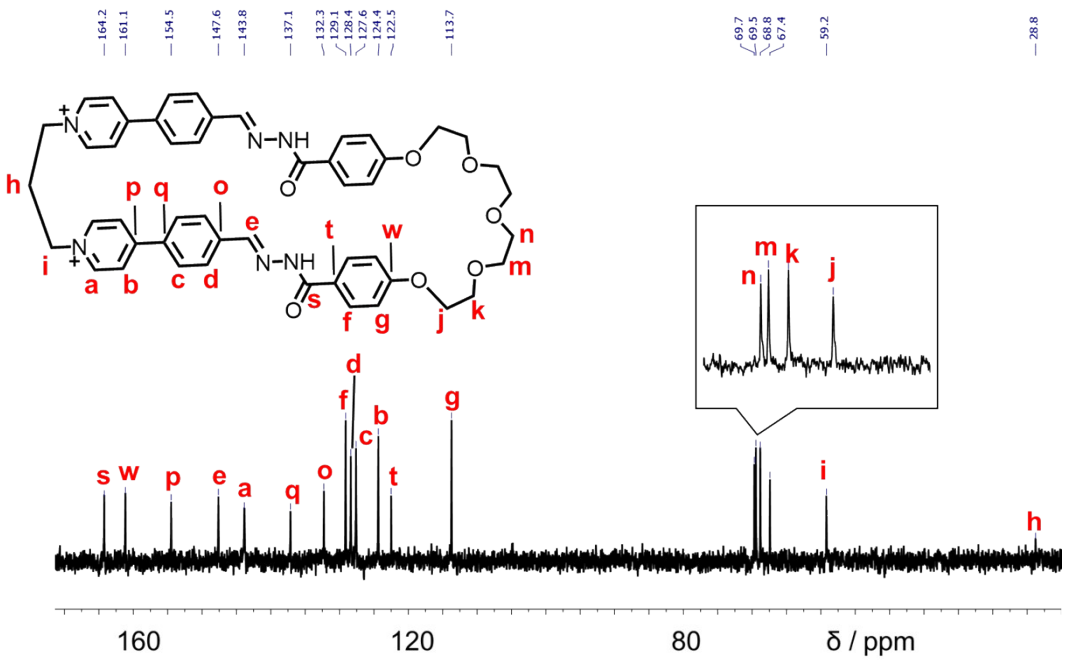

Figure S3. ^{13}C NMR spectrum (100 M Hz, 298 K, D_2O) of (**1a**$^{2+}$·**2**). Counteranions could be either Cl^- or Br^-.

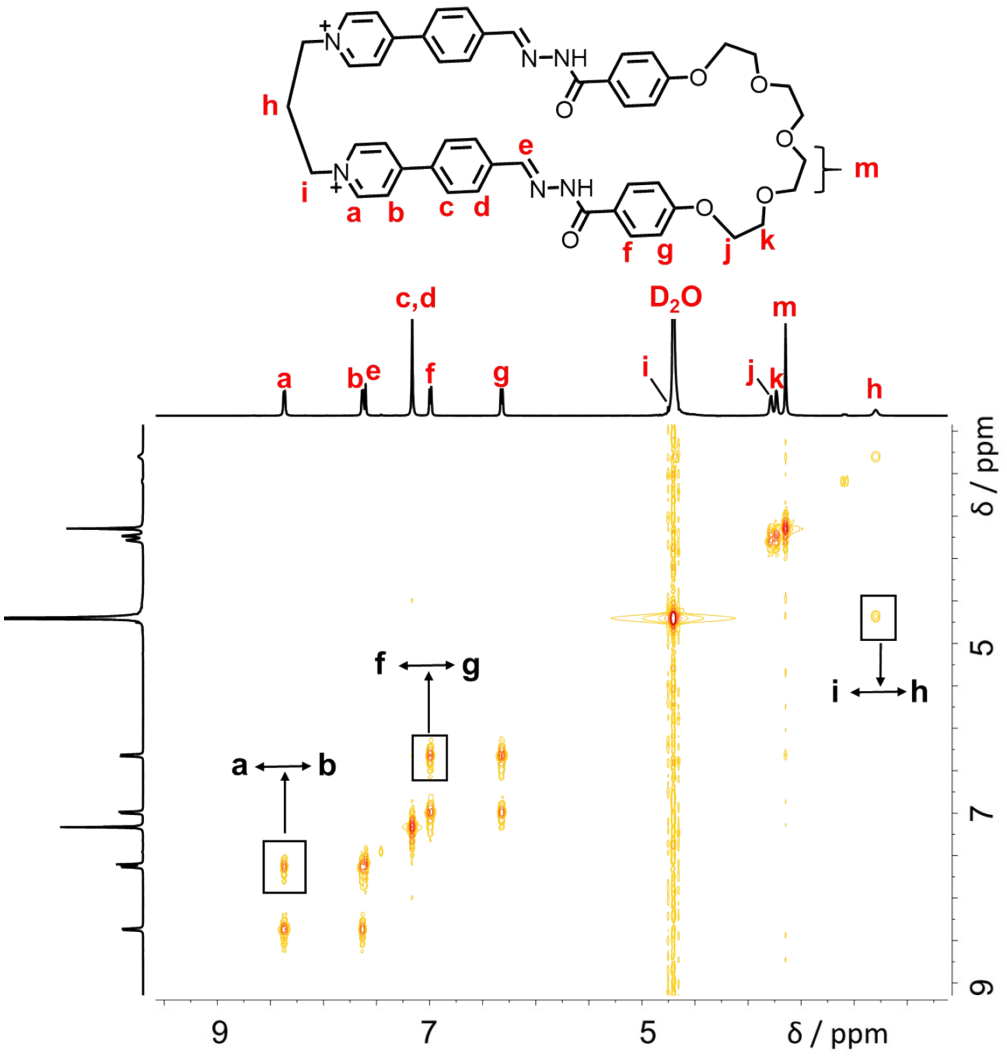

Figure S4. $^{1}H-^{1}H$ COSY spectrum (500 MHz, D_2O, 298 K) of (**1a**$^{2+}$·**2**). Counteranions could be either Cl^- or Br^-. Key correlation peaks are labeled in the spectrum.

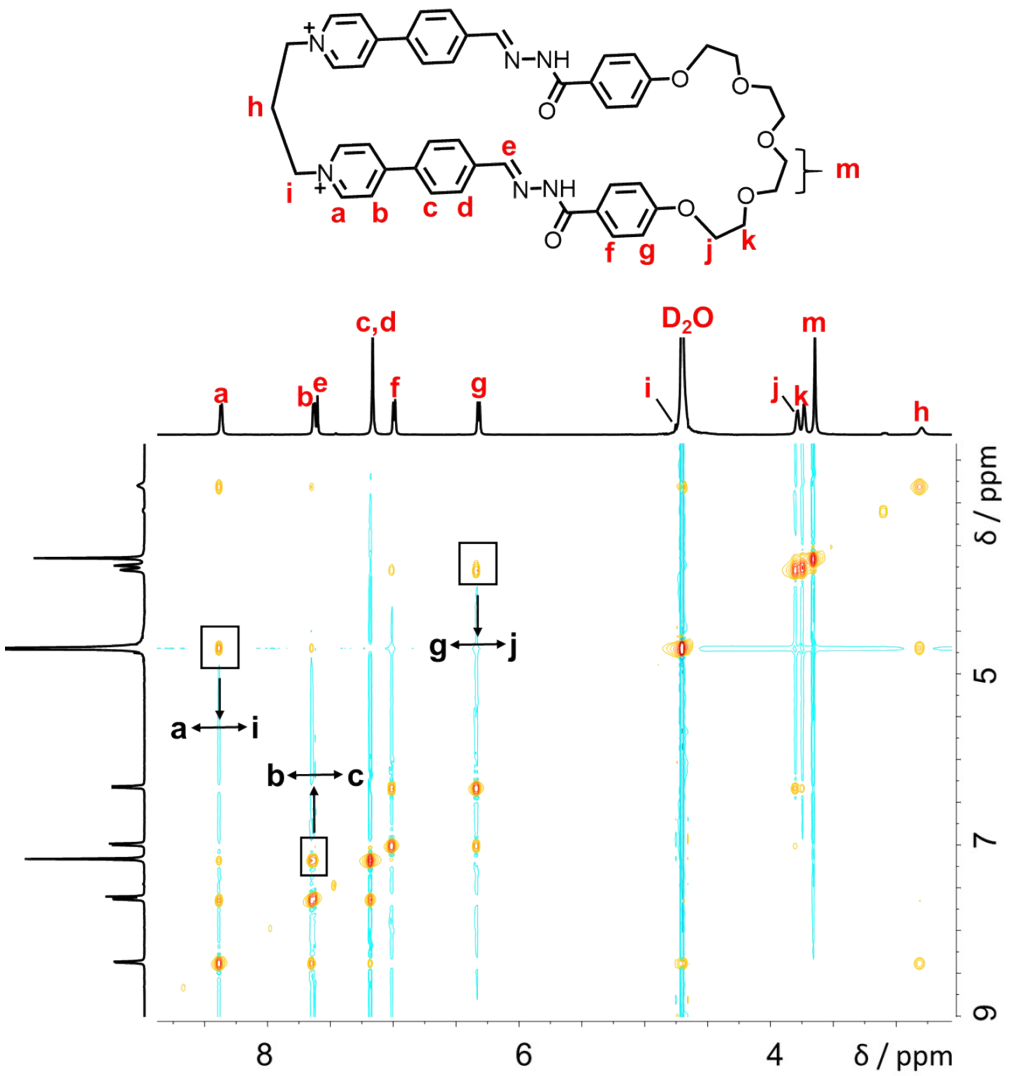

Figure S5. $^{1}H-^{1}H$ NOESY spectrum (500 MHz, D_2O, 298 K) of (**1a**$^{2+}$·**2**). Counteranions could be either Cl^- or Br^-. Key correlation peaks are labeled in the spectrum.

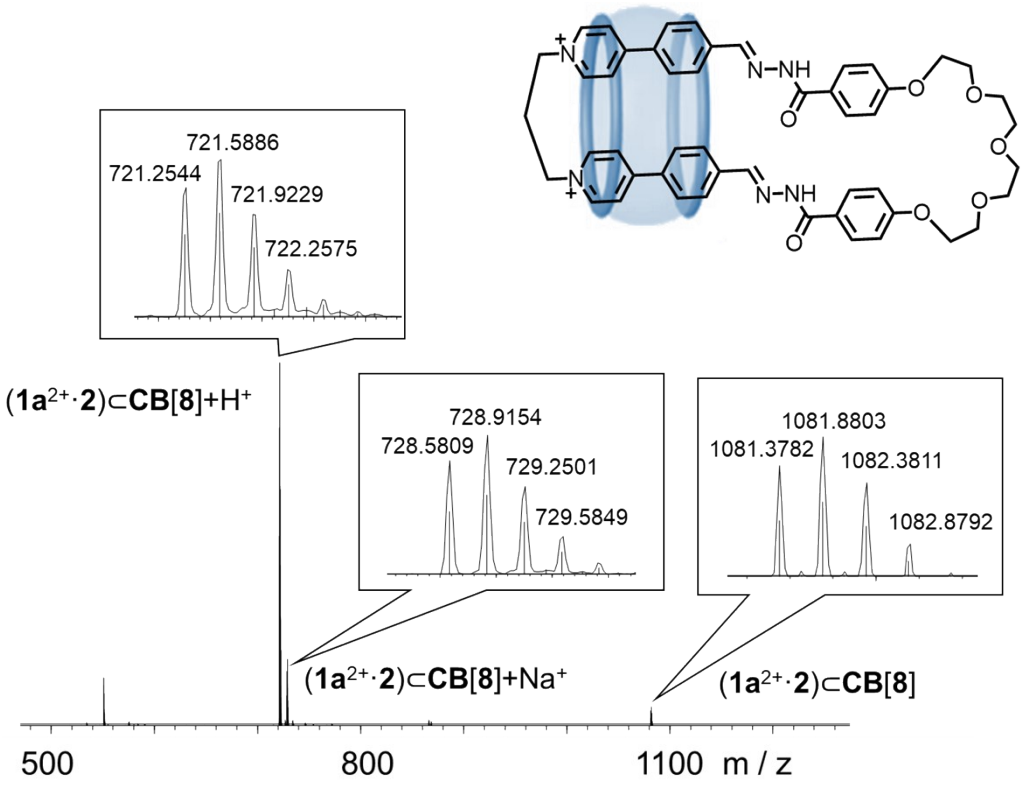

Figure S6. High-resolution LCMS-IT-TOF of (**1a**$^{2+}$·**2**)⊂**CB**[**8**]. Counteranions could be either Cl^- or Br^-.The signals labeled in the spectrum correspond to molecular cations that contain three and two positive charges, respectively. *m/z* [(**1a**$^{2+}$·**2**)⊂**CB**[**8**] + Na^+]$^{3+}$ calculated for $C_{97}H_{98}N_{38}NaO_{23}^{3+}$: 728.9194; found: 728.9154. [(**1a**$^{2+}$·**2**)⊂**CB**[**8**] + H^+]$^{3+}$ calculated for $C_{97}H_{99}N_{38}O_{23}^{3+}$: 721.5921; found: 721.5886. [(**1a**$^{2+}$·**2**)⊂**CB**[**8**]]$^{2+}$ calculated for $C_{97}H_{98}N_{38}O_{23}^{2+}$: 1081.8845; found: 1081.8803.

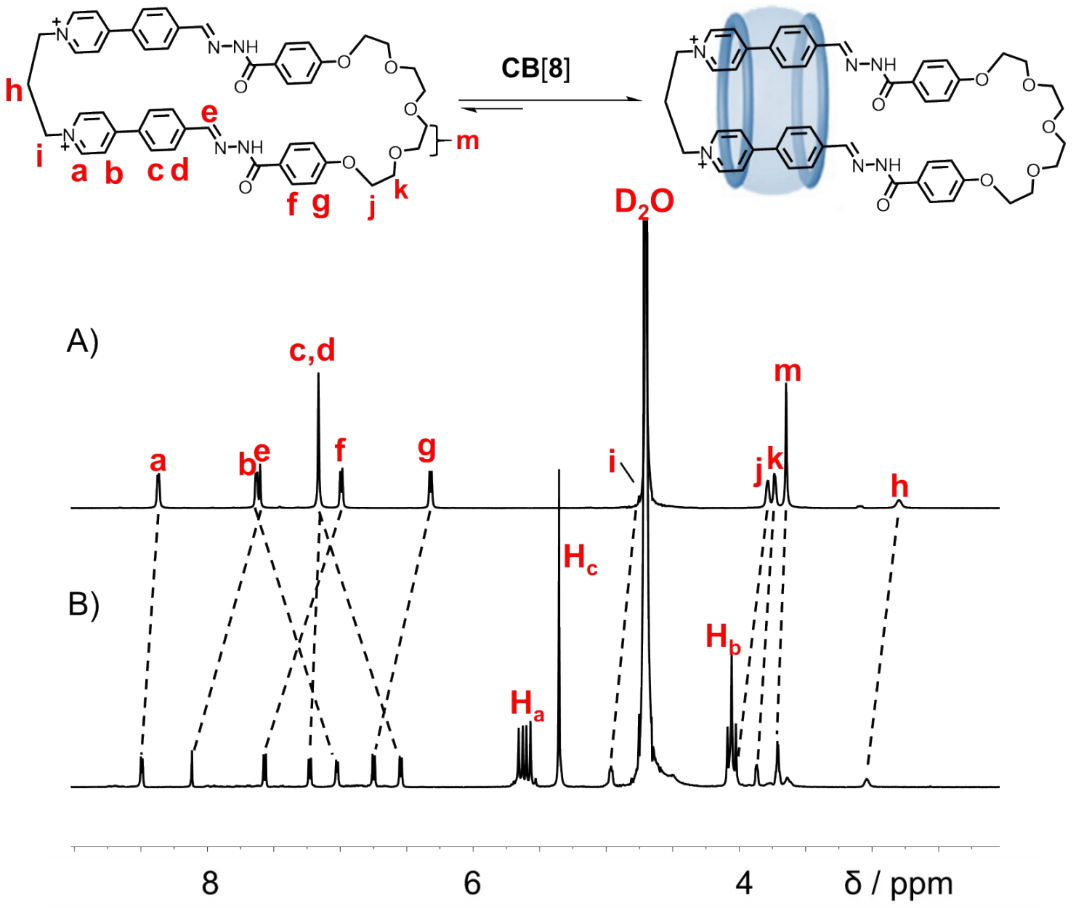

Figure S7. Partial ^{1}H NMR spectrum (500 MHz, D_2O, 298 K) of A) (**1a**$^{2+}$·**2**) and B) (**1a**$^{2+}$·**2**)⊂**CB**[**8**]. Counteranions could be either Cl^- or Br^-.

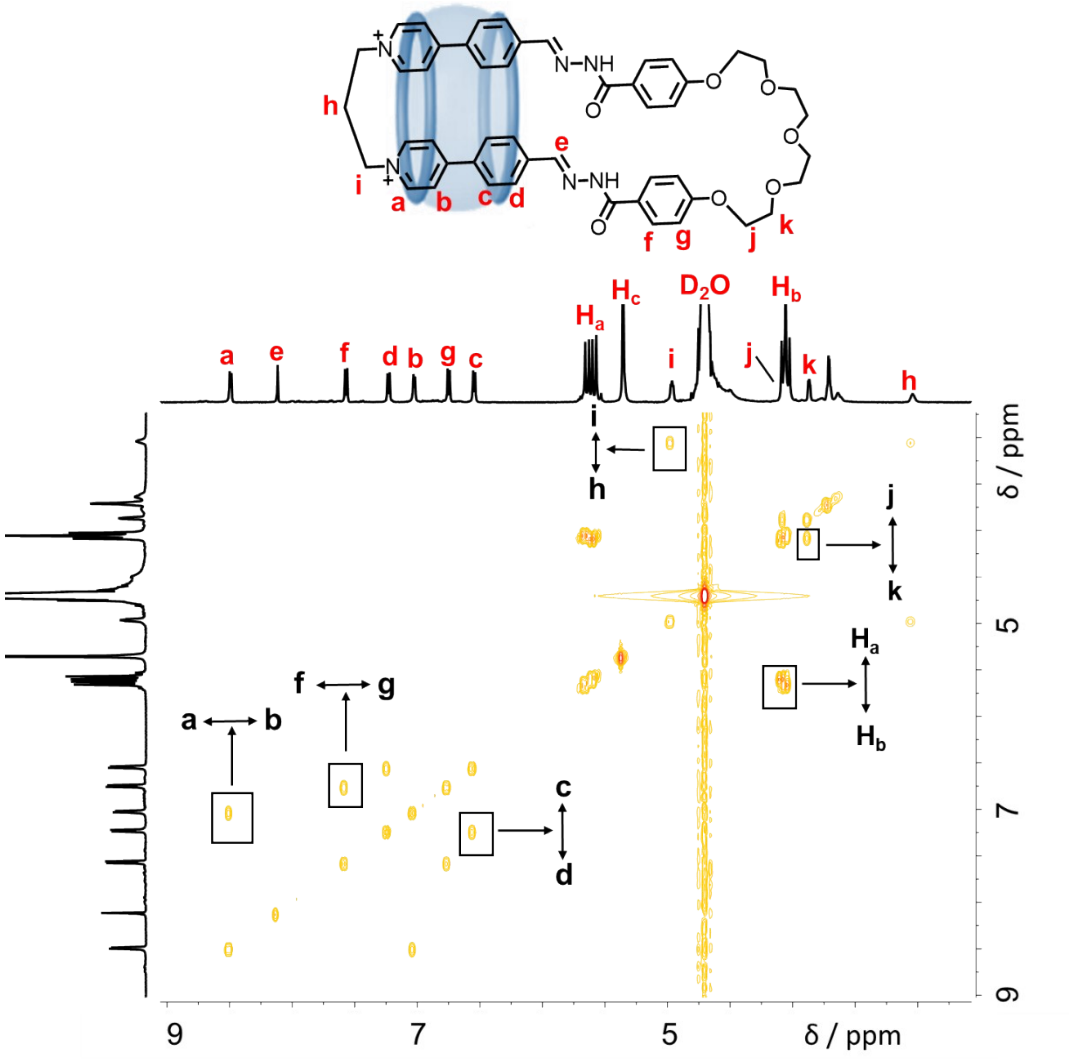

Figure S8. $^{1}H-^{1}H$ COSY spectrum (500 MHz, D_2O, 298 K) of (**1a**$^{2+}$·**2**)⊂**CB**[**8**]. Counteranions could be either Cl^- or Br^-. Key correlation peaks are labeled in the spectrum.

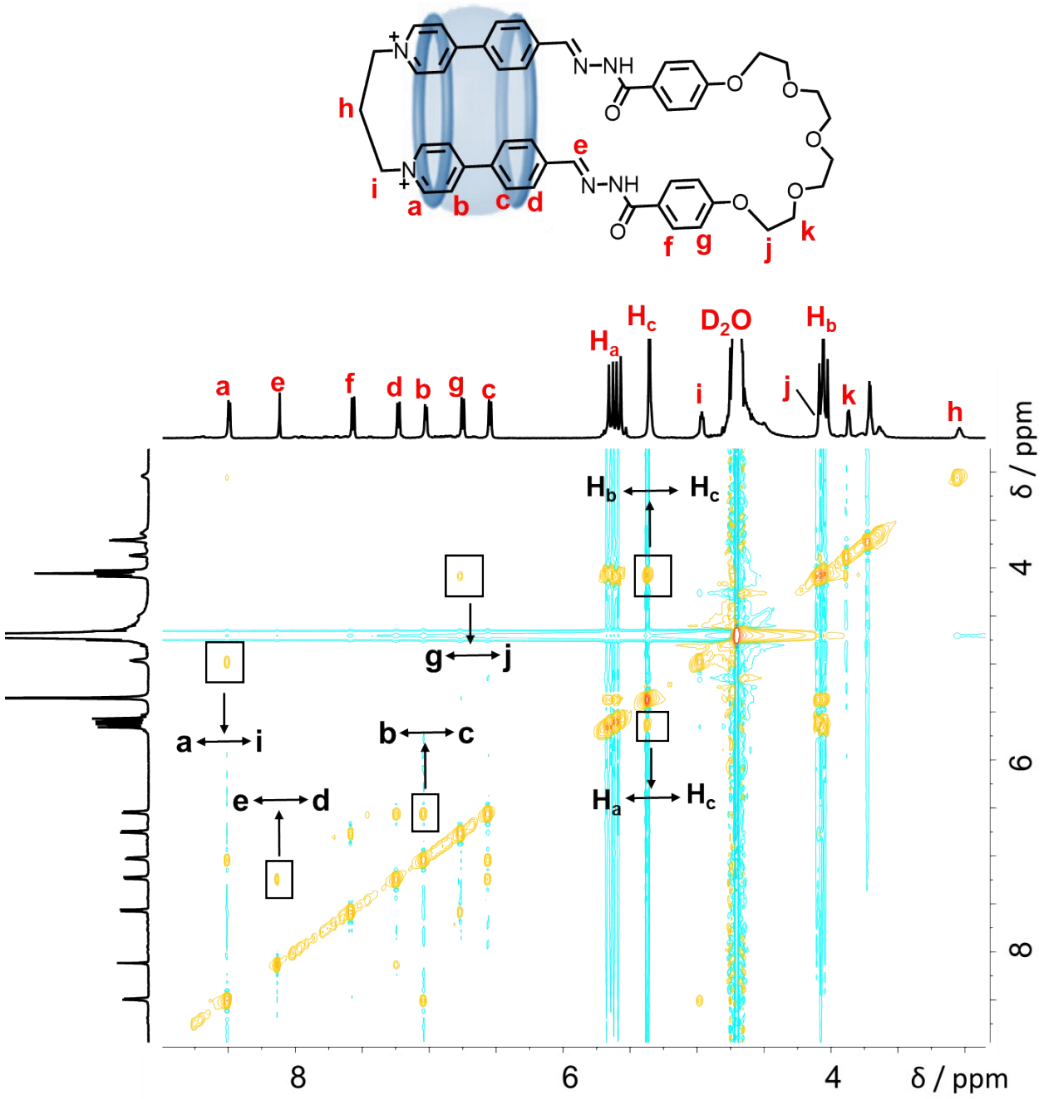

Figure S9. $^{1}H-^{1}H$ NOESY spectrum (500 MHz, D_2O, 298 K) of (**1a**$^{2+}$·**2**)⊂**CB**[**8**]. Counteranions could be either Cl^- or Br^-. Key correlation peaks are labeled in the spectrum.

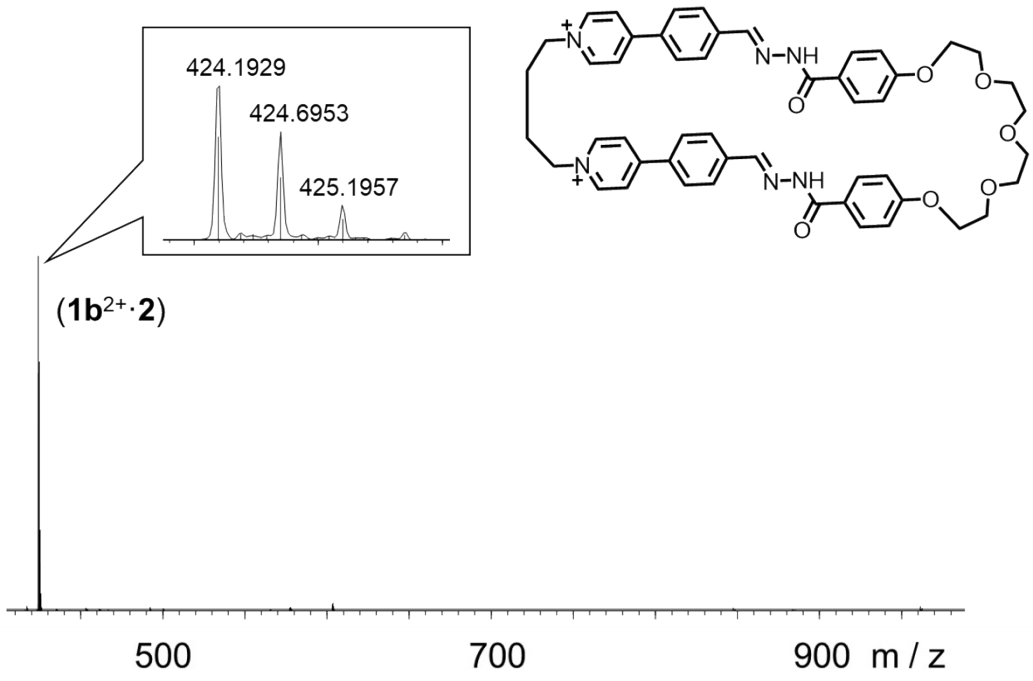

Figure S10. High-resolution LCMS-IT-TOF of (**1b**$^{2+}$·**2**). Counteranions could be either Cl^- or Br^-. The signal labeled in the spectrum correspond to molecular cation that contains two positive charges. *m/z* [(**1b**$^{2+}$·**2**)]$^{2+}$ calculated for $C_{50}H_{52}N_6O_7^{2+}$: 424.1943; found: 424.1929.

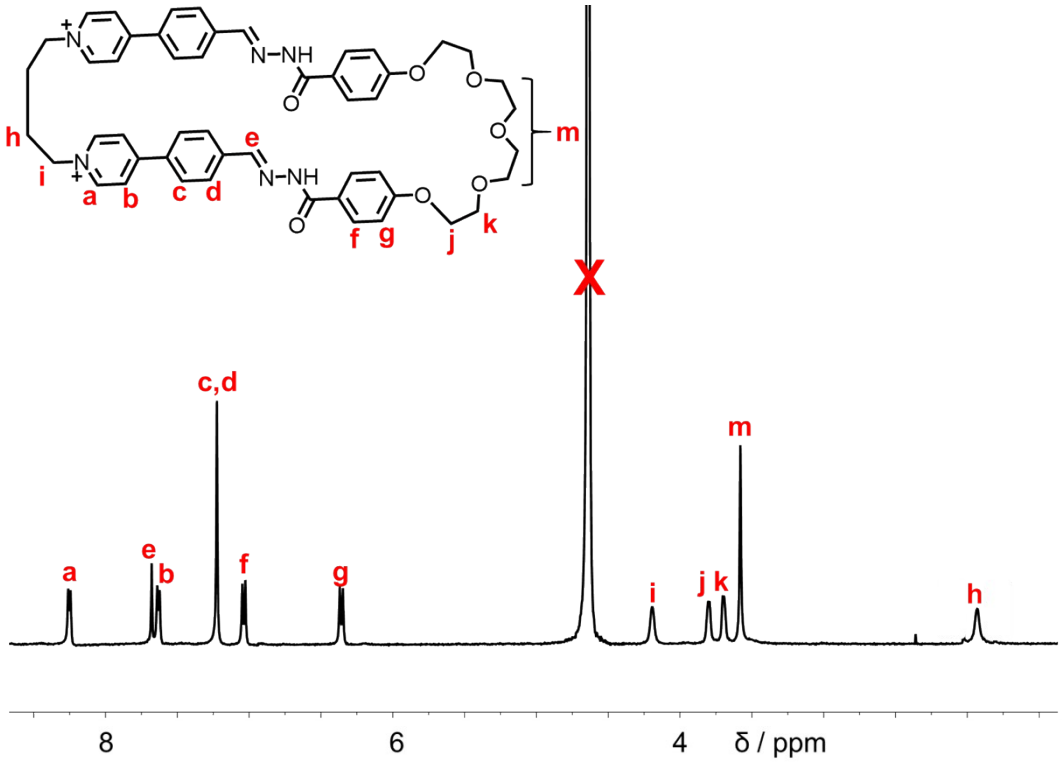

Figure S11. Partial ^{1}H NMR spectrum of (**1b**$^{2+}$·**2**) (500 MHz, D_2O, 298 K). Counteranions could be either Cl^- or Br^-.

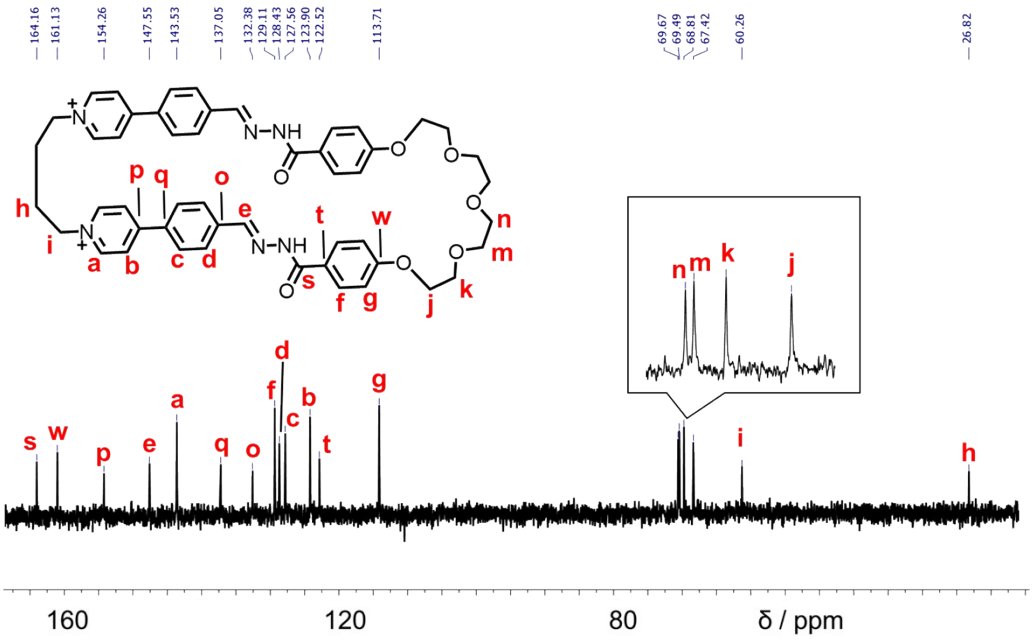

Figure S12. ^{13}C NMR spectrum (100 M Hz, 298 K, D_2O) of (**1b**$^{2+}$·**2**). Counteranions could be either Cl^- or Br^-.

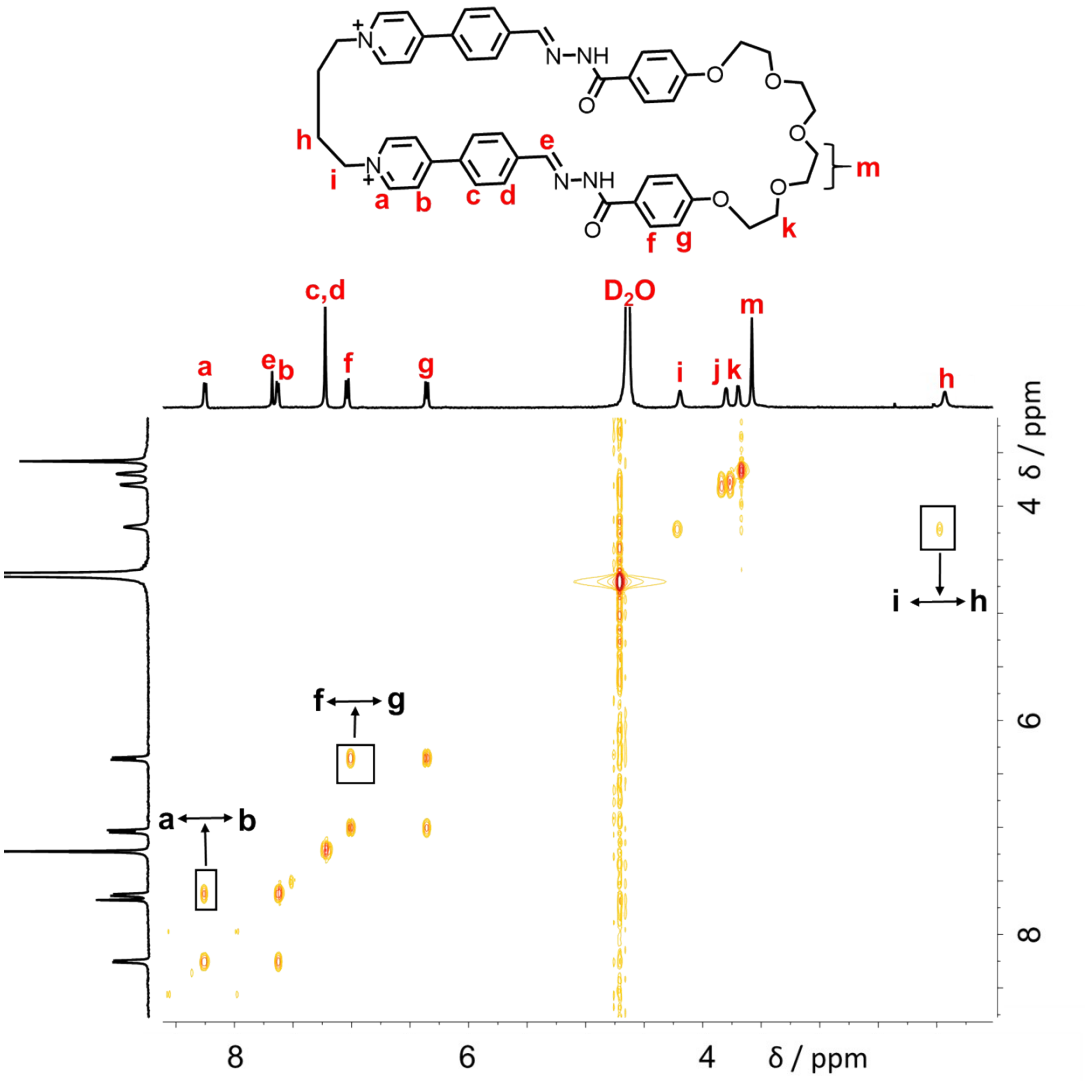

Figure S13. $^{1}H-^{1}H$ COSY spectrum (500 MHz, D_2O, 298 K) of (**1b**$^{2+}$·**2**). Counteranions could be either Cl^- or Br^-. Key correlation peaks are labeled in the spectrum.

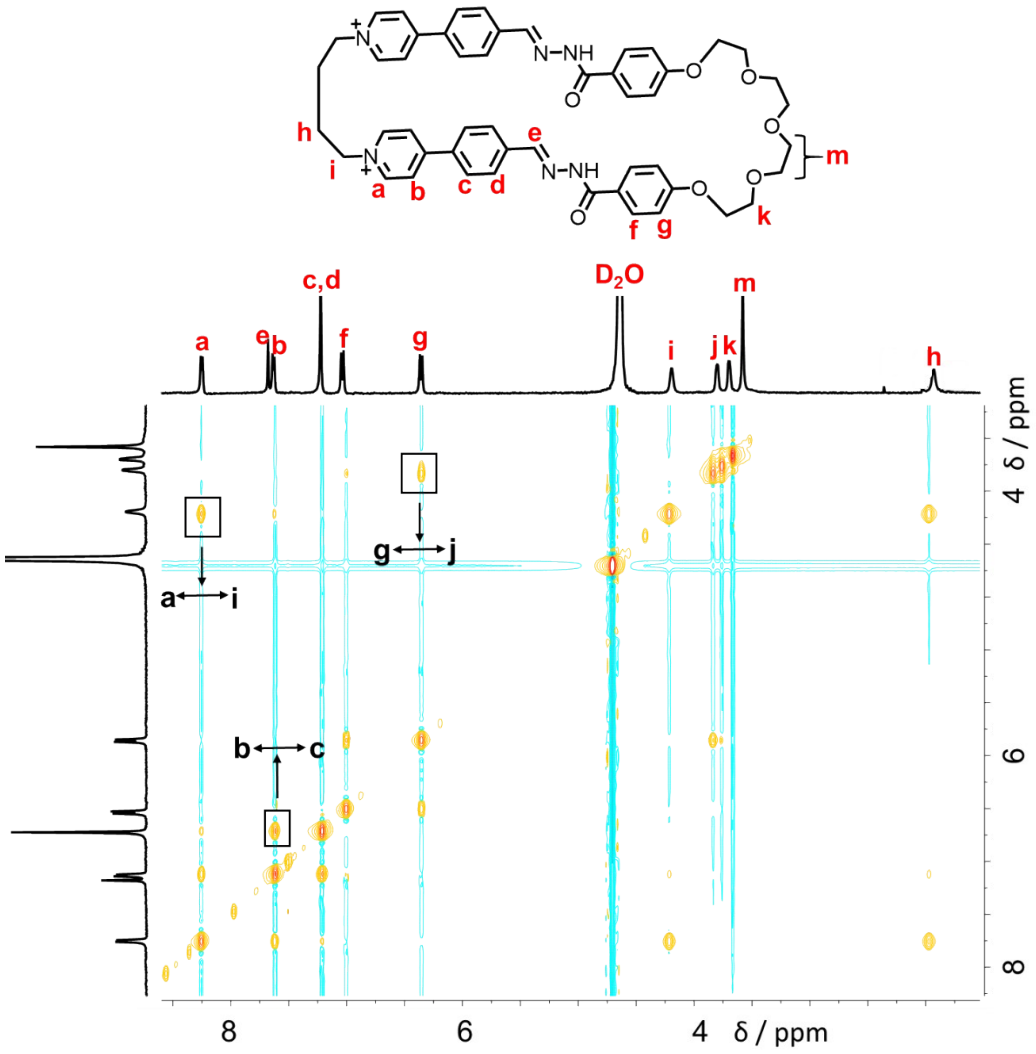

Figure S14. $^{1}H-^{1}H$ NOESY spectrum (500 MHz, D_2O, 298 K) of (**1b**$^{2+}$·**2**). Counteranions could be either Cl^- or Br^-. Key correlation peaks are labeled in the spectrum.

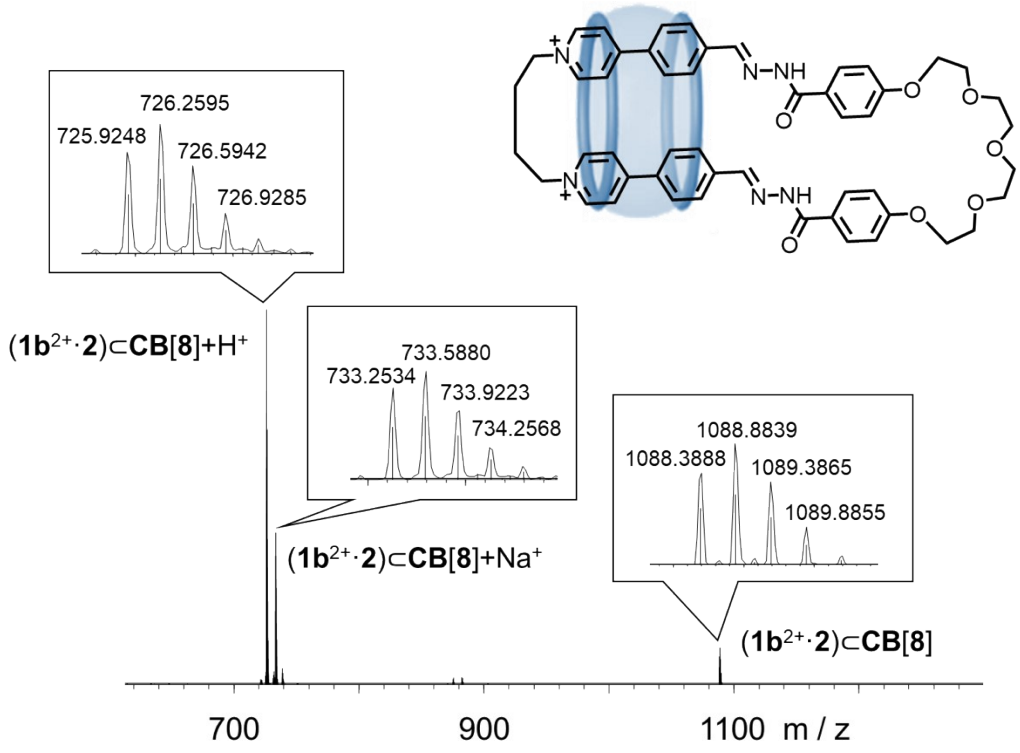

Figure S15. High-resolution LCMS-IT-TOF of (**1b**$^{2+}$·**2**)⊂**CB**[**8**]. Counteranions could be either Cl^- or Br^-.The signals labeled in the spectrum correspond to molecular cations that contain three and two positive charges, respectively. *m/z* [(**1b**$^{2+}$·**2**)⊂**CB**[**8**] + Na^+]$^{3+}$ calculated for $C_{98}H_{100}N_{38}NaO_{23}^{3+}$: 733.5913; found: 733.5880. [(**1b**$^{2+}$·**2**)⊂**CB**[**8**] + H^+]$^{3+}$ calculated for $C_{98}H_{101}N_{38}O_{23}^{3+}$: 726.2640; found: 726.2595. [(**1b**$^{2+}$·**2**)⊂**CB**[**8**]]$^{2+}$ calculated for $C_{98}H_{100}N_{38}O_{23}^{2+}$: 1088.8923; found: 1088.8839.

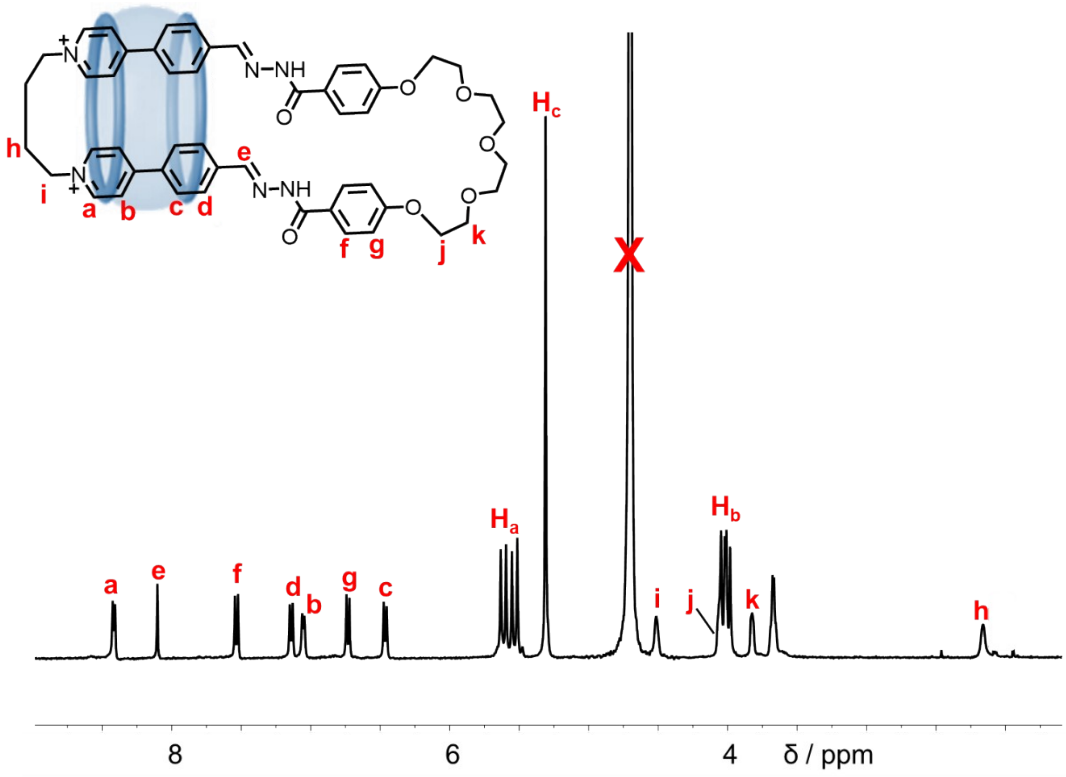

Figure S16. Partial ^{1}H NMR spectrum of (**1b**$^{2+}$·**2**)⊂**CB**[**8**] (500 MHz, D_2O, 298 K). Counteranions could be either Cl^- or Br^-.

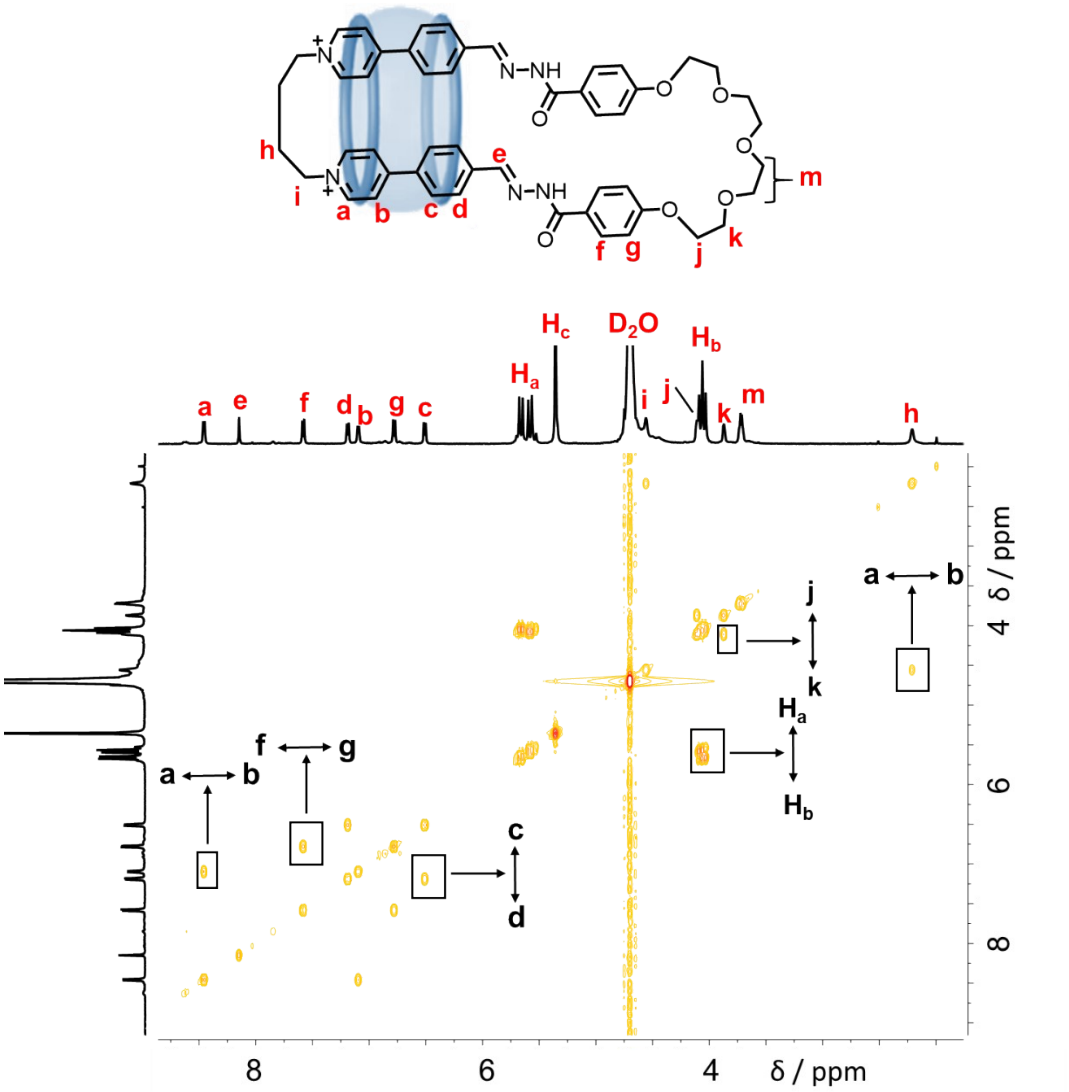

Figure S17. $^{1}H-^{1}H$ COSY spectrum (500 MHz, D_2O, 298 K) of (**1b**$^{2+}$·**2**)⊂**CB**[**8**]. Counteranions could be either Cl^- or Br^-. Key correlation peaks are labeled in the spectrum.

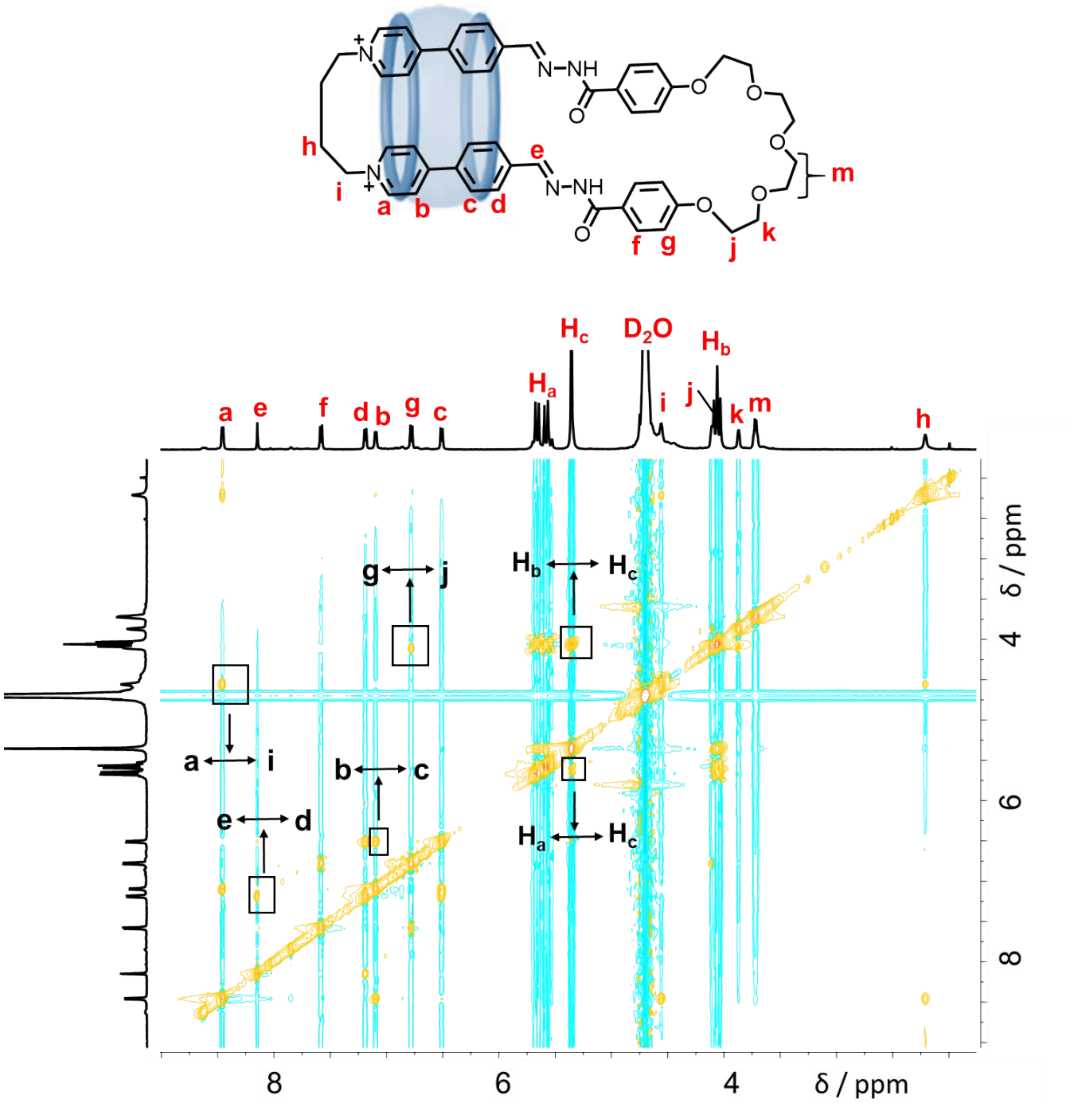

Figure S18. $^1H-^1H$ NOESY spectrum (500 MHz, D_2O, 298 K) of (**1b**$^{2+}$·**2**)⊂**CB**[**8**]. Counteranions could be either Cl^- or Br^-. Key correlation peaks are labeled in the spectrum.

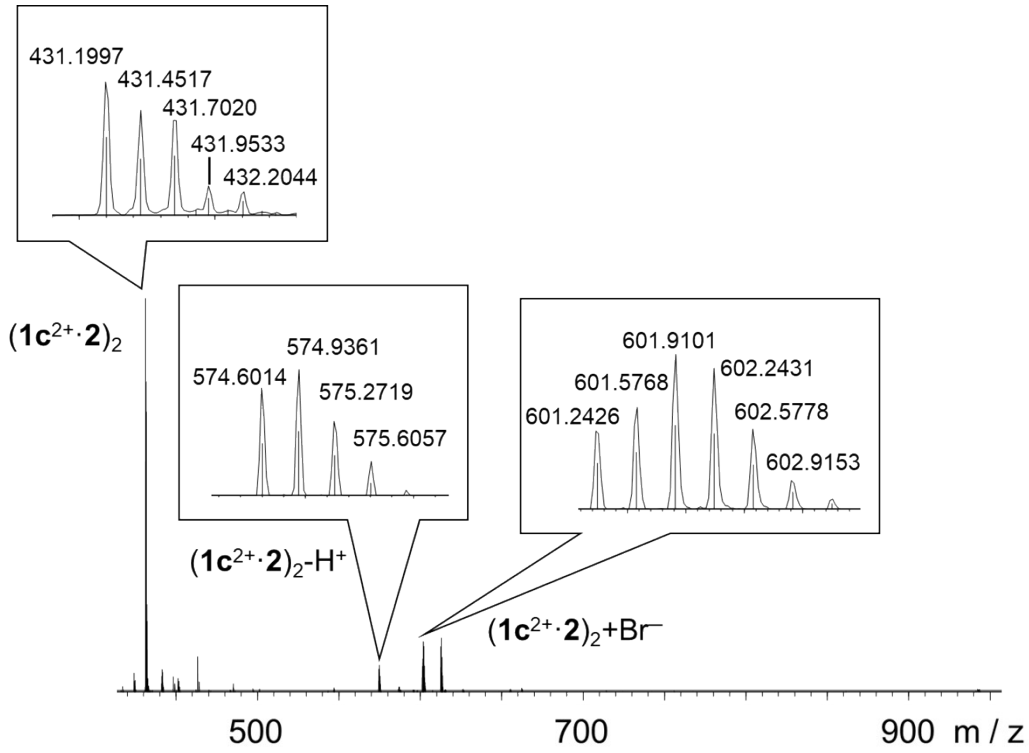

Figure S19. High-resolution LCMS-IT-TOF of the reaction mixture by condensing a 1:1 mixture of **1c**$^{2+}$2Br^{-} (4.5 mM) and **2** (4.5 mM). Counteranions could be either Cl^{-} or Br^{-}.The signals labeled in the spectrum correspond to molecular cations that contain four and three positive charges, respectively. *m/z* [(**1c**$^{2+}$·**2**)$_2$]$^{4+}$ calculated for $C_{102}H_{108}N_{12}O_{14}^{4+}$: 431.4530; found: 431.4517. [(**1c**$^{2+}$·**2**)$_2$ − H^{+}]$^{3+}$ calculated for $C_{102}H_{107}N_{12}O_{14}^{3+}$: 574.9349; found: 574.9361. [(**1c**$^{2+}$·**2**)$_2$ + Br^{-}]$^{3+}$ calculated for $C_{102}H_{108}BrN_{12}O_{14}^{4+}$: 602.2429; found: 602.2431.

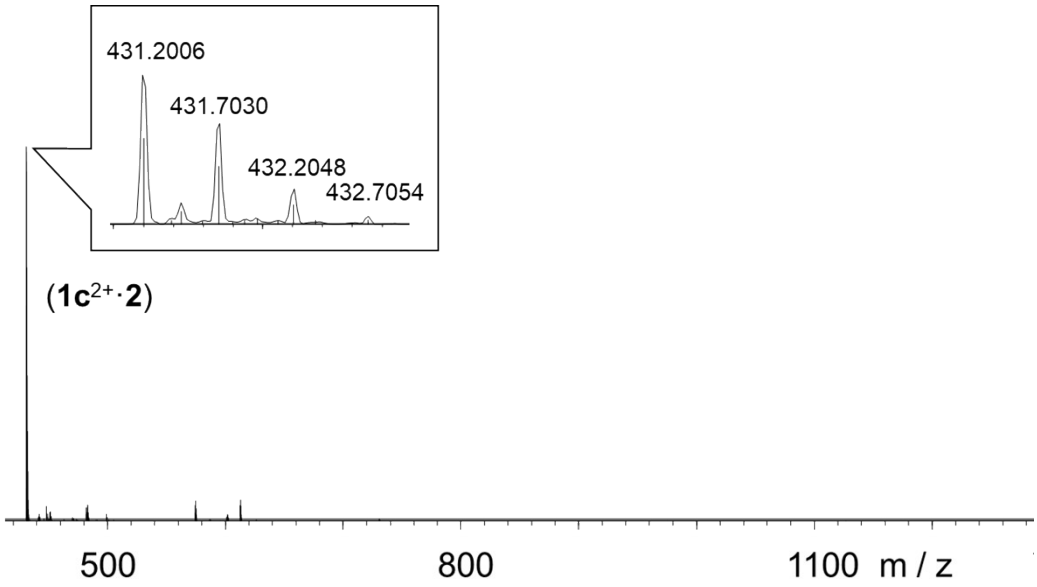

Figure S20. High-resolution LCMS-IT-TOF of the reaction mixture by condensing a 1:1 mixture of $\mathbf{1c}^{2+}2Br^-$ (0.6 mM) and **2** (0.6 mM). Counteranions could be either Cl^- or Br^-. The signal labeled in the spectrum correspond to molecular cation that contain two positive charges. *m/z* $[(\mathbf{1c}^{2+}\cdot\mathbf{2})]^{2+}$ calculated for $C_{51}H_{54}N_6O_7^{2+}$: 431.2022; found: 431.2006.

Figures S19 and S20 indicated that an equilibrium was established between the [2]catenane $(\mathbf{1c}^{2+}\cdot\mathbf{2})_2$ and the ring $(\mathbf{1c}^{2+}\cdot\mathbf{2})$. At higher concentration (Figure S19), the [2]catenane $(\mathbf{1c}^{2+}\cdot\mathbf{2})_2$ was observed as the major product; while at lower concentration, equilibrium shifted to the side of the ring $(\mathbf{1c}^{2+}\cdot\mathbf{2})$.

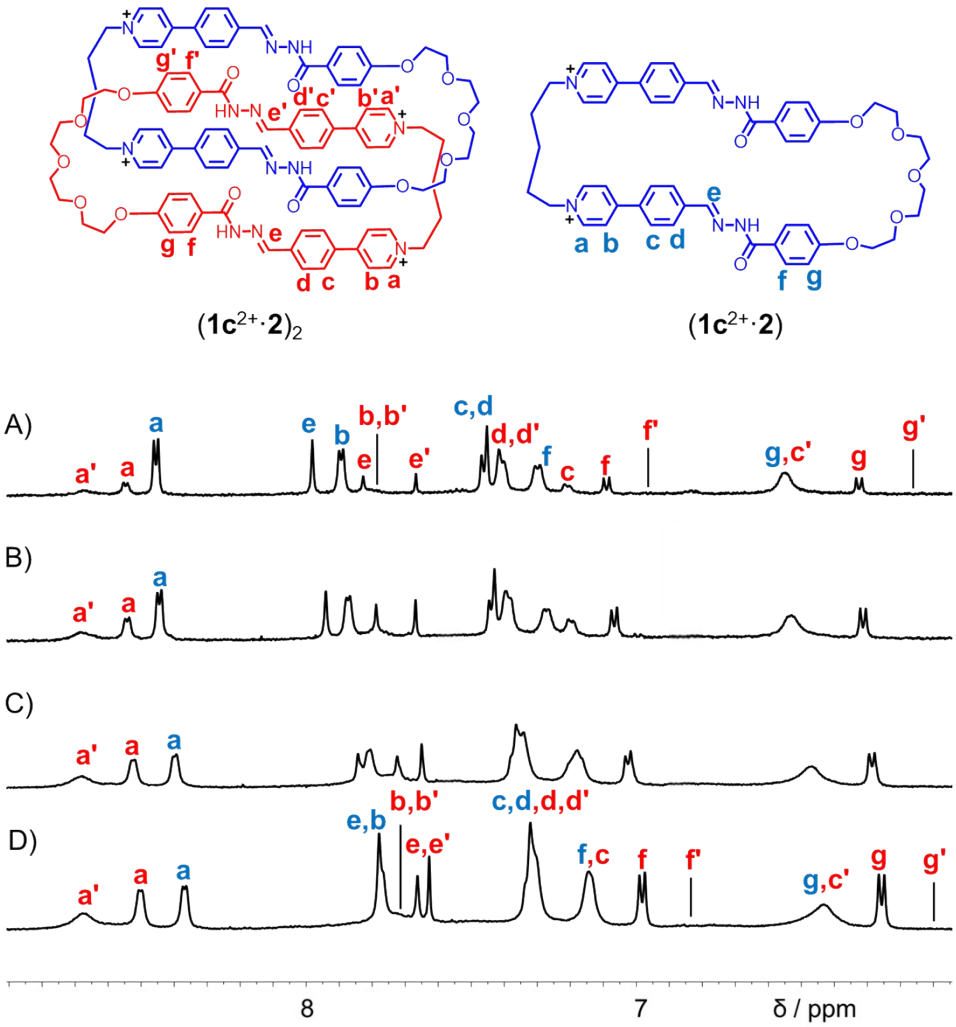

Figure S21. Partial ^{1}H NMR spectrum of the reaction mixture by condensing a 1:1 mixture of **1c**$^{2+}$2Br$^-$ and **2** at different concentrations (500 MHz, D_2O, 298 K): A) 0.6 mM, B) 1.2 mM, C) 2.5 mM, D) 4.5 mM . Counteranions could be either Cl^- or Br^-. All the spectra were recorded after the systems reached their equilibria.

The ^{1}H NMR spectra indicated that the products of condensing **1c**$^{2+}$2Br$^-$ and **2** were concentration dependent in D_2O. Generally, low reaction concentrations were observed to favor the ring production (**1c**$^{2+}$·**2**) over its corresponding catenane counterpart (**1c**$^{2+}$·**2**)$_2$ (Figure S21 A and S20). While at higher concentration, the [2]catenane (**1c**$^{2+}$·**2**)$_2$ became more favored (Figure S21 and S19).

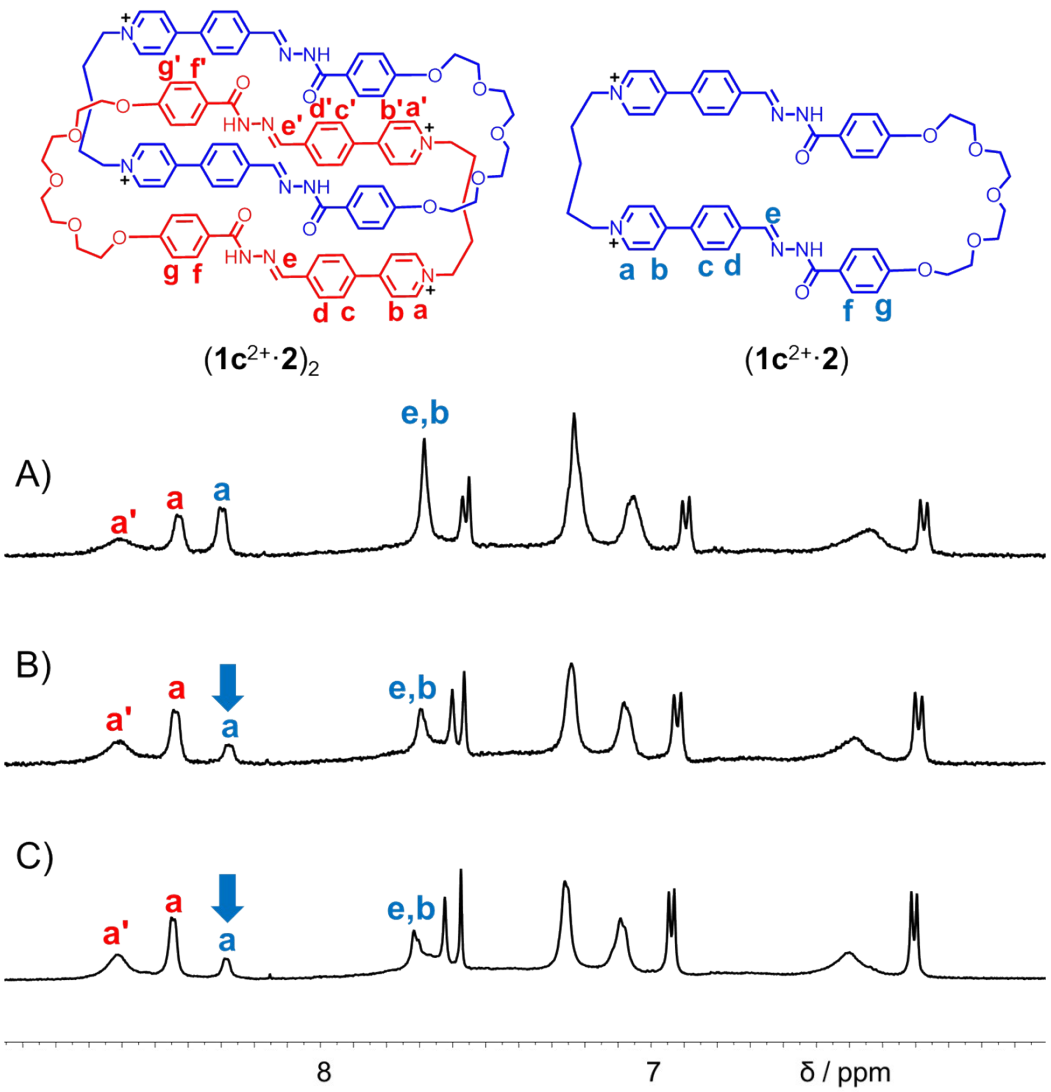

Figure S22. Partial ^{1}H NMR spectrum of the reaction mixture by condensing a 1:1 mixture of **1c**$^{2+}$2Br$^-$ and **2** (4.5 mM) (500 MHz, D_2O, 298 K), which were recorded after the reactants were mixed for A) 12 h, B) 4 d and C) 6 d. Counterions could be either Cl$^-$ or Br$^-$.

^{1}H NMR spectra indicate that in the early stage of reaction (Figure S22 A), the resonances corresponding to the macrocycle (**1c**$^{2+}$·**2**) are much stronger than those after the system reached the equilibrium (Figure S22 C). Such observation indicated that the ring is a kinetic product, while the [2]catenane is the thermodynamic favored product at higher concentration namely 4.5 mM.

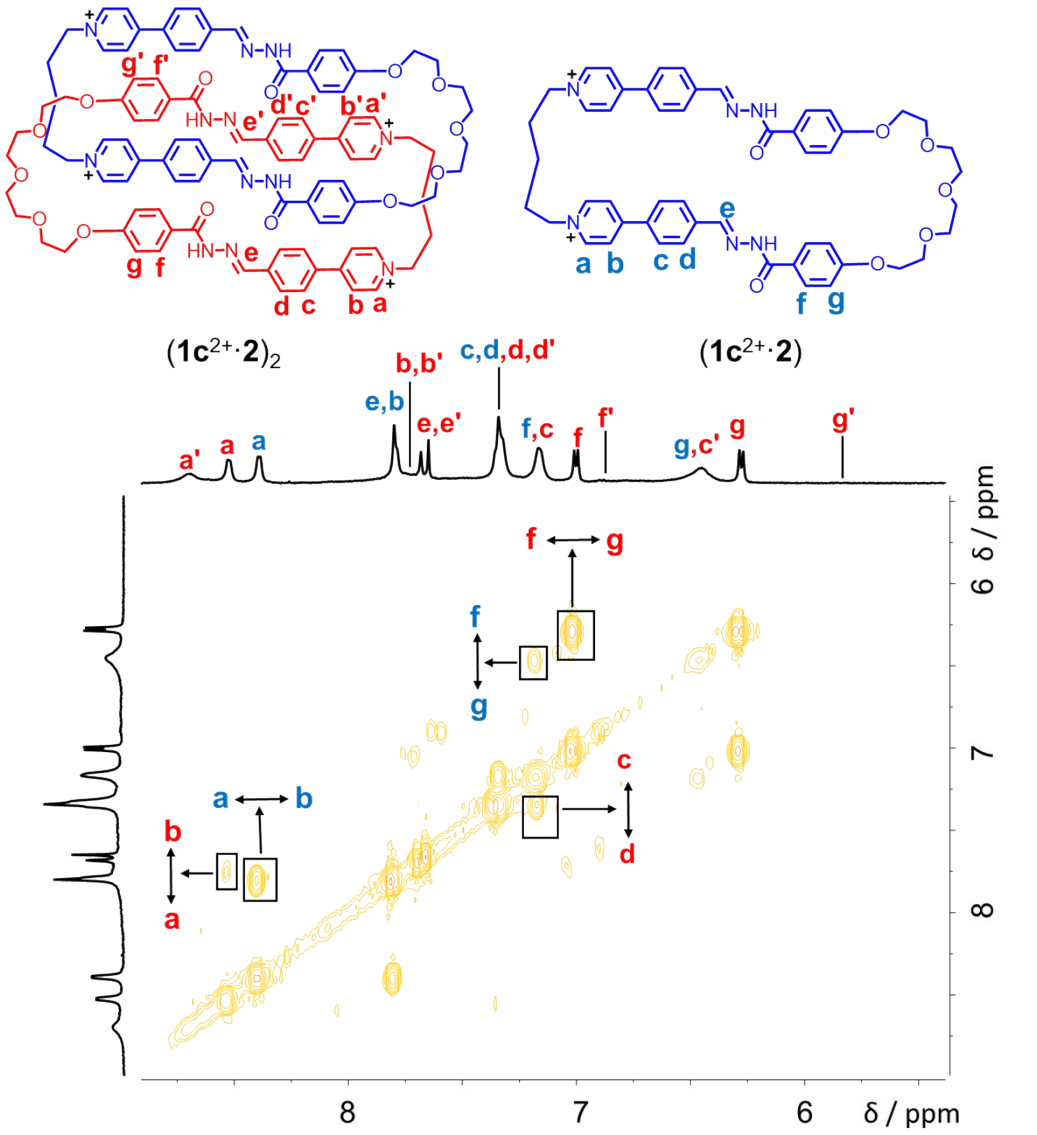

Figure S23. $^{1}H-^{1}H$ COSY spectrum (500 MHz, D_2O, 298 K) of the reaction mixture by condensing a 1:1 mixture of **1c**$^{2+}$2Br^{-} (4.5 mM) and **2** (4.5 mM). Counteranions could be either Cl^{-} or Br^{-}. Key correlation peaks are labeled in the spectrum.

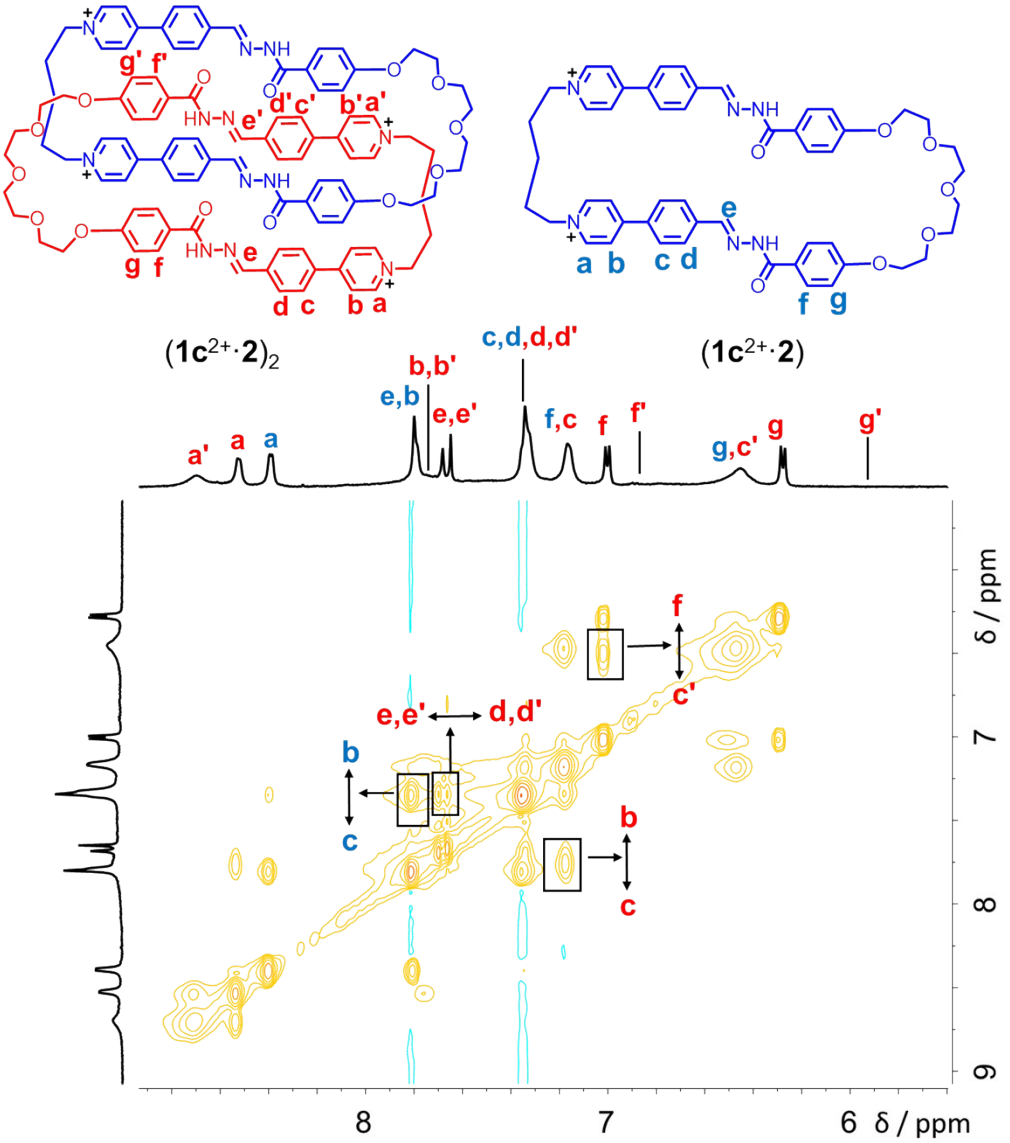

Figure S24. $^{1}H-^{1}H$ NOESY spectrum (500 MHz, D_2O, 298 K) of the reaction mixture by condensing a 1:1 mixture of **1c**$^{2+}$2Br^{-} (4.5 mM) and **2** (4.5 mM). Counteranions could be either Cl^{-} or Br^{-}. Key correlation peaks are labeled in the spectrum.

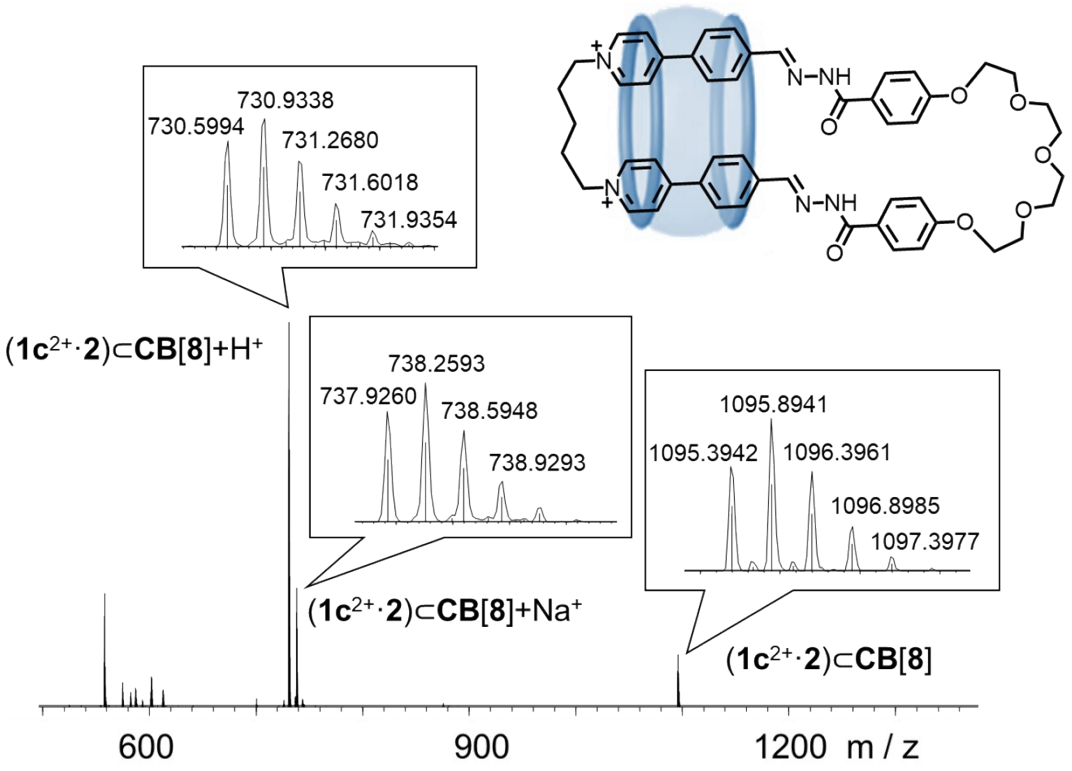

Figure S25. High-resolution LCMS-IT-TOF of (**1c**$^{2+}$·**2**)⊂**CB**[**8**]. Counteranions could be either Cl^- or Br^-.The signals labeled in the spectrum correspond to molecular cations that contain three and two positive charges, respectively. *m/z* [(**1c**$^{2+}$·**2**)⊂**CB**[**8**] + Na^+]$^{3+}$ calculated for $C_{99}H_{102}N_{38}NaO_{23}^{3+}$: 738.2632; found: 738.2593. [(**1c**$^{2+}$·**2**)⊂**CB**[**8**] + H^+]$^{3+}$ calculated for $C_{99}H_{103}N_{38}O_{23}^{3+}$: 730.9358; found: 930.9338. [(**1c**$^{2+}$·**2**)⊂**CB**[**8**]]$^{2+}$ calculated for $C_{99}H_{102}N_{38}O_{23}^{2+}$: 1095.9001; found: 1095.8941.

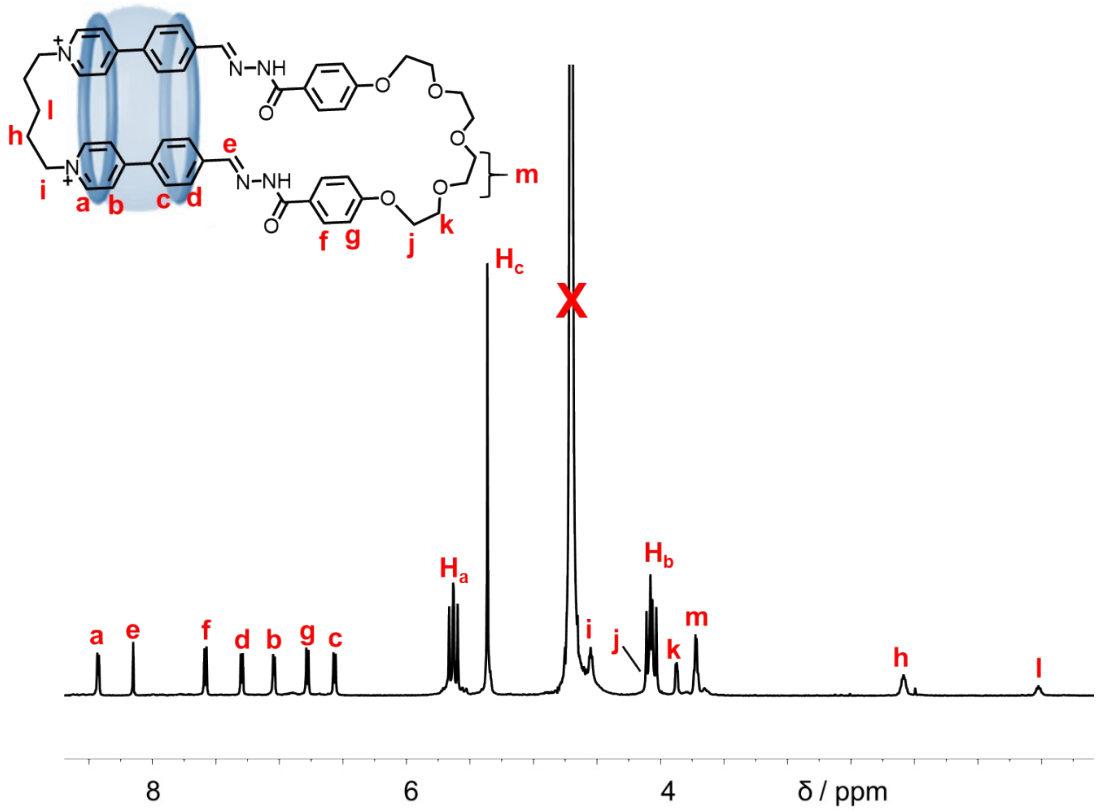

Figure S26. Partial ^{1}H NMR spectrum of (**1c**$^{2+}$·**2**)⊂**CB**[**8**] (500 MHz, D_2O, 298 K). Counteranions could be either Cl^- or Br^-.

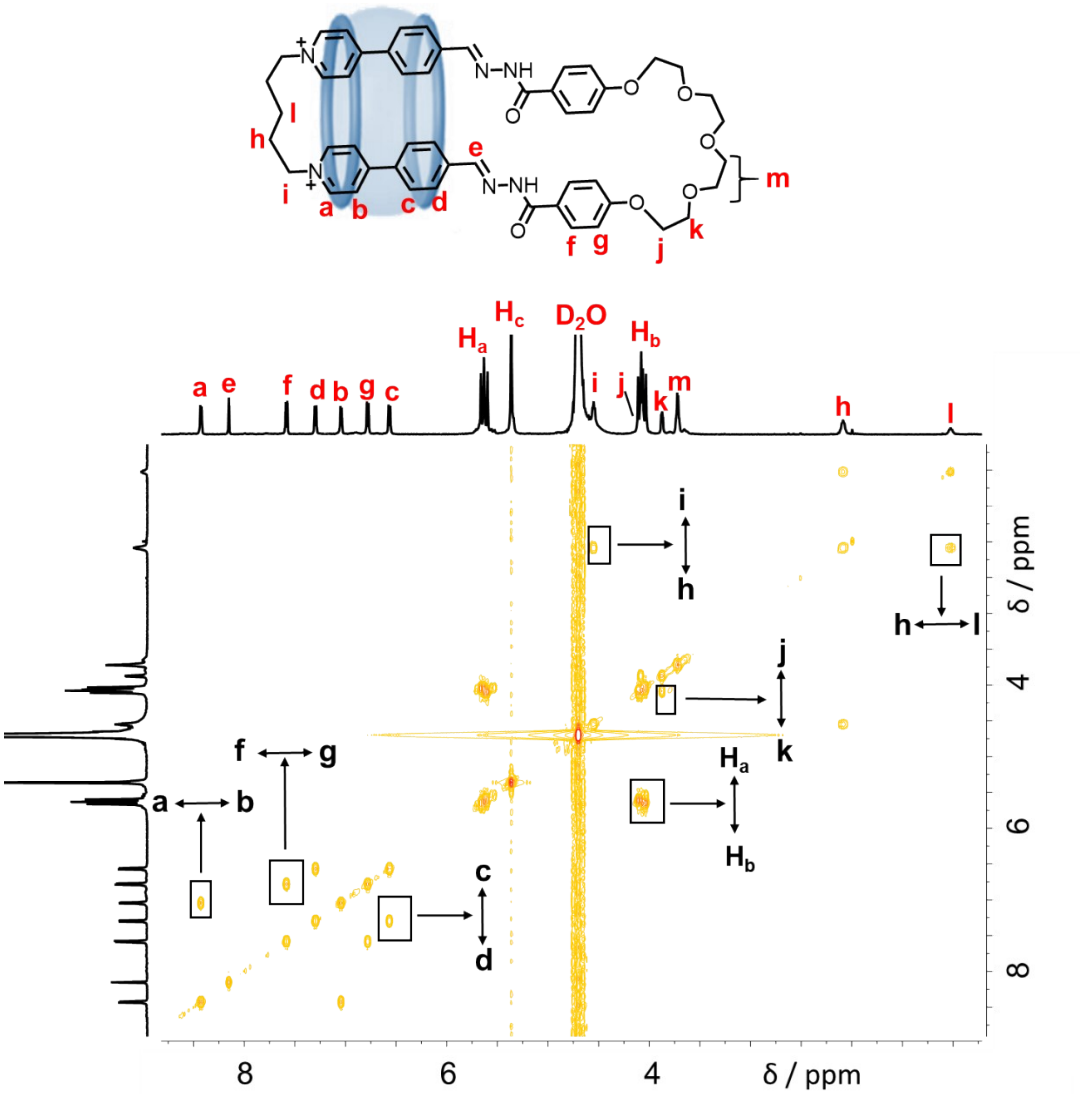

Figure S27. $^{1}H-^{1}H$ COSY spectrum (500 MHz, D_2O, 298 K) of (**1c**$^{2+}$·**2**)⊂**CB**[**8**]. Counteranions could be either Cl^- or Br^-. Key correlation peaks are labeled in the spectrum.

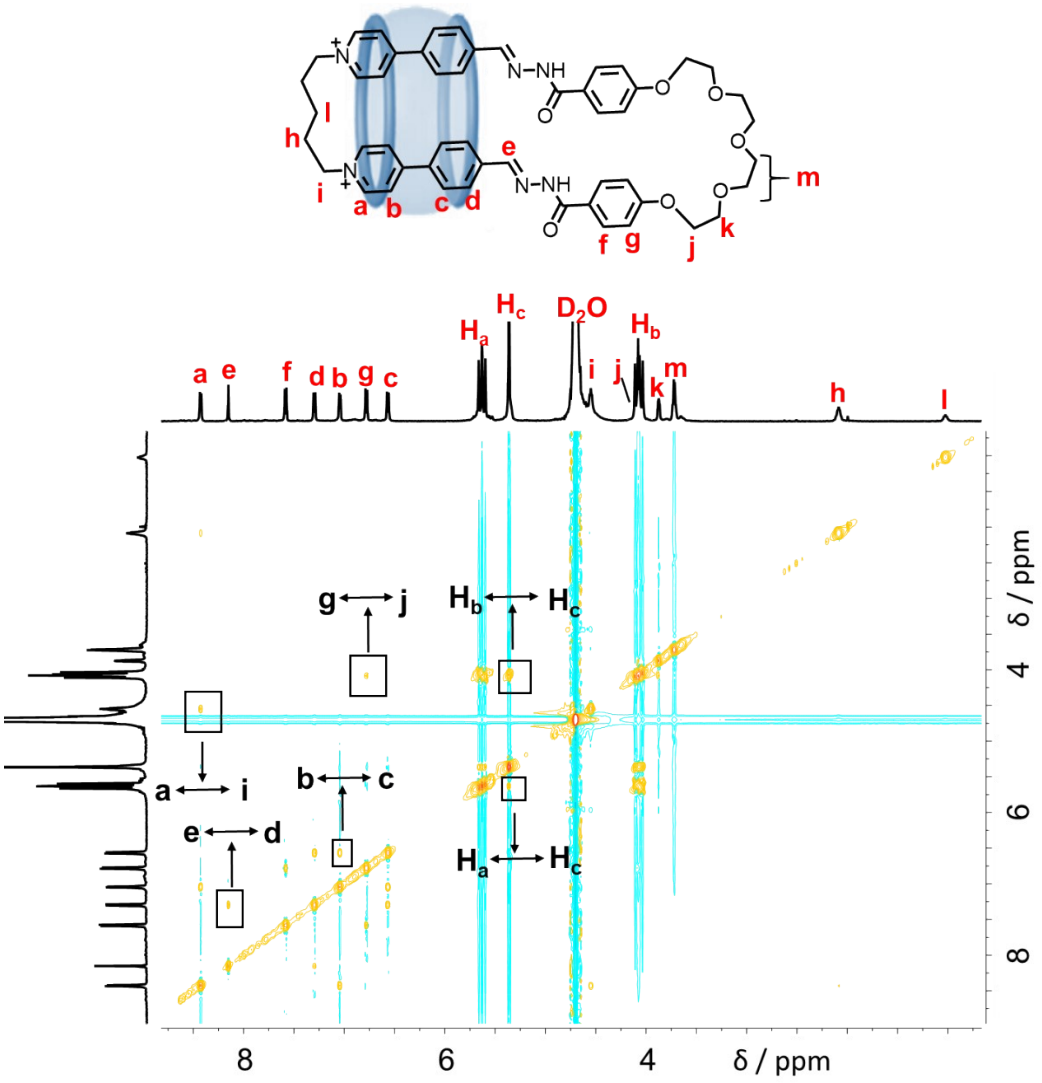

Figure S28. ^{1}H–^{1}H NOESY spectrum (500 MHz, D_2O, 298 K) of (**1c**$^{2+}$·**2**)⊂**CB**[**8**]. Counteranions could be either Cl^- or Br^-. Key correlation peaks are labeled in the spectrum.

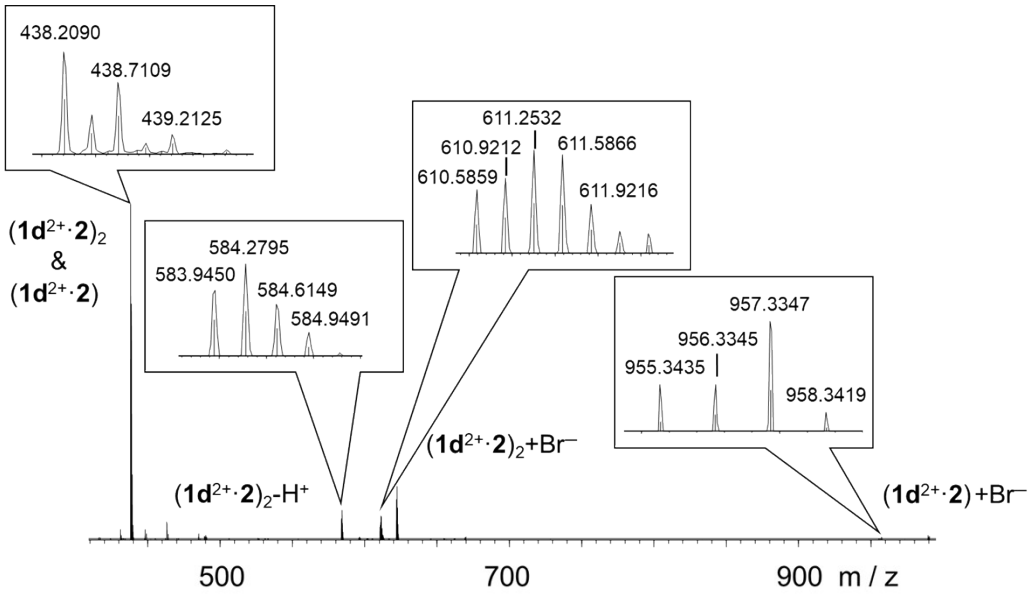

Figure S29. High-resolution LCMS-IT-TOF of the reaction mixture by condensing a 1:1 mixture of **1d**$^{2+}$2Br^{-} (2.5 mM) and **2** (2.5 mM) in water. Counteranions could be either Cl^{-} or Br^{-}.The signals labeled in the spectrum correspond to molecular cations that contain four, three, two and one positive charges, respectively. *m/z* [(**1d**$^{2+}$·**2**)$_2$ − H^{+}]$^{3+}$ calculated for $C_{104}H_{111}N_{12}O_{14}^{3+}$: 584.2787; found: 584.2795. [(**1d**$^{2+}$·**2**)$_2$ + Br^{-}]$^{3+}$ calculated for $C_{104}H_{112}BrN_{12}O_{14}^{4+}$: 611.5867; found: 611.5866. [(**1d**$^{2+}$·**2**) + Br^{-}]$^{+}$ calculated for $C_{104}H_{112}BrN_{12}O_{14}^{4+}$: 955.3388; found: 955.3435.

In mass spectrum, peaks corresponding to both the [2]catenane (**1d**$^{2+}$·**2**)$_2$ and the macrocycle (**1d**$^{2+}$·**2**) (Figure S29) were observed.

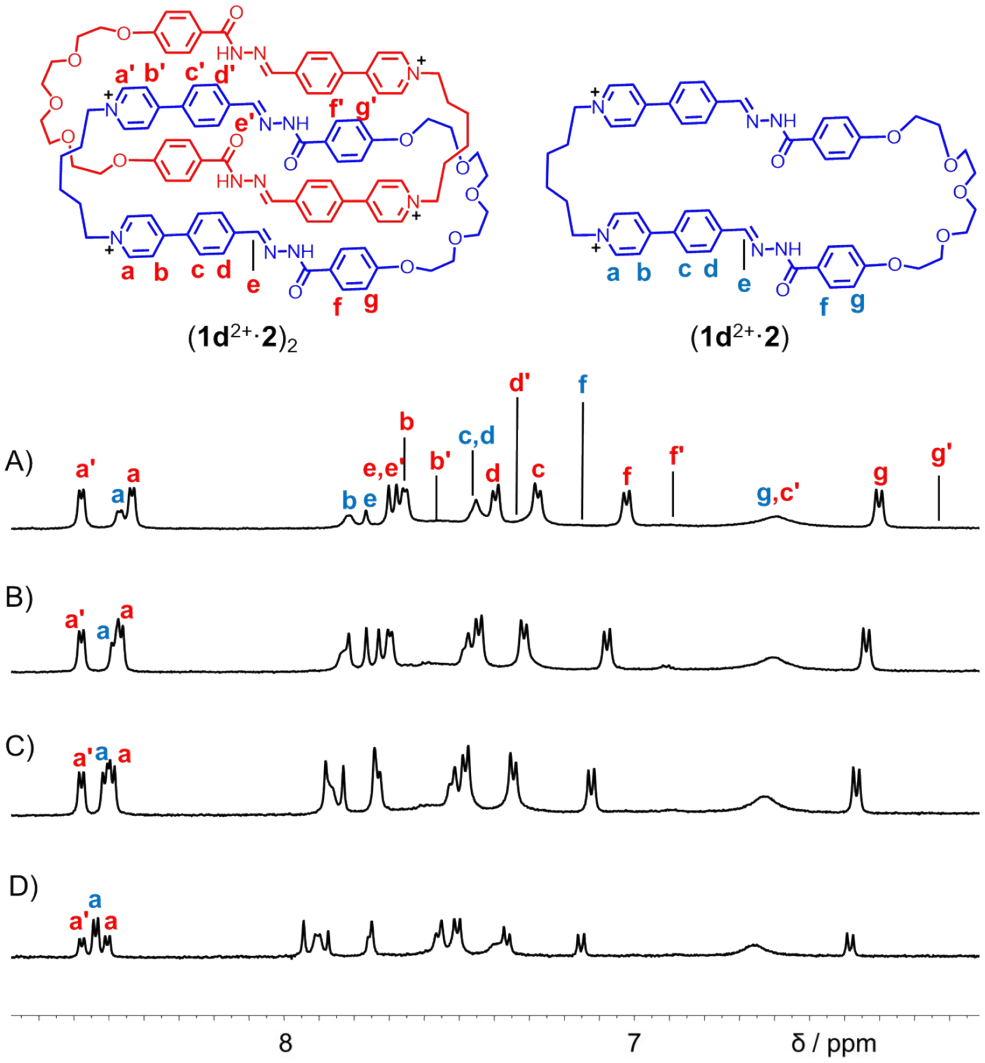

Figure S30. Partial ^{1}H NMR spectrum of the reaction mixture by condensing a 1:1 mixture of **1d**$^{2+}$2Br$^-$ and **2** at different concentrations (500 MHz, D_2O, 298 K), including A) 4.5 mM, B) 2.5 mM, C) 1.2 mM, D) 0.6 mM . Counteranions could be either Cl$^-$ or Br$^-$.

The ^{1}H NMR spectra indicated that the reaction products of condensing **1d**$^{2+}$2Br$^-$ and **2** in water is concentration dependent. Generally, at lower reaction concentration (Figure S30 D), the ring (**1d**$^{2+}$·**2**) is more favored compared that observed at higher concentration (Figure S30 A).

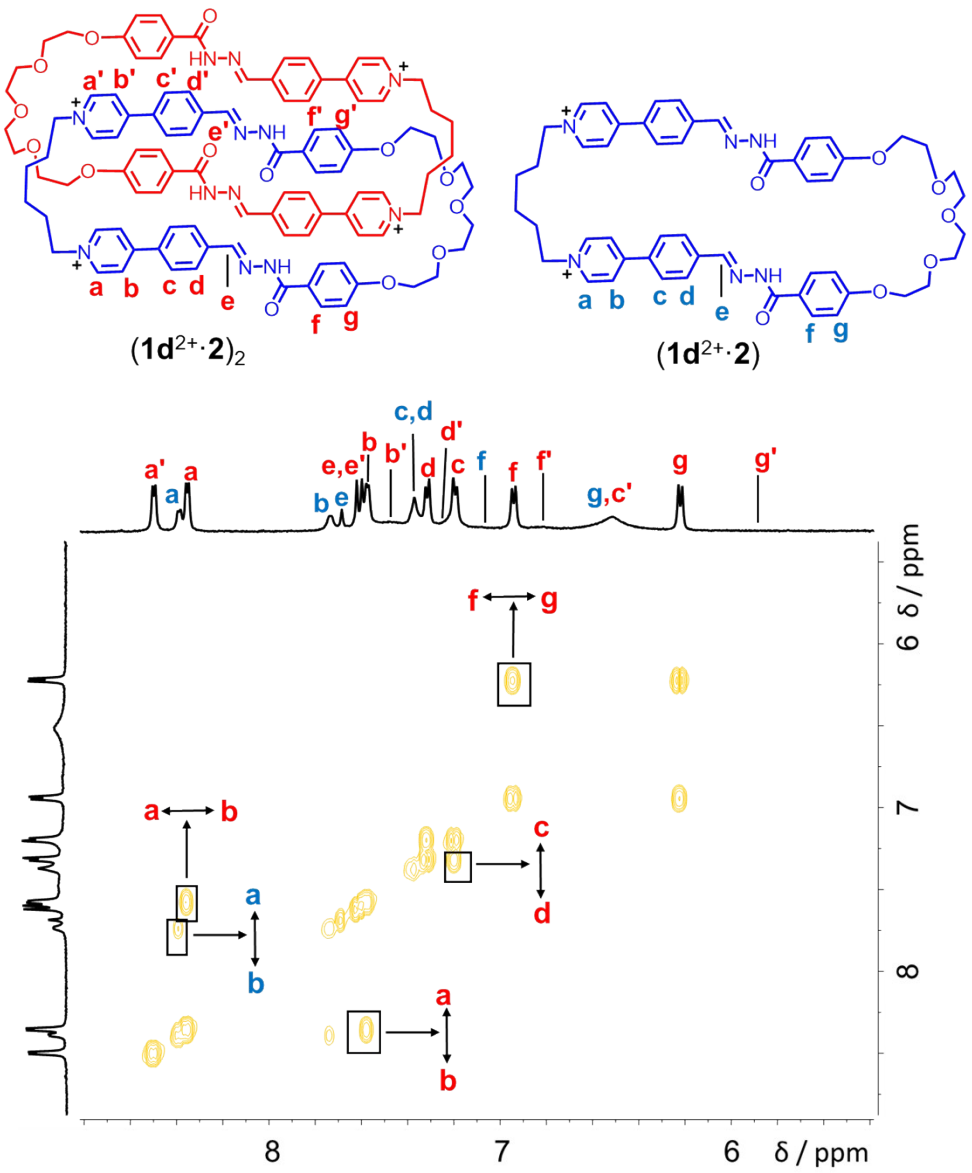

Figure S31. $^{1}H-^{1}H$ COSY spectrum (500 MHz, D_2O, 298 K) of the reaction mixture by condensing a 1:1 mixture of **1d**$^{2+}$2Br^{-} (4.5 mM) and **2** (4.5 mM). Counteranions could be either Cl^{-} or Br^{-}. Key correlation peaks are labeled in the spectrum.

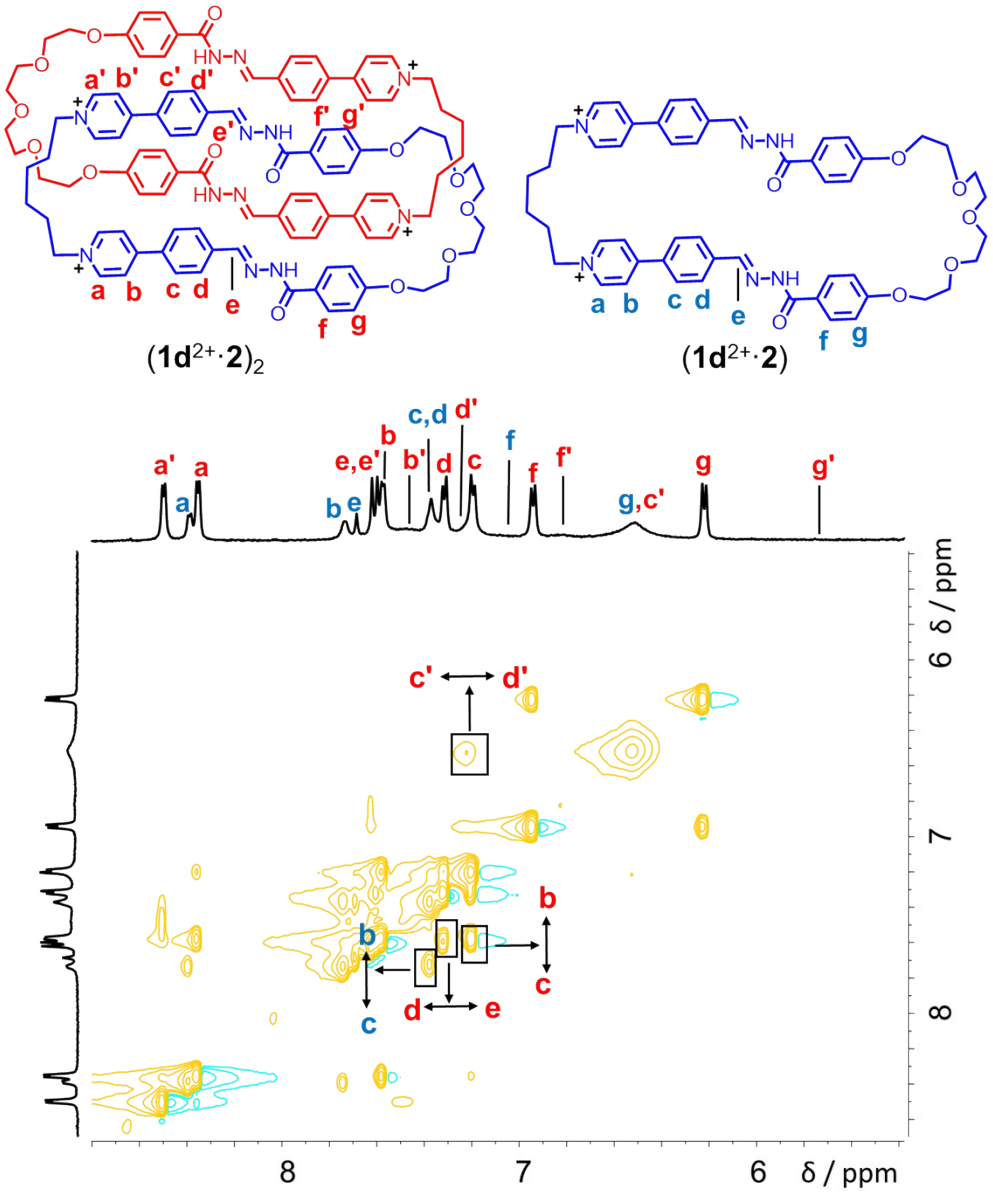

Figure S32. $^{1}H-^{1}H$ NOESY spectrum (500 MHz, D_2O, 298 K) of the reaction mixture by condensing a 1:1 mixture of **1d**$^{2+}$2Br^{-} (4.5 mM) and **2** (4.5 mM). Counteranions could be either Cl^{-} or Br^{-}. Key correlation peaks are labeled in the spectrum.

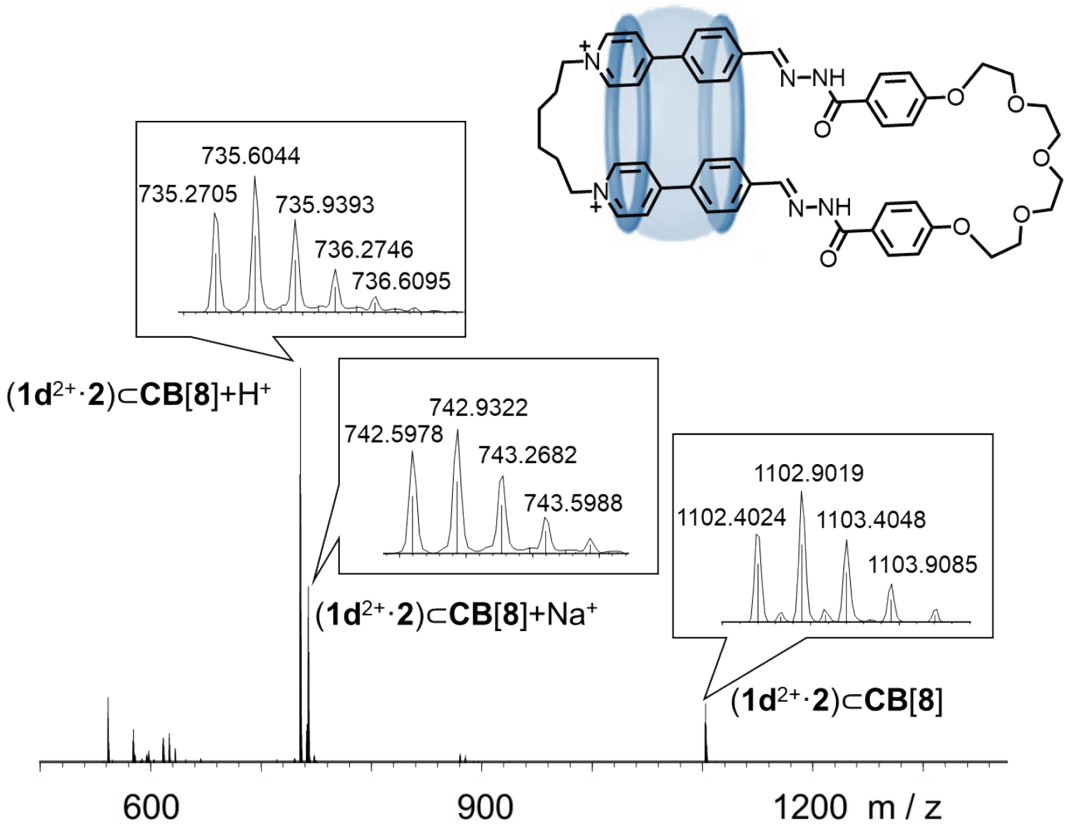

Figure S33. High-resolution LCMS-IT-TOF of (**1d**$^{2+}$·**2**)⊂**CB**[**8**]. Counteranions could be either Cl^- or Br^-. The signals labeled in the spectrum correspond to molecular cations that contain three and two positive charges, respectively. *m/z* [(**1d**$^{2+}$·**2**)⊂**CB**[**8**] + Na^+]$^{3+}$ calculated for $C_{100}H_{104}N_{38}NaO_{23}^{3+}$: 742.9350; found: 742.9322. [(**1d**$^{2+}$·**2**)⊂**CB**[**8**] + H^+]$^{3+}$ calculated for $C_{100}H_{105}N_{38}O_{23}^{3+}$: 735.6077; found: 735.6044. [(**1d**$^{2+}$·**2**)⊂**CB**[**8**]]$^{2+}$ calculated for $C_{100}H_{104}N_{38}O_{23}^{2+}$: 1102.9080; found: 1102.9019.

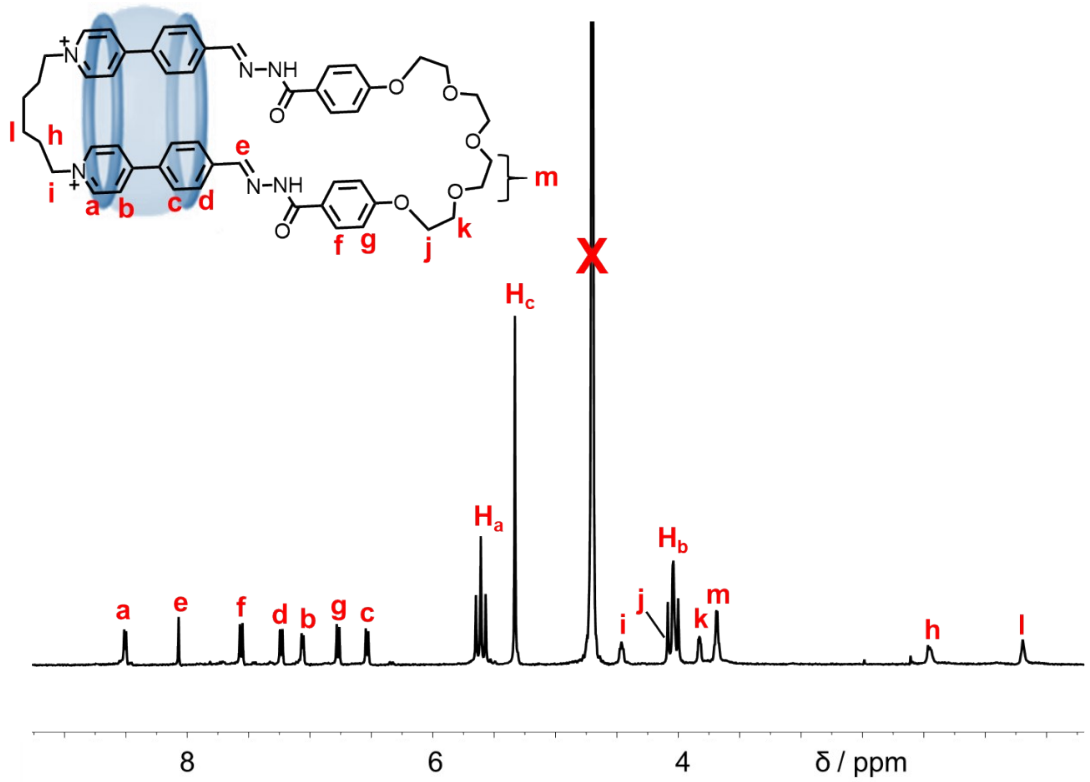

Figure S34. Partial ^{1}H NMR spectrum of (**1d**$^{2+}$·**2**)⊂**CB**[**8**] (500 MHz, D_2O, 298 K). Counteranions could be either Cl^- or Br^-.

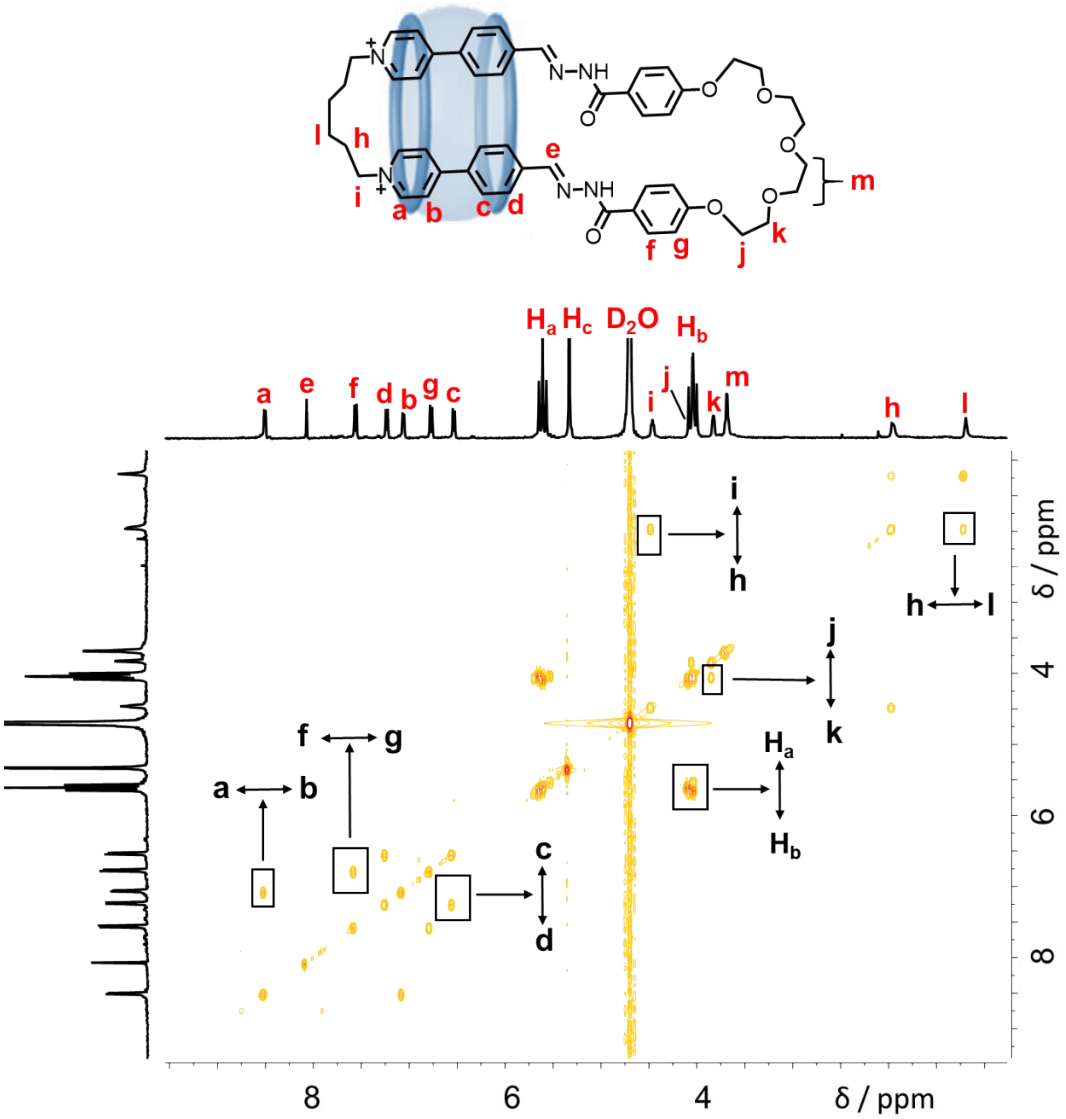

Figure S35. ^{1}H–^{1}H COSY spectrum (500 MHz, D_2O, 298 K) of (**1d**$^{2+}$·**2**)⊂**CB**[**8**]. Counteranions could be either Cl^- or Br^-. Key correlation peaks are labeled in the spectrum.

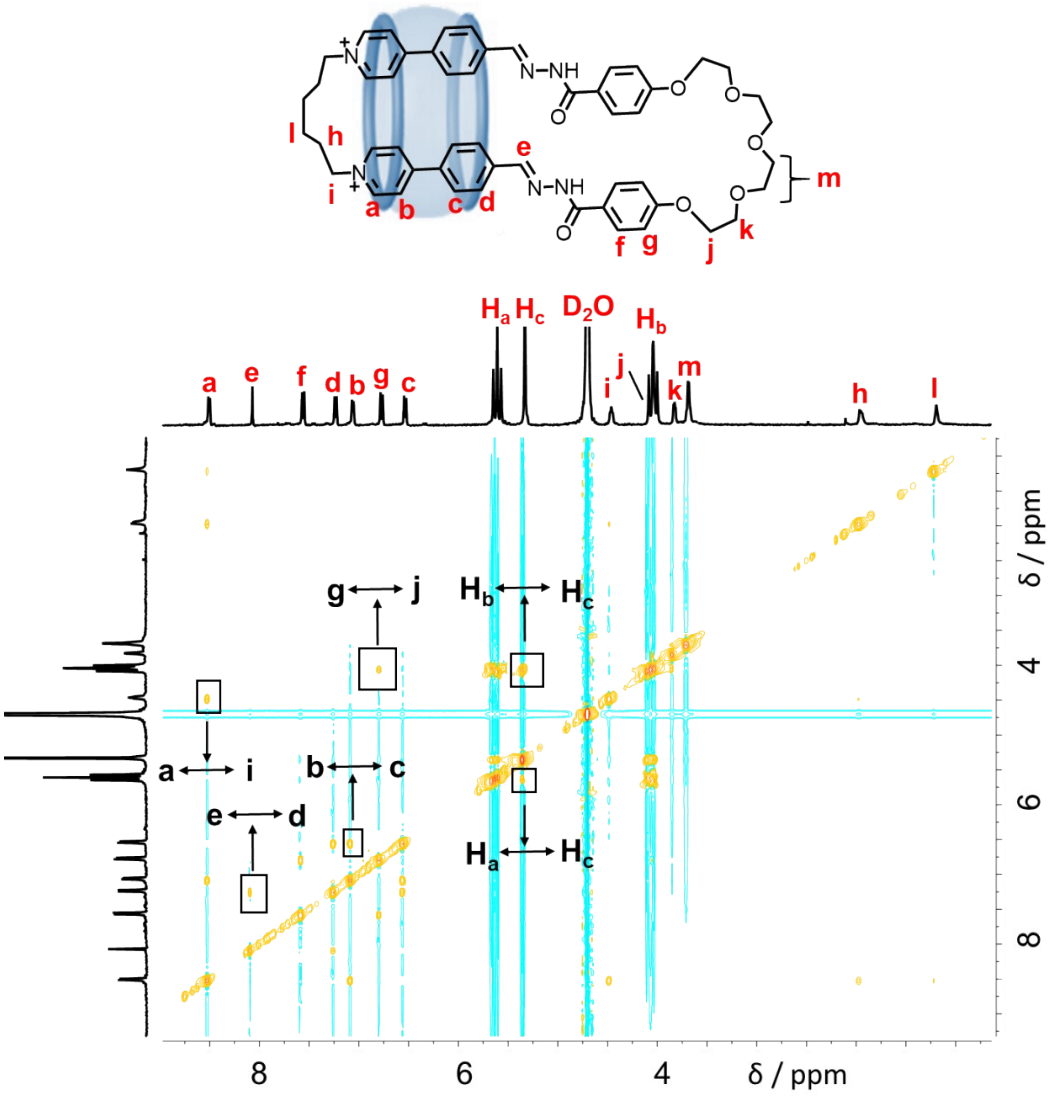

Figure S36. ^{1}H–^{1}H NOESY spectrum (500 MHz, D_2O, 298 K) of (**1d**$^{2+}$·**2**)⊂**CB**[**8**]. Counteranions could be either Cl^- or Br^-. Key correlation peaks are labeled in the spectrum.

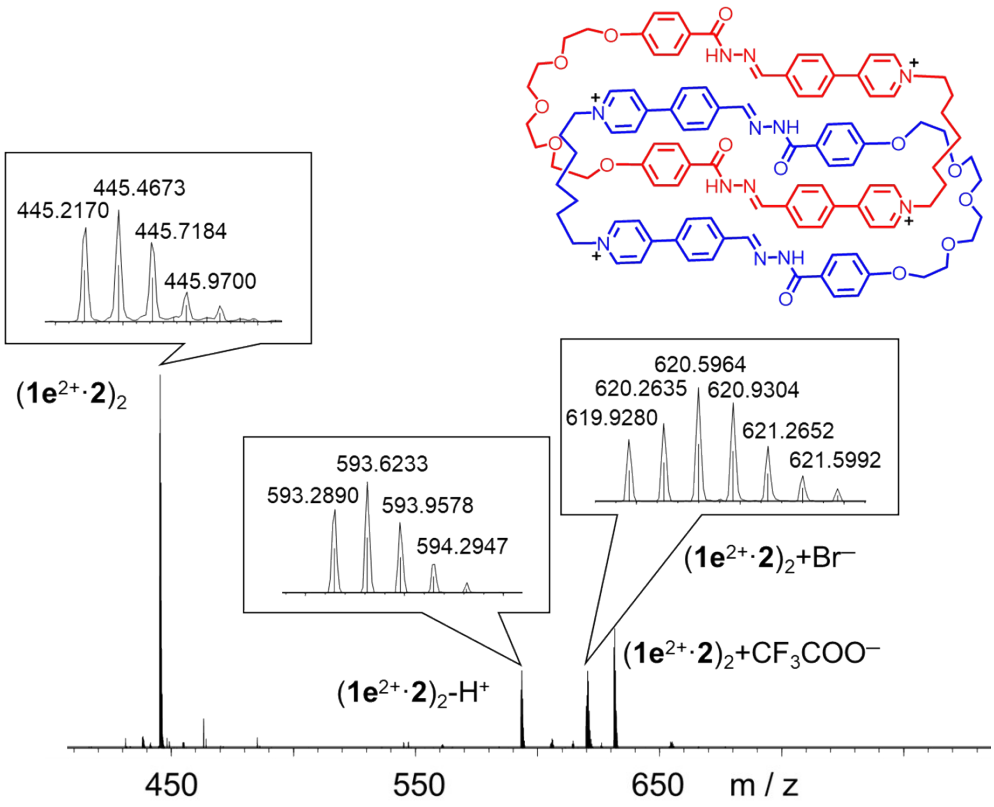

Figure S37. High-resolution LCMS-IT-TOF of [2]catenane $(\mathbf{1e}^{2+}\cdot\mathbf{2})_2$. Counteranions could be either Cl^- or Br^-. The signals labeled in the spectrum correspond to molecular cations that contain four and three positive charges, respectively. *m/z* $[(\mathbf{1e}^{2+}\cdot\mathbf{2})_2]^{4+}$ calculated for $C_{106}H_{116}N_{12}O_{14}^{3+}$: 445.4686; found: 445.4673. $[(\mathbf{1e}^{2+}\cdot\mathbf{2})_2 - H^+]^{3+}$ calculated for $C_{106}H_{115}N_{12}O_{14}^{3+}$: 593.6224; found: 593.6233. $[(\mathbf{1e}^{2+}\cdot\mathbf{2})_2 + Br^-]^{3+}$ calculated for $C_{106}H_{116}BrN_{12}O_{14}^{4+}$: 620.2645; found: 620.2635.

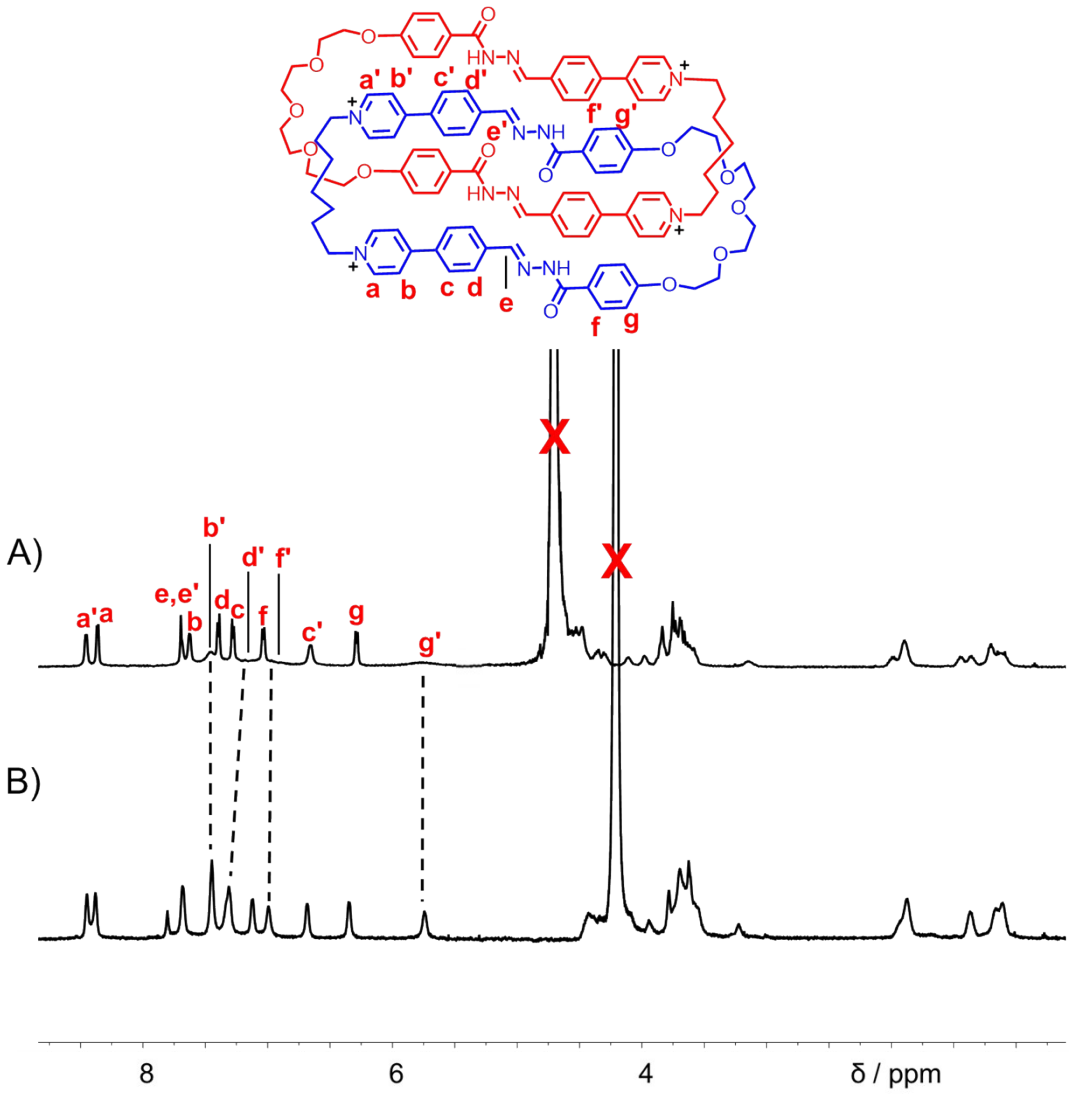

Figure S38. Partial ^{1}H NMR spectra of A) $(\mathbf{1e}^{2+}\cdot\mathbf{2})_2$ (600 MHz, D_2O, 298 K), B) $(\mathbf{1e}^{2+}\cdot\mathbf{2})_2$ (600 MHz, D_2O, 333 K). Counteranions could be either Cl^- or Br^-.

The ^{1}H NMR spectra of $(\mathbf{1e}^{2+}\cdot\mathbf{2})_2\cdot 4Cl^-$ are temperature dependent in D_2O. At room temperature (25 °C), the resonances of the protons b', d', c', f' and g' (see Figure S38) are relatively broad. This observation could be explained by the fact that, within the cavity of one of the two interlocked rings, the circumvolution movement corresponding parts is significantly slowed down. At elevated temperature such as 60 °C, these peaks become sharper, indicating that the circumvolution motion is "speeded up" at higher temperature.

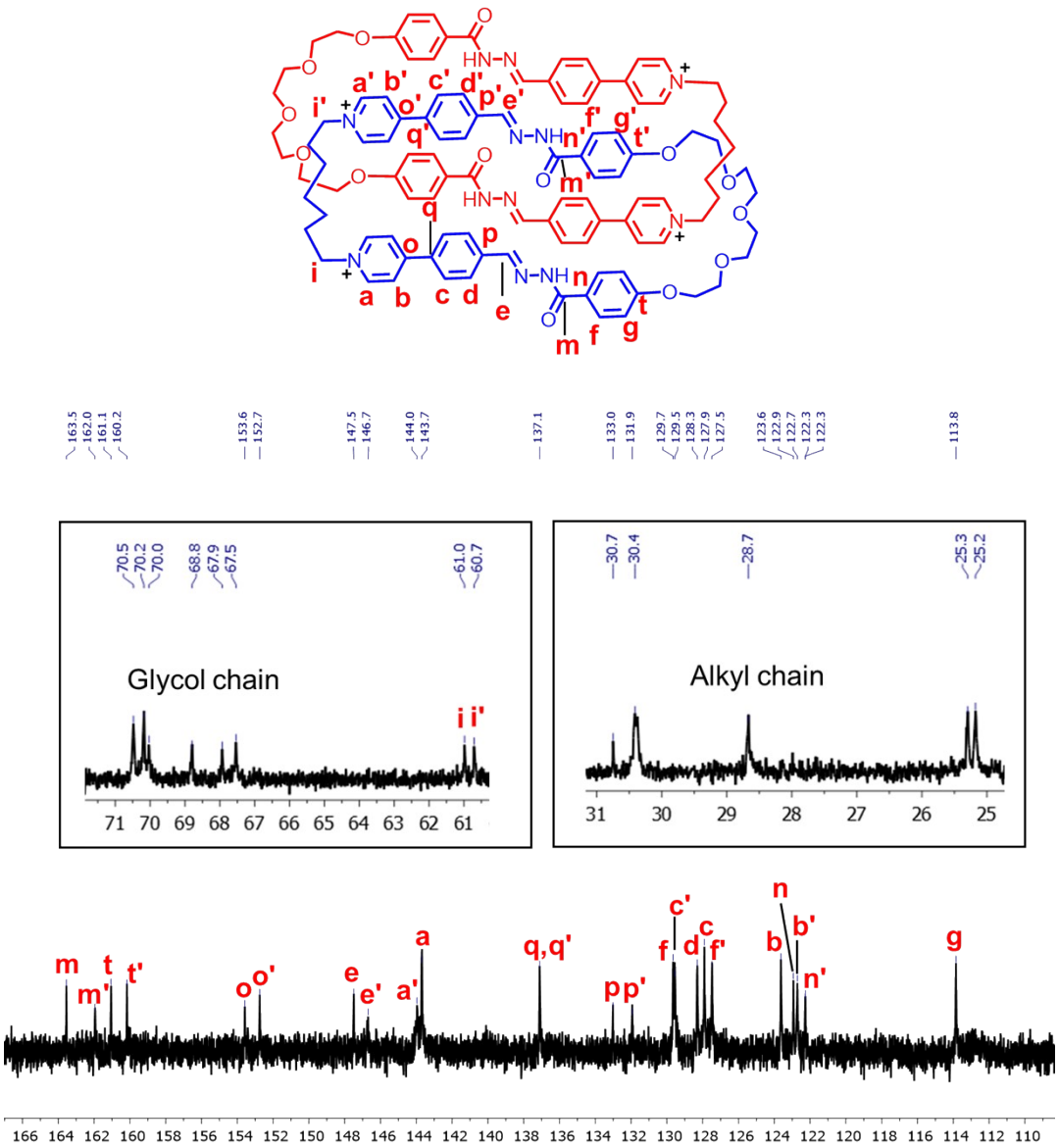

Figure S39. ^{13}C NMR spectrum (150 M Hz, 298 K, D_2O:DMSO = 4:3) of $(\mathbf{1e}^{2+}\cdot\mathbf{2})_2$. Counteranions could be either Cl^- or Br^-.

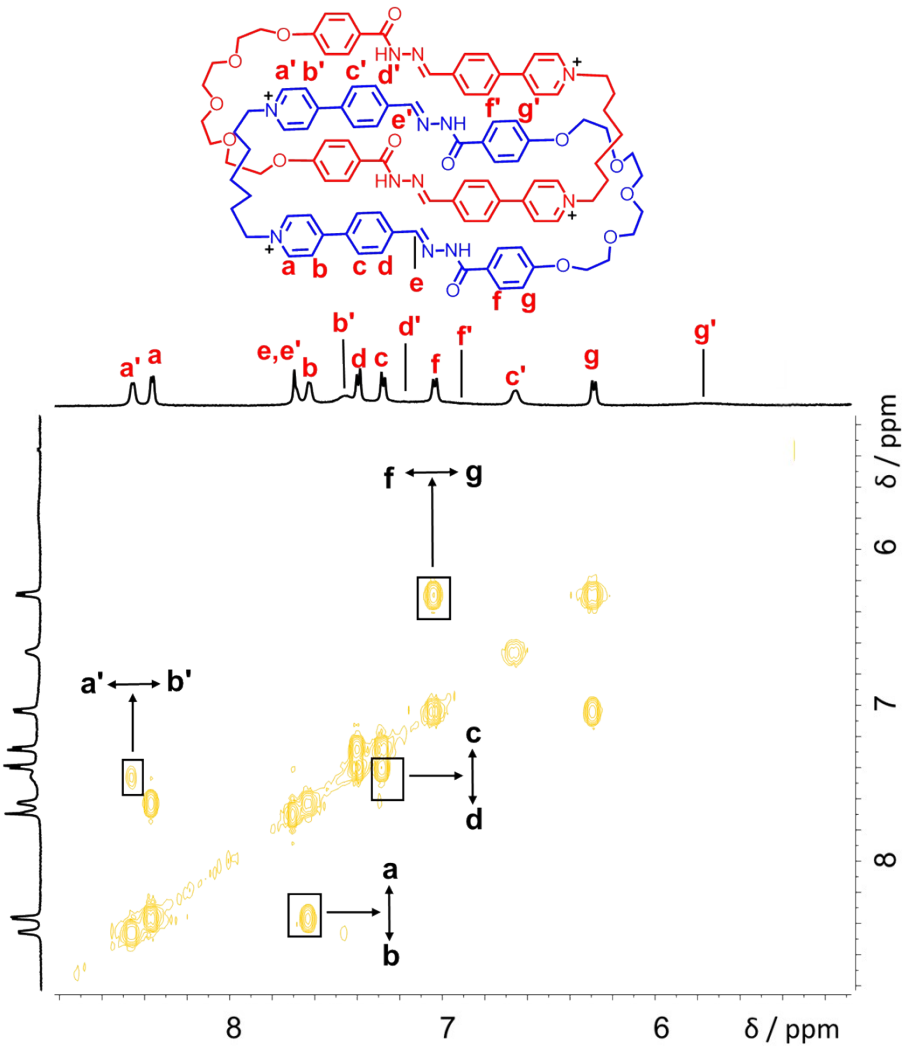

Figure S40. $^{1}H-^{1}H$ COSY spectrum (500 MHz, D_2O, 298 K) of [2]catenane (**1e**$^{2+}$·**2**)$_2$. Counteranions could be either Cl^- or Br^-. Key correlation peaks are labeled in the spectrum.

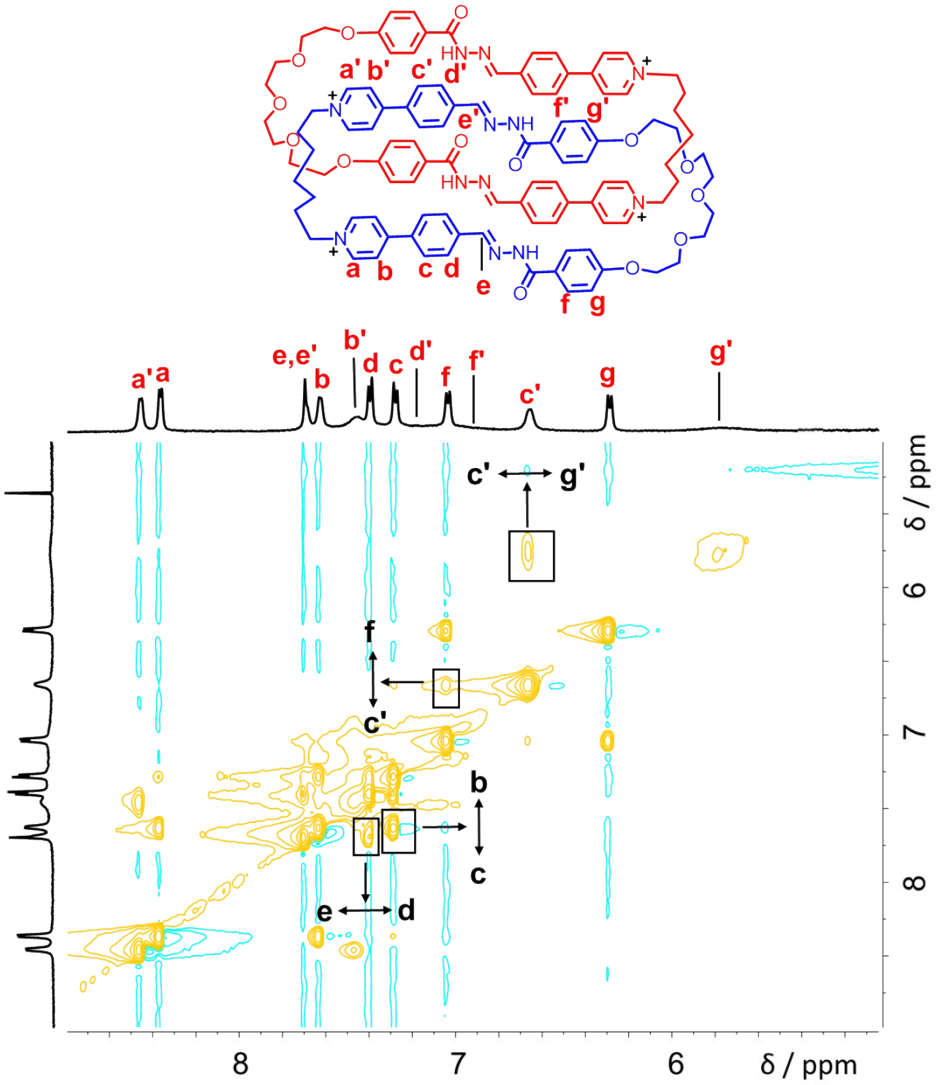

Figure S41. $^{1}H-^{1}H$ NOESY spectrum (500 MHz, D_2O, 298 K) of [2]catenane (**1e**$^{2+}$·**2**)$_2$. Counteranions could be either Cl^- or Br^-. Key correlation peaks are labeled in the spectrum.

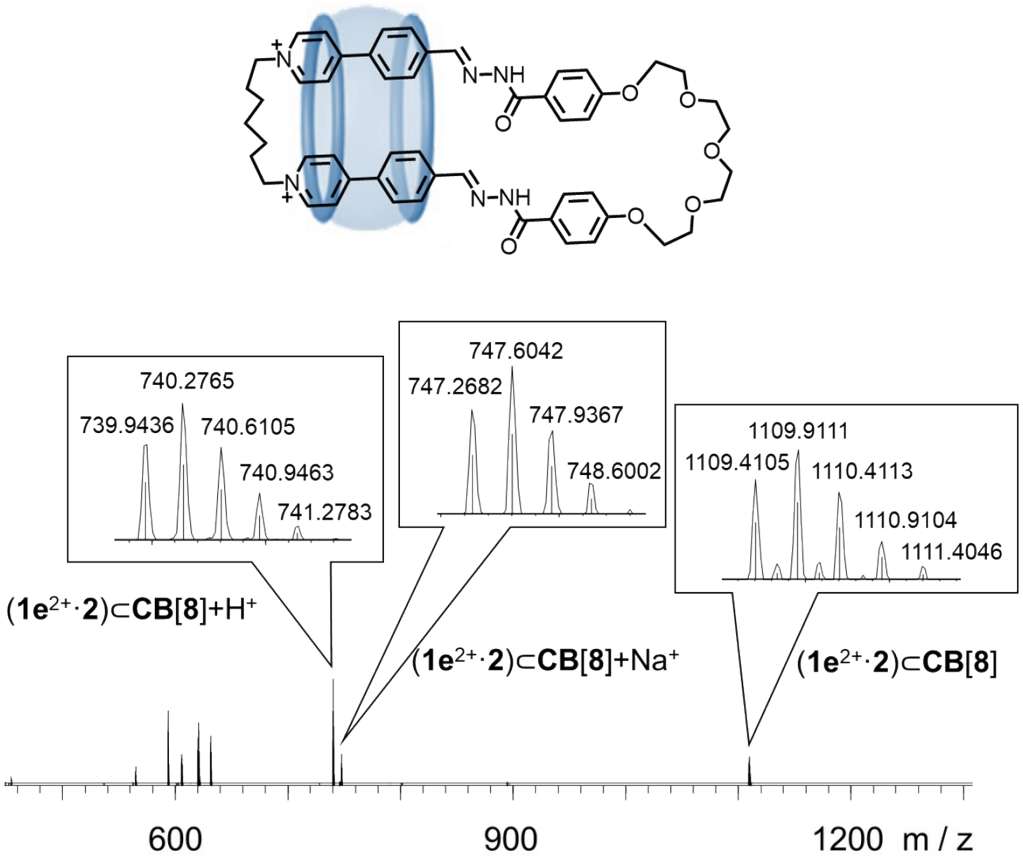

Figure S42. High-resolution LCMS-IT-TOF of (**1e**$^{2+}$·**2**)⊂**CB**[**8**]. Counteranions could be either Cl^- or Br^-.The signals labeled in the spectrum correspond to molecular cations that contain four, three and two positive charges, respectively. *m/z* [(**1e**$^{2+}$·**2**)⊂**CB**[**8**] + Na^+]$^{3+}$ calculated for $C_{101}H_{106}N_{38}NaO_{23}^{3+}$: 747.6069; found: 747.6042. [(**1e**$^{2+}$·**2**)⊂**CB**[**8**] + H^+]$^{3+}$ calculated for $C_{101}H_{107}N_{38}O_{23}^{3+}$: 740.2796; found: 740.2765. [(**1e**$^{2+}$·**2**)⊂**CB**[**8**]]$^{2+}$ calculated for $C_{101}H_{106}N_{38}O_{23}^{2+}$: 1109.9158; found: 1109.9111.

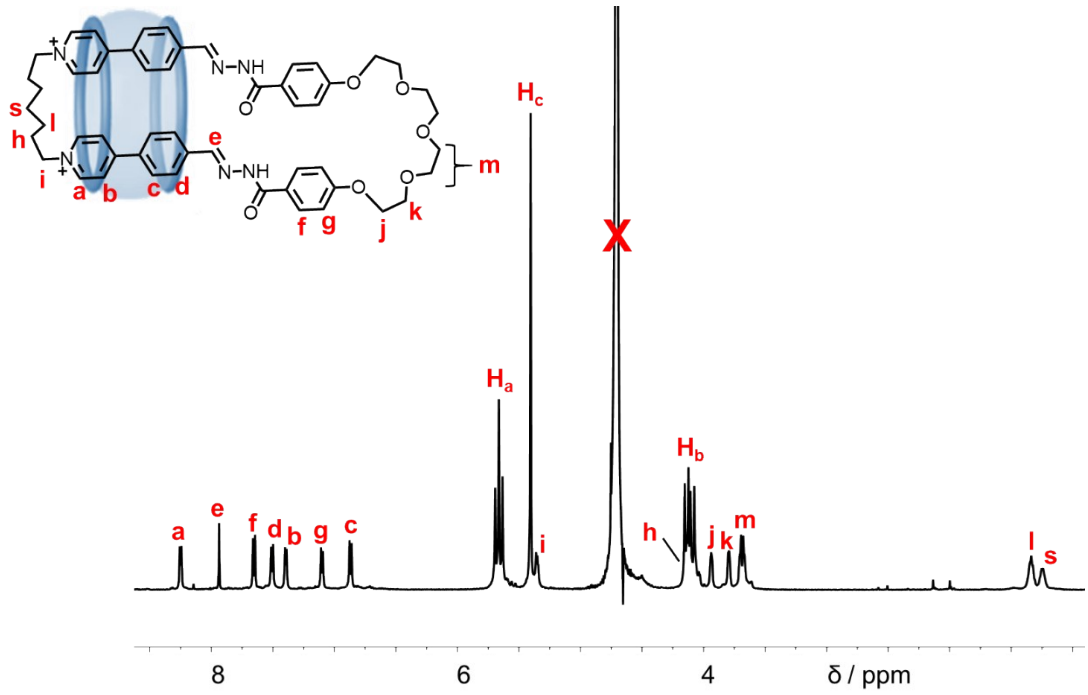

Figure S43. Partial ^{1}H NMR spectrum of (**1e**$^{2+}$·**2**)⊂**CB**[**8**] (500 MHz, D_2O, 298 K). Counteranions could be either Cl^- or Br^-.

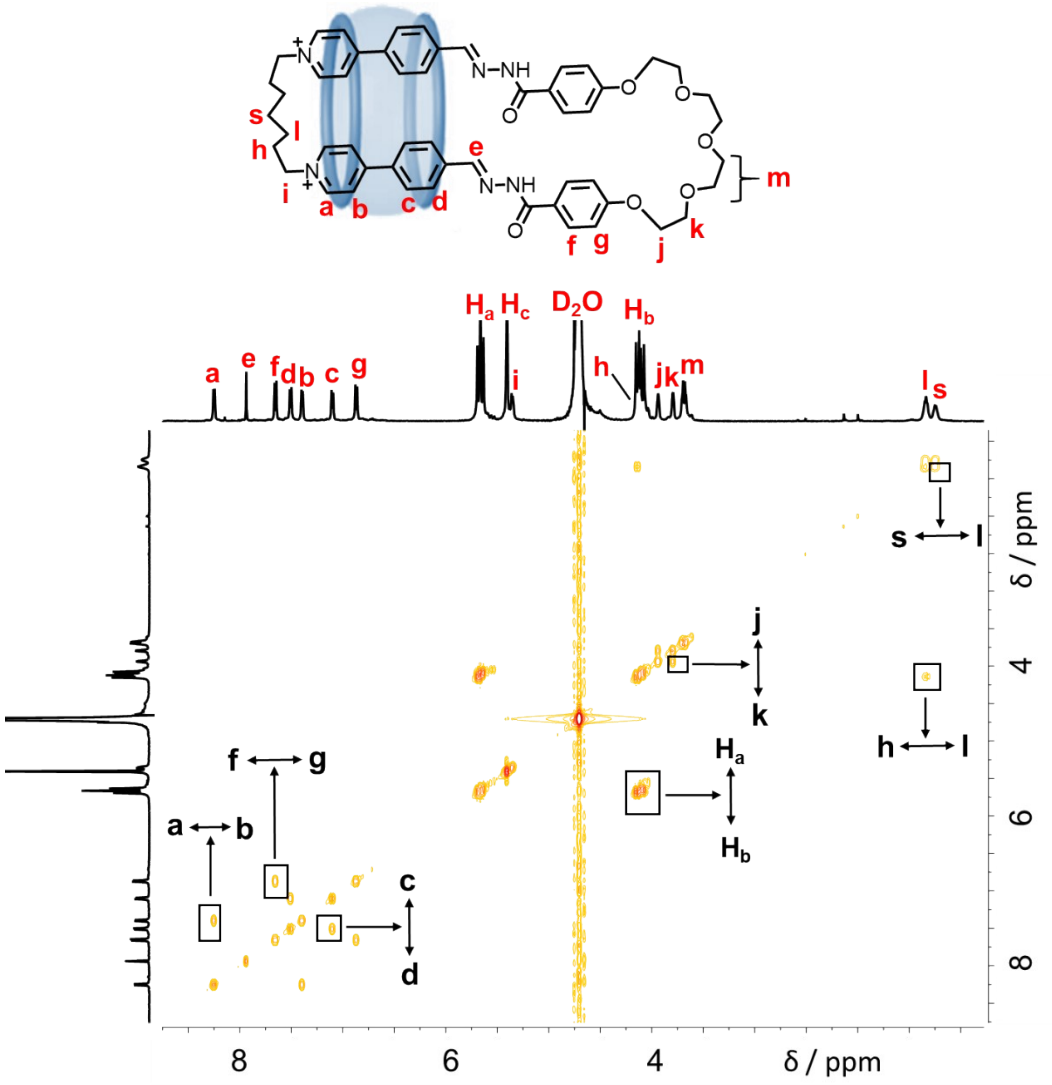

Figure S44. ^1H–^1H COSY spectrum (500 MHz, D_2O, 298 K) of (**1e**$^{2+}$·**2**)⊂**CB**[**8**]. Counteranions could be either Cl^- or Br^-. Key correlation peaks are labeled in the spectrum.

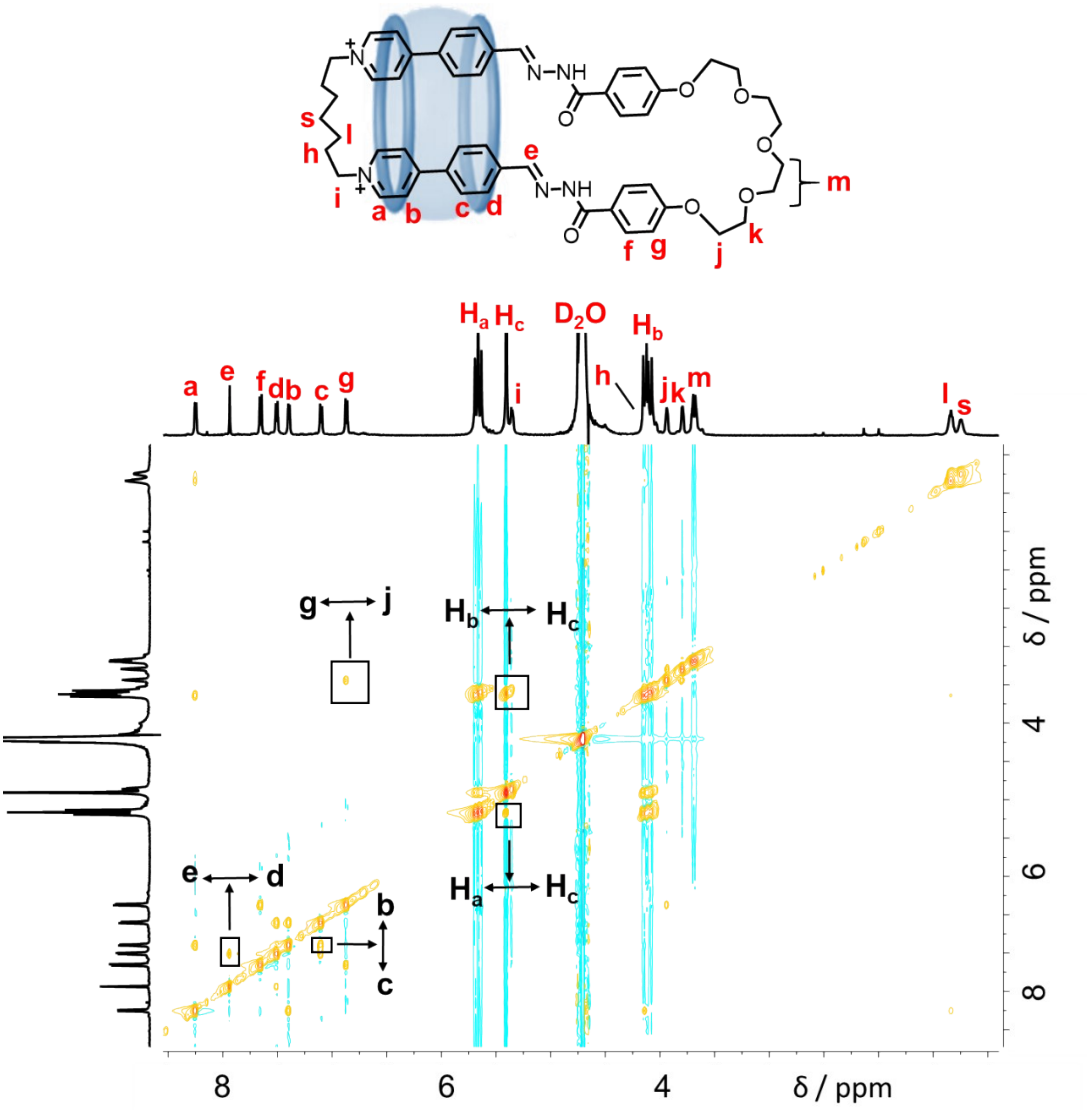

Figure S45. $^1H-^1H$ NOESY spectrum (500 MHz, D_2O, 298 K) of (**1e**$^{2+}$·**2**)⊂**CB**[**8**]. Counteranions could be either Cl^- or Br^-. Key correlation peaks are labeled in the spectrum.

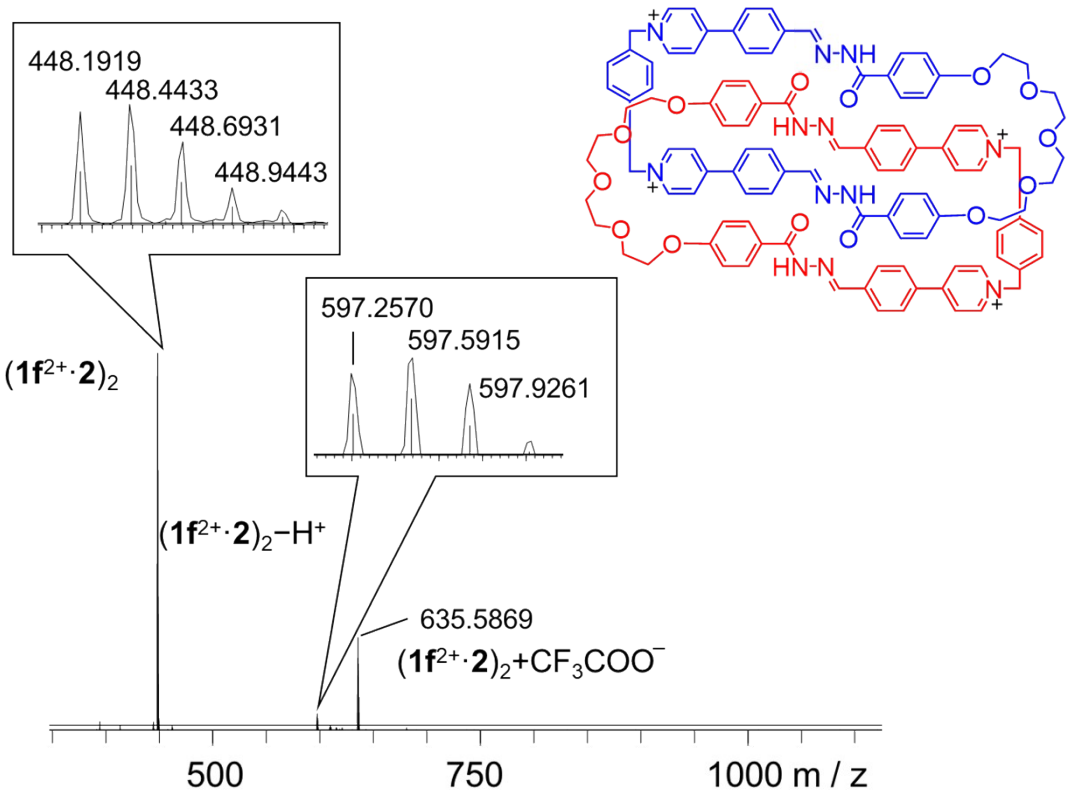

Figure S46. High-resolution LCMS-IT-TOF of $(\mathbf{1f}^{2+}\cdot\mathbf{2})_2\cdot 4Cl^-$. The signals labeled in the spectrum correspond to molecular cations that contain four and three positive charges, respectively. *m/z* $[(\mathbf{1f}^{2+}\cdot\mathbf{2})_2]^{4+}$ calculated for $C_{108}H_{104}N_{12}O_{14}^{4+}$: 448.4452; found: 448.4433. $[(\mathbf{1f}^{2+}\cdot\mathbf{2})_2 - H^+]^{3+}$ calculated for $C_{108}H_{103}N_{12}O_{14}^{3+}$: 597.5911; found: 597.5915.

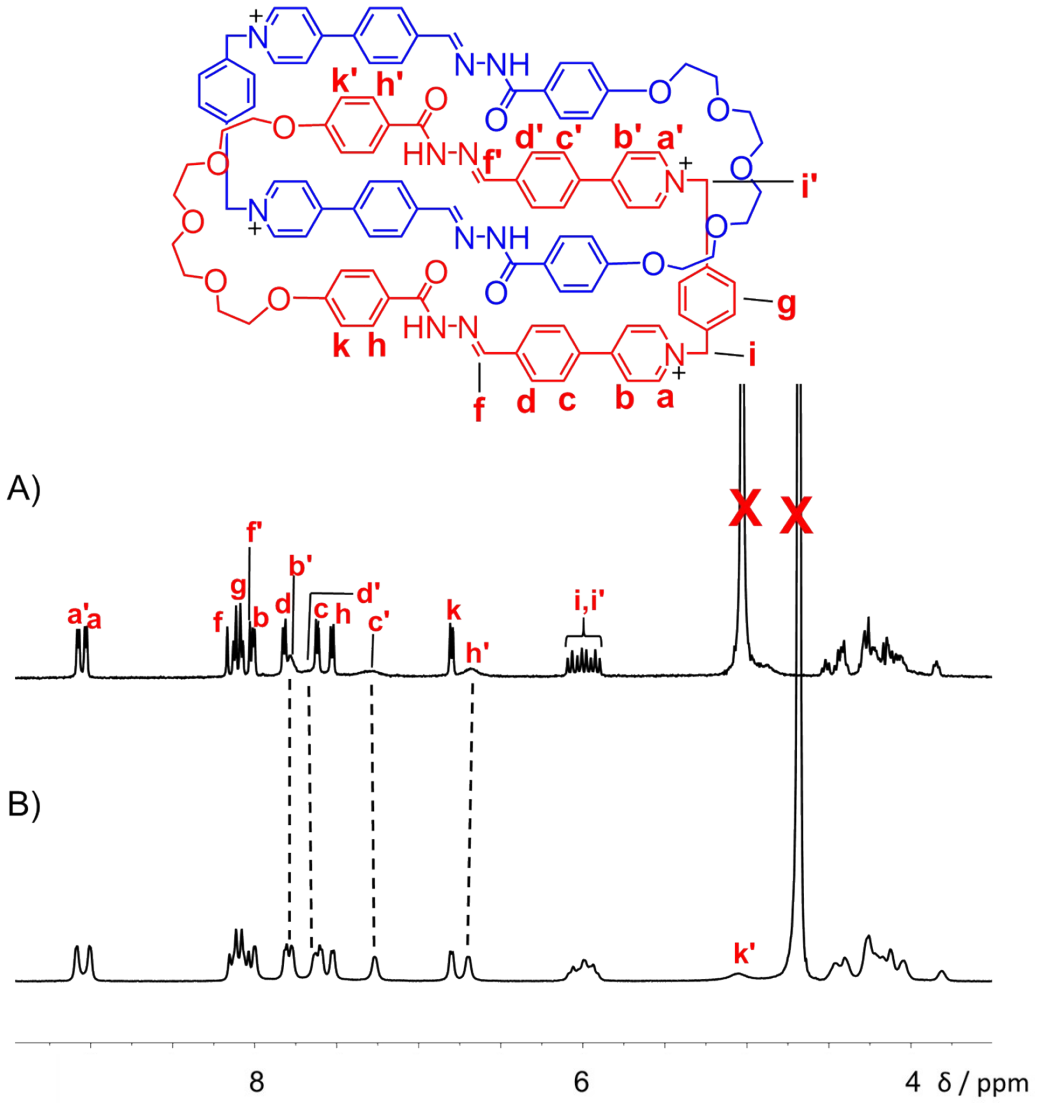

Figure S47. Partial ^{1}H NMR spectra of A) (**1f**$^{2+}$·**2**)$_2$·4Cl$^-$ (600 MHz, D_2O, 298 K), B) (**1f**$^{2+}$·**2**)$_2$·4Cl$^-$ (600 MHz, D_2O, 333 K).

The ^{1}H NMR spectra of (**1f**$^{2+}$·**2**)$_2$·4Cl$^-$ are temperature dependent in D_2O. At room temperature (25 °C), the resonances of the protons b', d', c', h' and k' (see Figure S47) are relatively broad. This observation could be explained by the fact that, within the cavity of one of the two interlocked rings, the circumvolution movement corresponding parts is significantly slowed down. At elevated temperature such as 60 °C, these peaks become sharper, indicating that the circumvolution motion is "speeded up" at higher temperature.

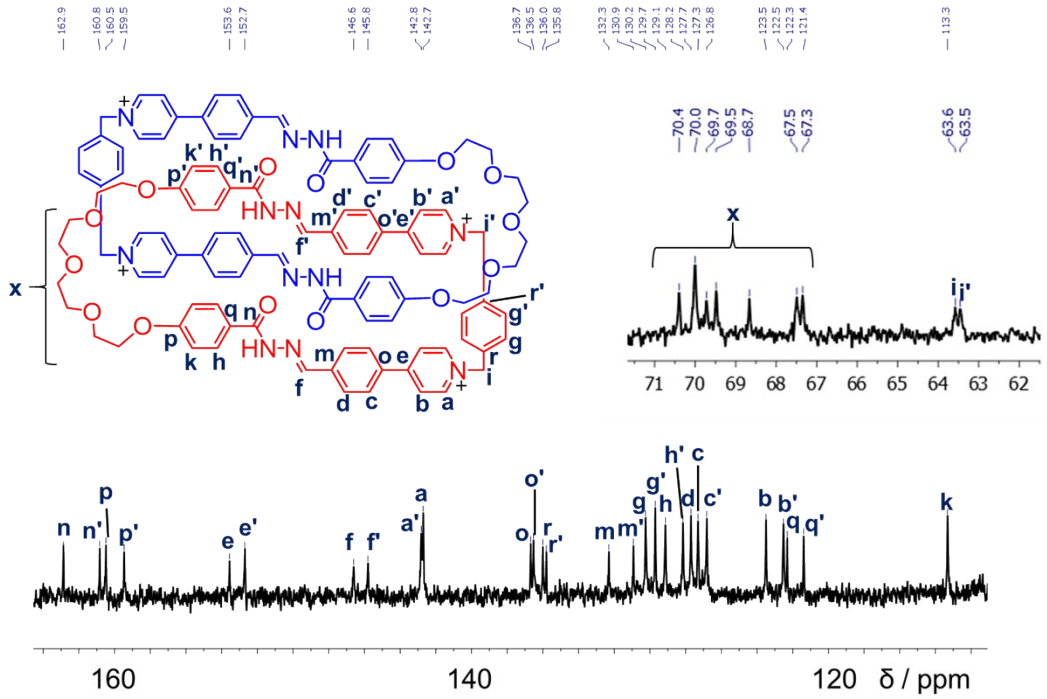

Figure S48. ^{13}C NMR spectrum (125 M Hz, 298 K, D_2O:DMSO = 4:3) of $(\mathbf{1f}^{2+}\cdot\mathbf{2})_2\cdot 4Cl^-$.

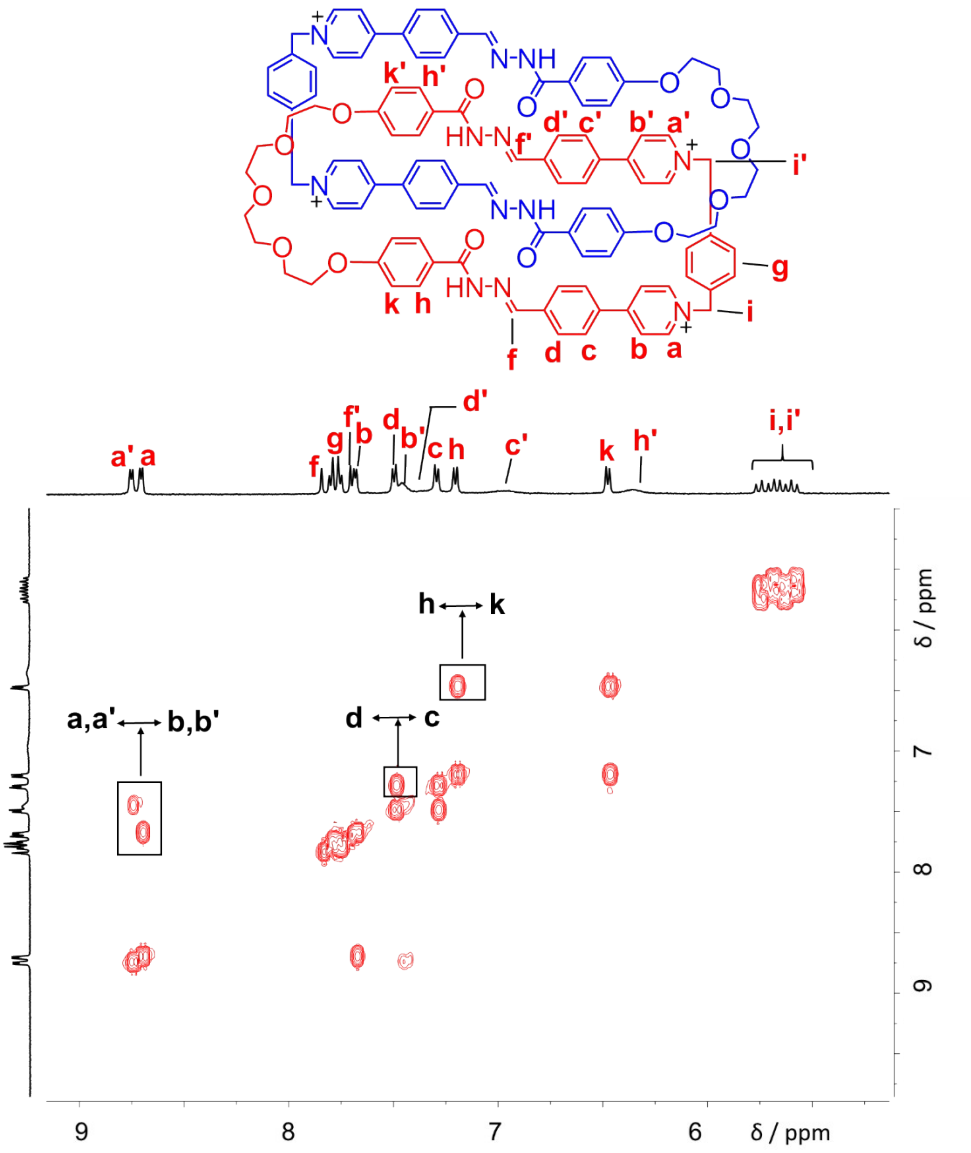

Figure S49. $^{1}H-^{1}H$ COSY spectrum (500 MHz, D_2O, 298 K) of $(\mathbf{1f}^{2+}\cdot\mathbf{2})_2\cdot 4Cl^-$. Key correlation peaks are labeled in the spectrum.

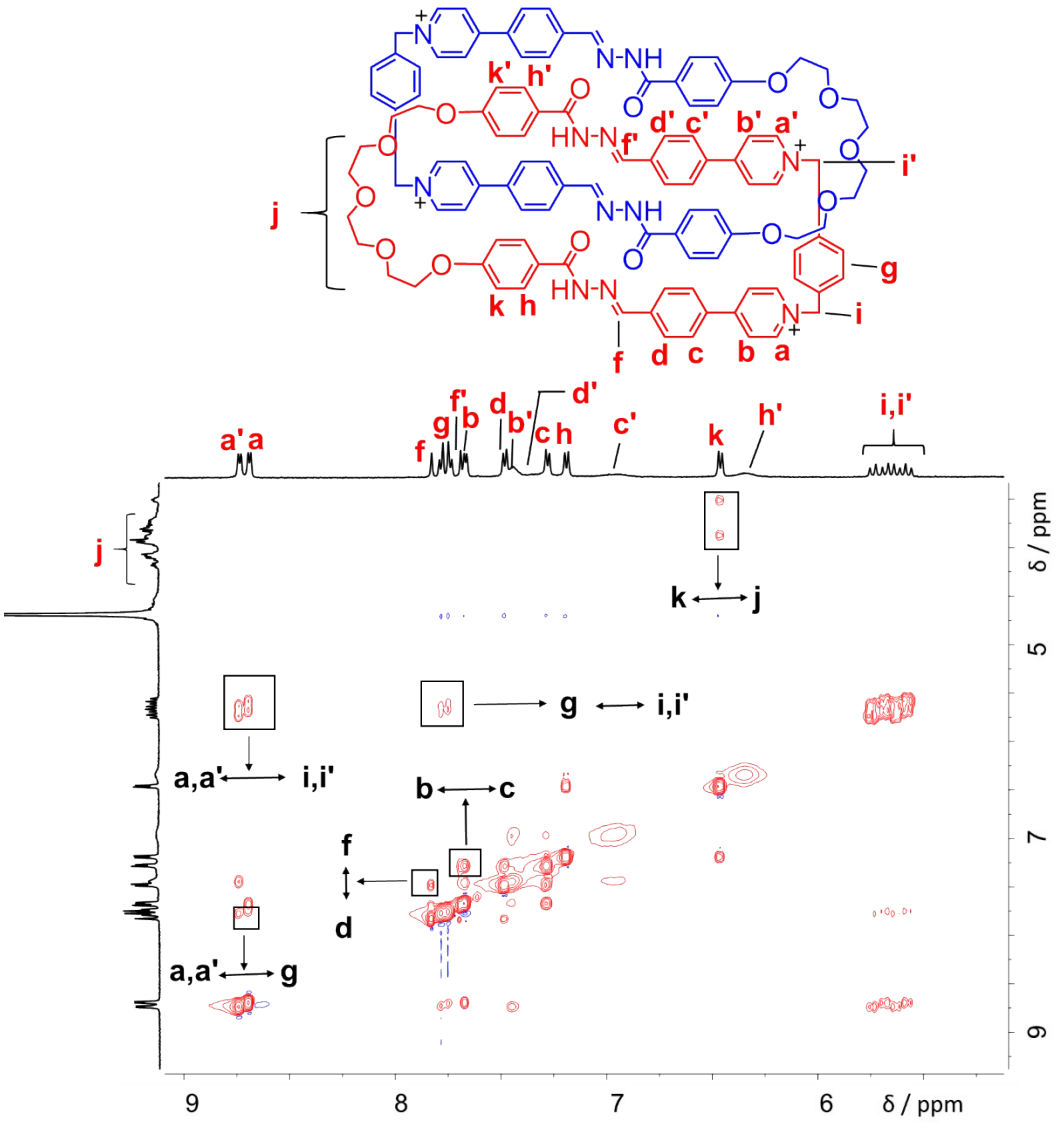

Figure S50. $^{1}H-^{1}H$ NOESY spectrum (500 MHz, D_2O, 298 K) of $(\mathbf{1f}^{2+}\cdot\mathbf{2})_2\cdot 4Cl^-$. Key correlation peaks are labeled in the spectrum.

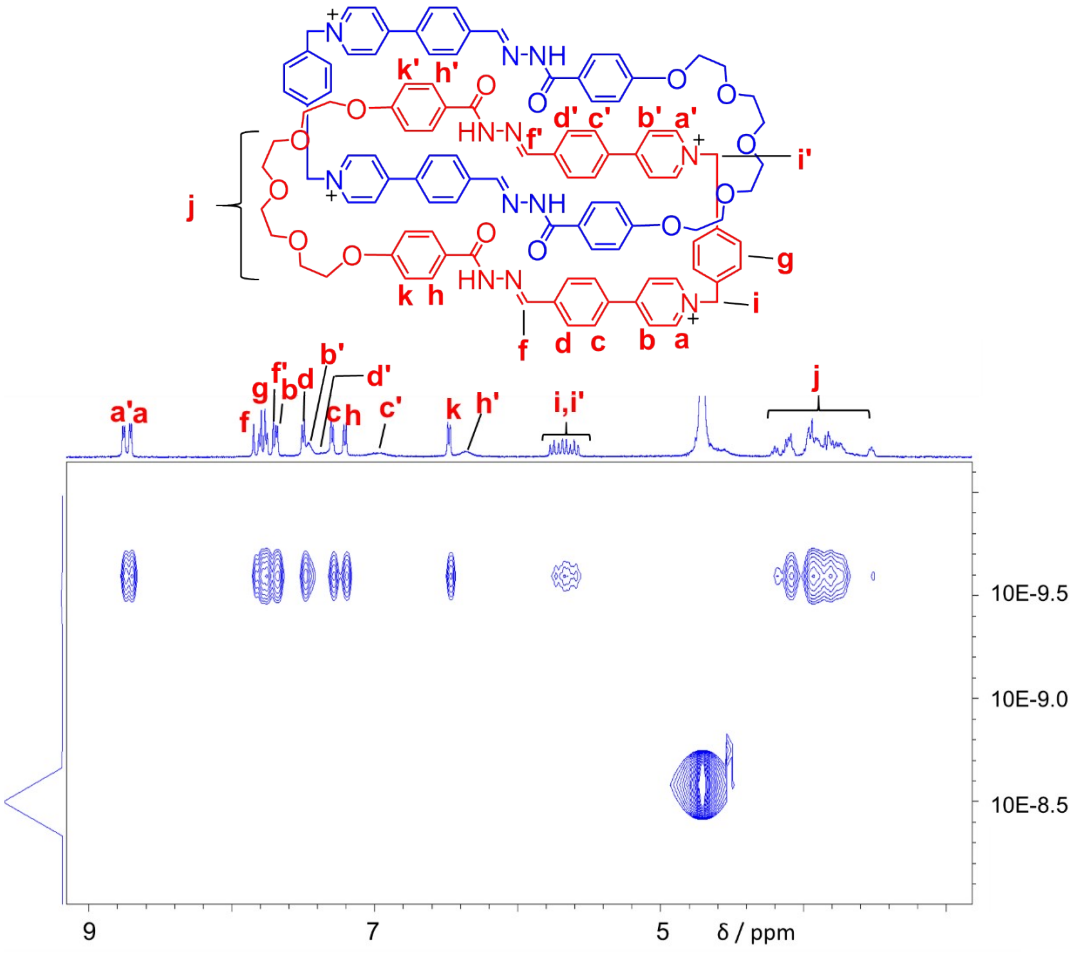

Figure S51. DOSY spectrum (500 MHz, D_2O, 298 K) of $(\mathbf{1f}^{2+}\cdot\mathbf{2})_2\cdot 4Cl^-$.

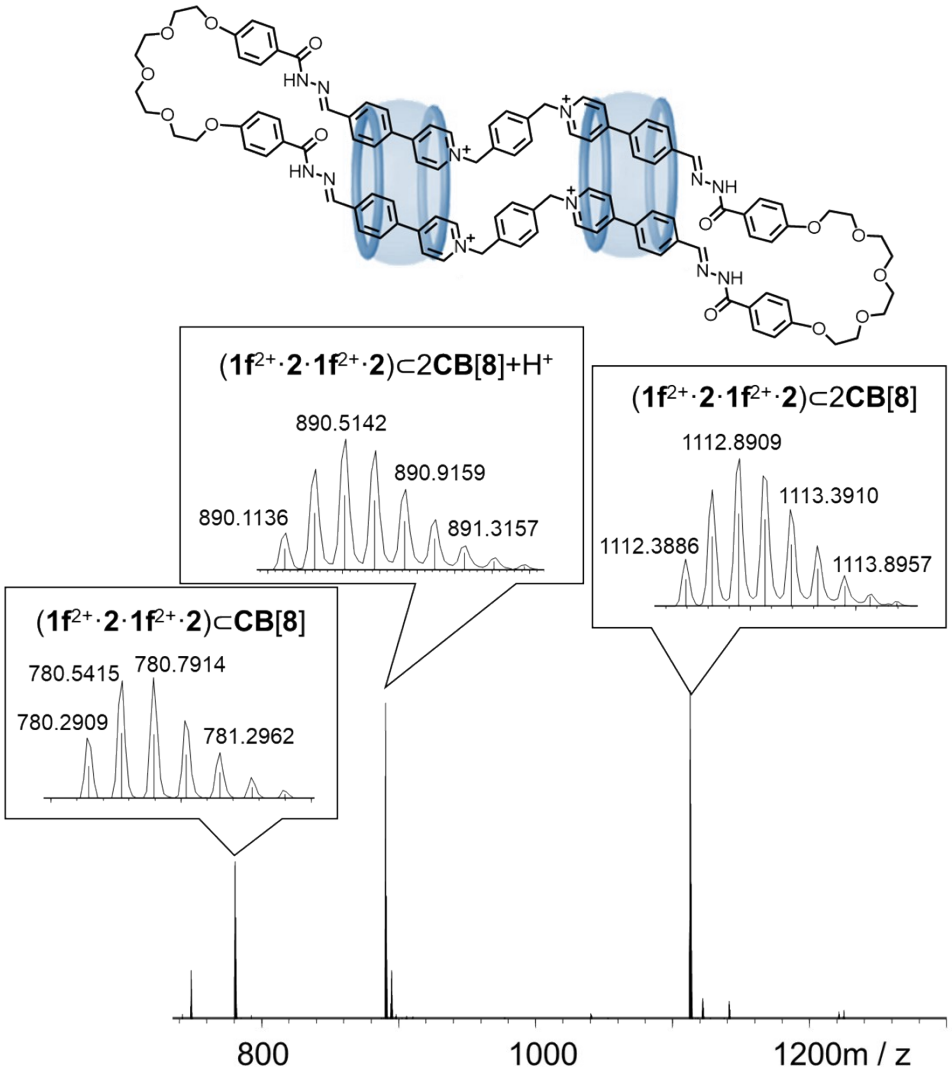

Figure S52. High-resolution LCMS-IT-TOF of (**1f**$^{2+}$·**2**·**1f**$^{2+}$·**2**)⊂2**CB**[**8**]. Charges are balanced by chloride counteranions. The signals labeled in the spectrum correspond to molecular cations that contain five and four positive charges, respectively. *m/z* [(**1f**$^{2+}$·**2**·**1f**$^{2+}$·**2**)⊂**CB**[**8**]]$^{4+}$ calculated for $C_{156}H_{152}N_{44}O_{30}^{4+}$: 780.5433; found: 780.5415. [(**1f**$^{2+}$·**2**·**1f**$^{2+}$·**2**)⊂2**CB**[**8**]]$^{4+}$ calculated for $C_{204}H_{200}N_{76}O_{46}^{4+}$: 1112.8923; found: 1112.8909. [(**1f**$^{2+}$·**2**·**1f**$^{2+}$·**2**)⊂2**CB**[**8**]+H^{+}]$^{5+}$ calculated for $C_{204}H_{201}N_{76}O_{46}^{5+}$: 890.5153; found: 890.5142.

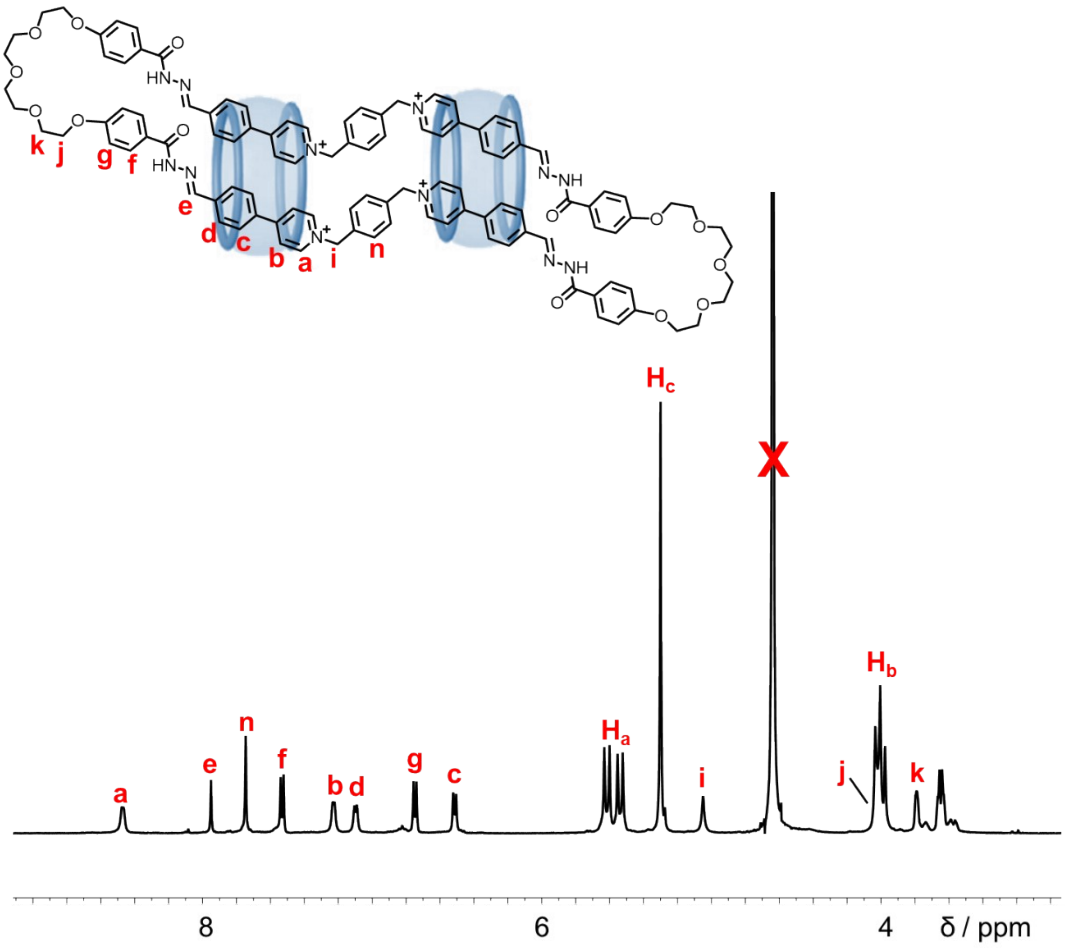

Figure S53. Partial ^{1}H NMR spectra of (**1f**$^{2+}$·**2**·**1f**$^{2+}$·**2**)⊂2**CB**[**8**] (500 MHz, D_2O, 298 K). Charges are balanced by chloride counteranions.

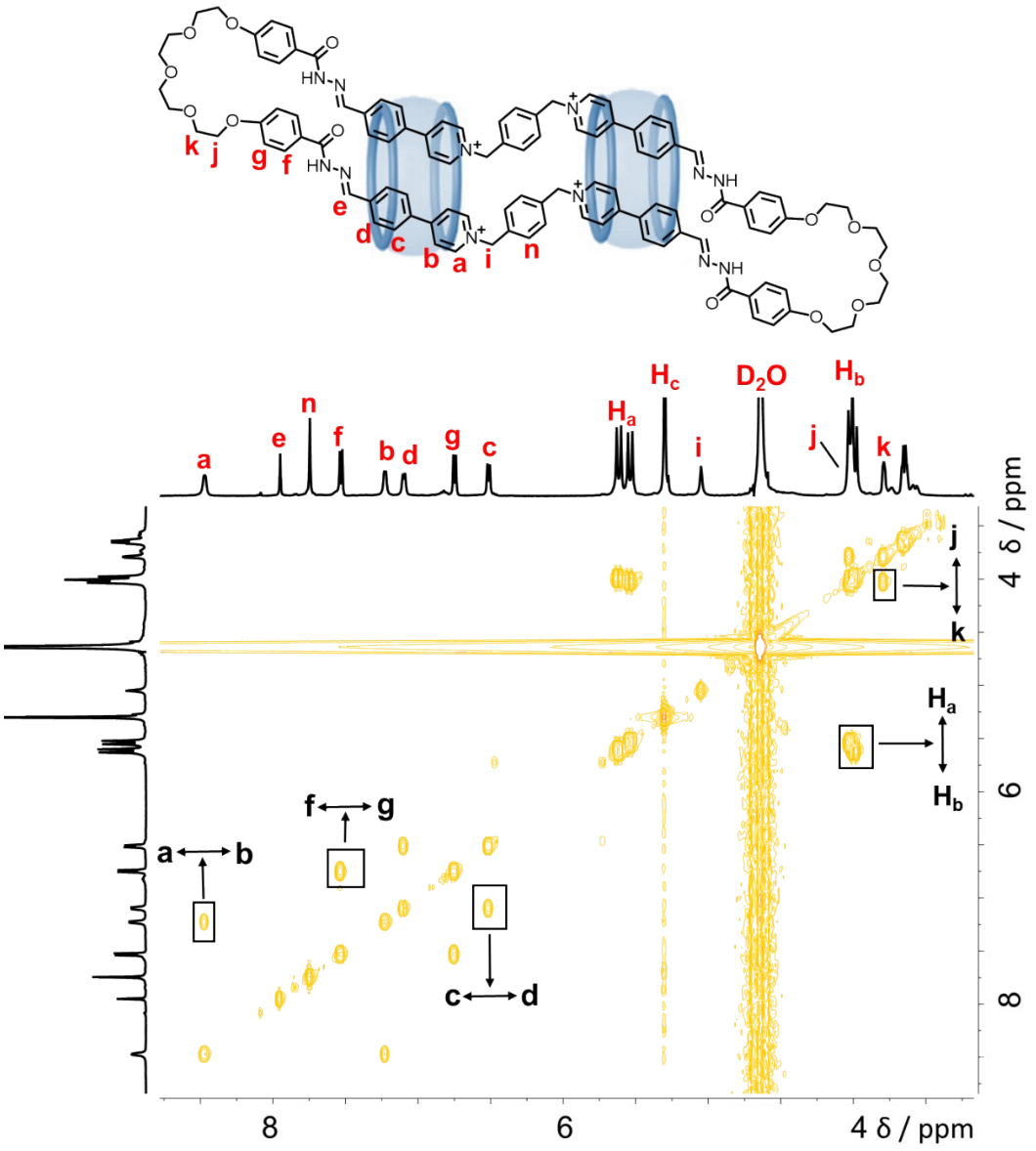

Figure S54. $^{1}H-^{1}H$ COSY spectrum (500 MHz, D_2O, 298 K) of (**1f**$^{2+}$·**2**·**1f**$^{2+}$·**2**)⊂2**CB**[**8**]. Charges are balanced by chloride counteranions. Key correlation peaks are labeled in the spectrum.

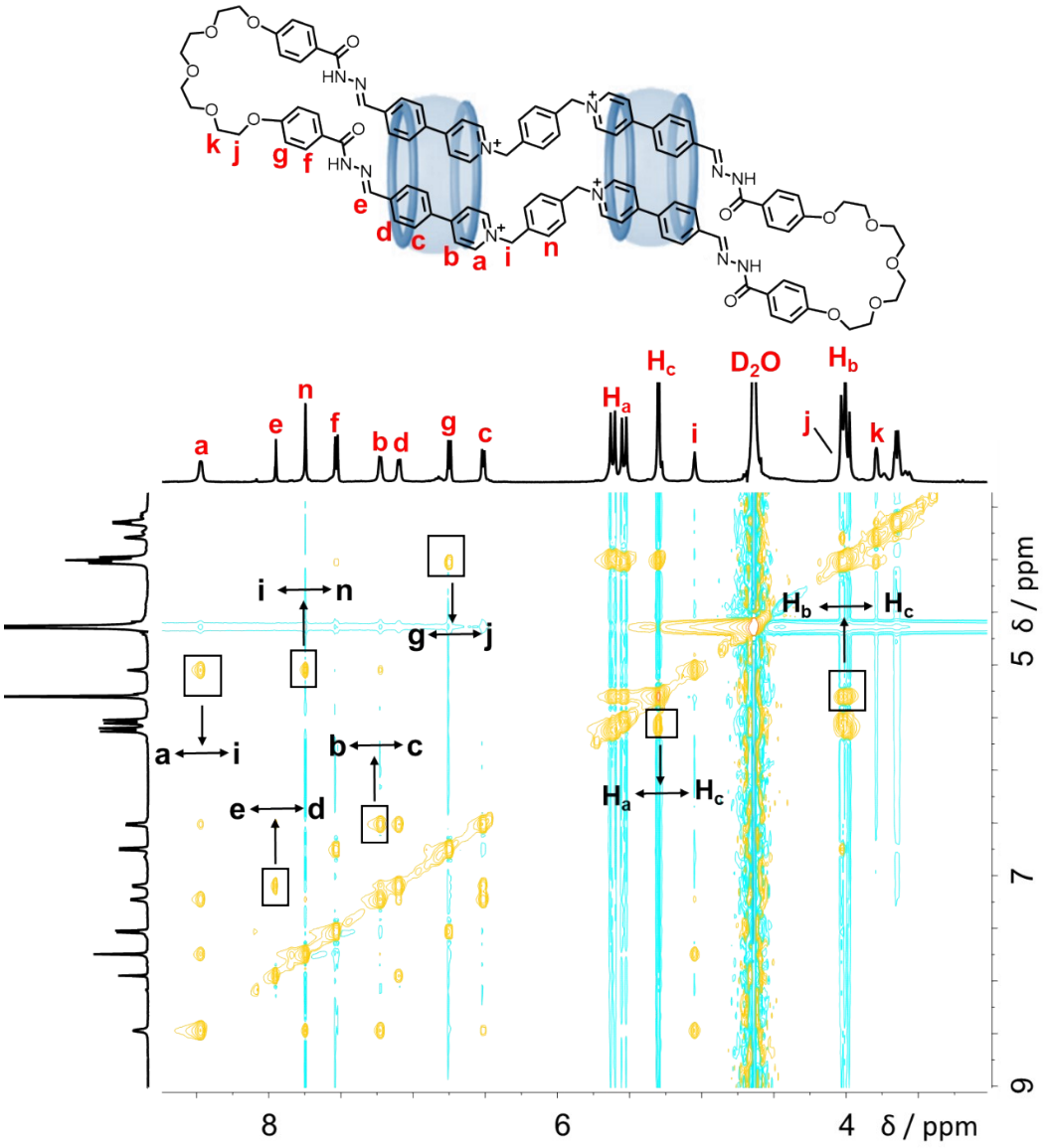

Figure S55. ^{1}H−^{1}H NOESY spectrum (500 MHz, D_2O, 298 K) of (**1f**$^{2+}$·**2**·**1f**$^{2+}$·**2**)⊂2**CB**[**8**]. Charges are balanced by chloride counteranions. Key correlation peaks are labeled in the spectrum.

4. Interconversion between $(\mathbf{1f}^{2+}\cdot\mathbf{2})_2$ and $(\mathbf{1f}^{2+}\cdot\mathbf{2}\cdot\mathbf{1f}^{2+}\cdot\mathbf{2})\subset 2\mathbf{CB[8]}$

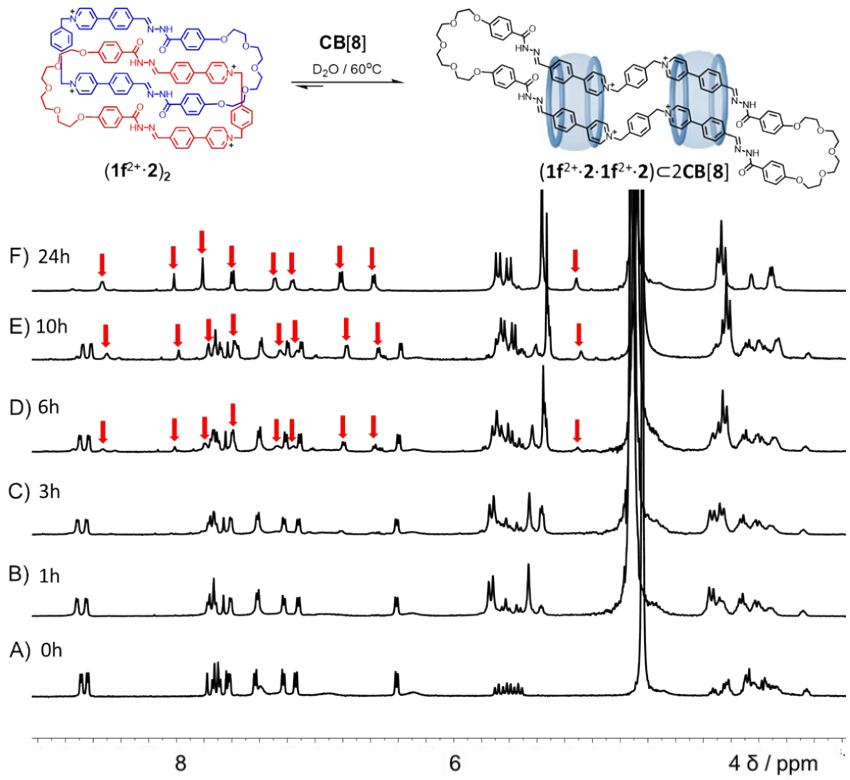

Figure S56. The ^{1}H NMR spectra (500 MHz, D_2O, 298 K) of the [2]catenane $(\mathbf{1f}^{2+}\cdot\mathbf{2})_2$, after adding two equiv. of CB[8] for certain amount of time. The resonances corresponding to the [3] pseudorotaxane $(\mathbf{1f}^{2+}\cdot\mathbf{2}\cdot\mathbf{1f}^{2+}\cdot\mathbf{2})\subset 2\mathbf{CB[8]}$ gradually appeared, which are marked with red arrows.

We added two equivalents of **CB[8]** to a D_2O solution of [2]catenane $(\mathbf{1f}^{2+}\cdot\mathbf{2})_2$ at 60 °C. The reaction progress was monitored by recording its ^{1}H NMR spectra in D_2O (Figure S56) during the reaction course. ^{1}H NMR spectra indicated that, after heating and sonicating the reaction mixture for about 6 h, a new set of sharp resonances was observed in the ^{1}H NMR spectrum (Figure S56 D), indicating the formation of a new thermodynamically stable product, namely $(\mathbf{1f}^{2+}\cdot\mathbf{2}\cdot\mathbf{1f}^{2+}\cdot\mathbf{2})\subset 2\mathbf{CB[8]}$. After approximate 24 h, the resonances corresponding to the [2]catenane $(\mathbf{1f}^{2+}\cdot\mathbf{2})_2$ almost completely disappeared, accompanied with the appearance of a set of resonances corresponding to $(\mathbf{1f}^{2+}\cdot\mathbf{2}\cdot\mathbf{1f}^{2+}\cdot\mathbf{2})\subset 2\mathbf{CB[8]}$. It is noteworthy that during the reaction course, no other reaction intermediates were observed, such as the [2]pseudorotaxane $(\mathbf{1f}^{2+}\cdot\mathbf{2}\cdot\mathbf{1f}^{2+}\cdot\mathbf{2})\subset\mathbf{CB[8]}$.

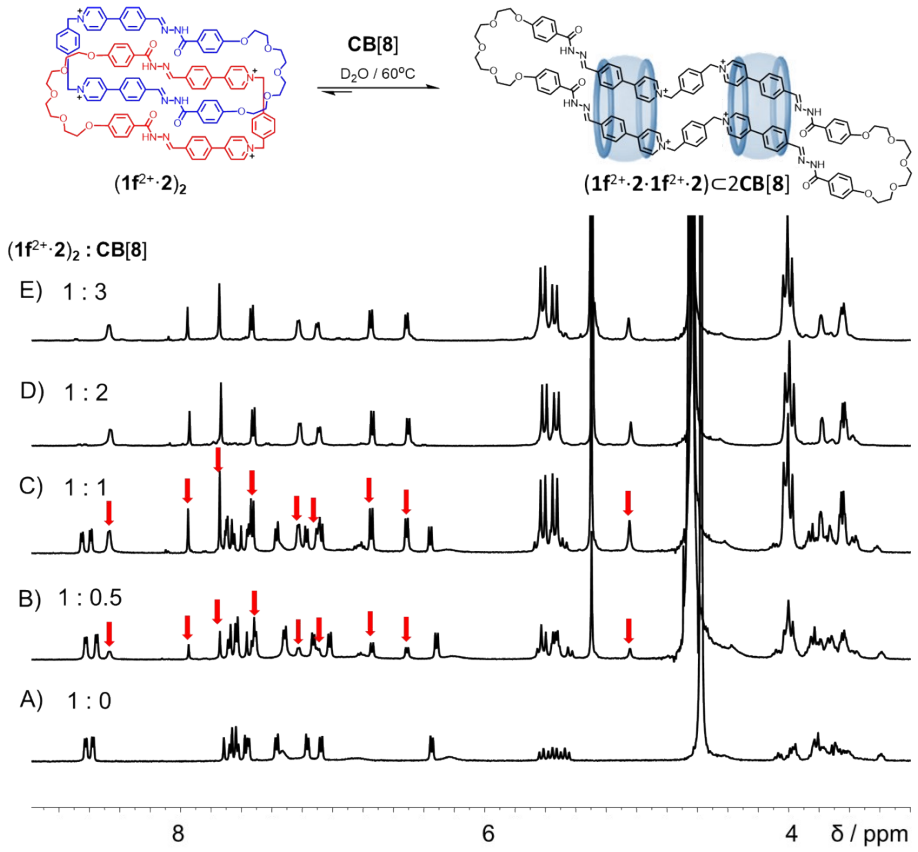

Figure S57. The ^{1}H NMR spectrum (500 MHz, D_2O, 298 K) of the [2]catenane $(\mathbf{1f}^{2+}\cdot\mathbf{2})_2$ after adding different amount of **CB**[**8**]. All spectra were recorded after the systems reached their equilibria. The ratio of $(\mathbf{1f}^{2+}\cdot\mathbf{2})_2$ and **CB**[**8**] is A) 1:0, B) 1:0.5, C) 1:1, D) 1:2 and E) 1:3. The resonances corresponding to $(\mathbf{1f}^{2+}\cdot\mathbf{2}\cdot\mathbf{1f}^{2+}\cdot\mathbf{2})\subset 2\mathbf{CB}[\mathbf{8}]$ are marked with red arrows.

We added different equivalents of **CB**[**8**] into [2]catenane $(\mathbf{1f}^{2+}\cdot\mathbf{2})_2$ at 60 °C for 24 h in D_2O. ^{1}H NMR spectra indicate that, when the **CB**[**8**]/catenane ratio is less than 2:1, both $(\mathbf{1f}^{2+}\cdot\mathbf{2})_2$ and $(\mathbf{1f}^{2+}\cdot\mathbf{2}\cdot\mathbf{1f}^{2+}\cdot\mathbf{2})\subset 2\mathbf{CB}[\mathbf{8}]$ were observed (Figure S57 B and C). No other products such as the [2]pseudorotaxane $(\mathbf{1f}^{2+}\cdot\mathbf{2}\cdot\mathbf{1f}^{2+}\cdot\mathbf{2})\subset\mathbf{CB}[\mathbf{8}]$ was observed, indicating that the formation of the [3]pseudorotaxane $(\mathbf{1f}^{2+}\cdot\mathbf{2}\cdot\mathbf{1f}^{2+}\cdot\mathbf{2})\subset 2\mathbf{CB}[\mathbf{8}]$ is positively cooperative. After the **CB**[**8**]/catenane ratio reached 2:1, further addition of **CB**[**8**] did not lead to any changes in the ^{1}H NMR spectrum (Figure S57 E).

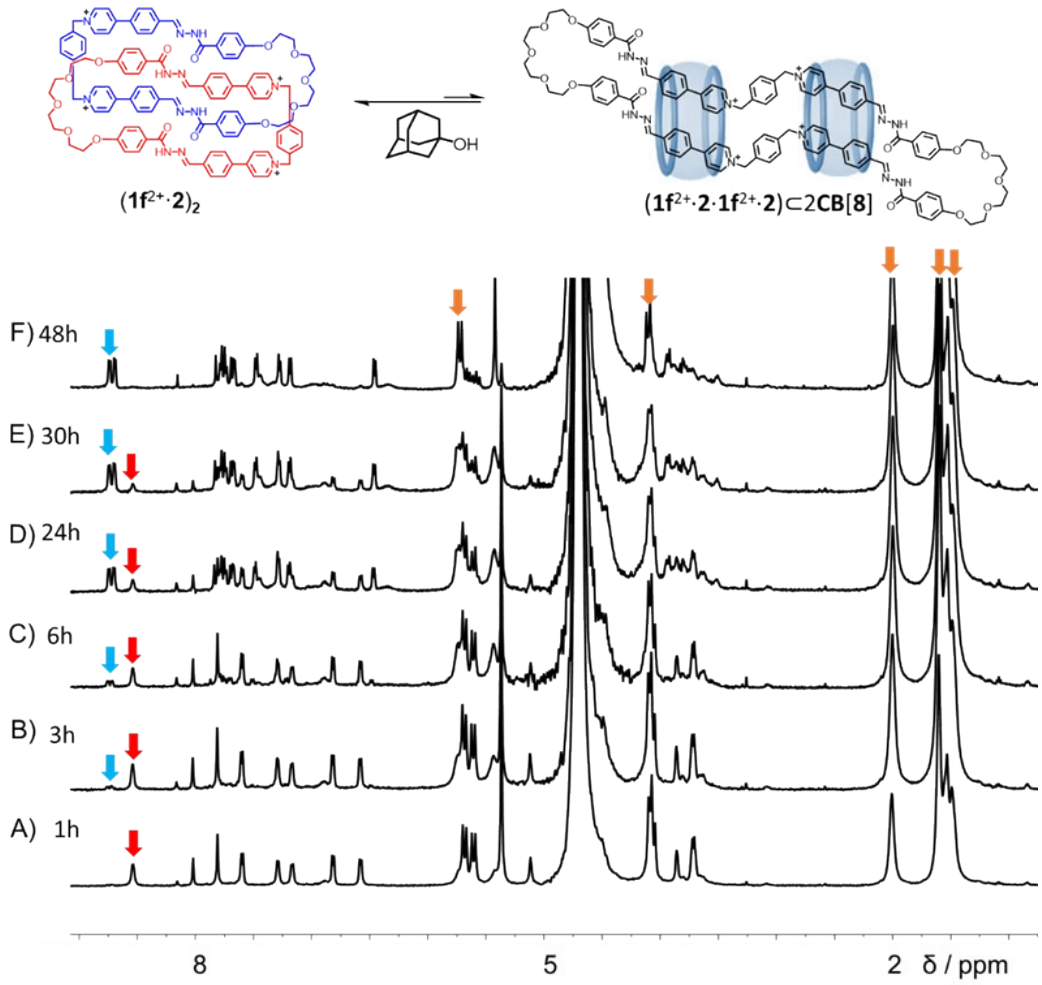

Figure S58. ^{1}H NMR spectra (500 MHz, D_2O, 298 K) of (**1f**$^{2+}$·**2**·**1f**$^{2+}$·**2**)⊂2**CB**[**8**] after removing the **CB[8]** ring by adding excess amount of adamantan-1-ol for certain amount of time. The resonances of (**1f**$^{2+}$·**2**)$_2$, (**1f**$^{2+}$·**2**·**1f**$^{2+}$·**2**)⊂2**CB**[**8**] and adamantan-1-ol⊂**CB**[**8**] are marked with blue arrows, red arrows and orange arrows, respectively., indicating that after removing the **CB[8]** ring, the [2]catenane was gradually recovered within 48 h.

5. The process of generating (**1f**$^{2+}$·**2**·**1f**$^{2+}$·**2**)⊂2**CB[8]** by means of one-pot procedure

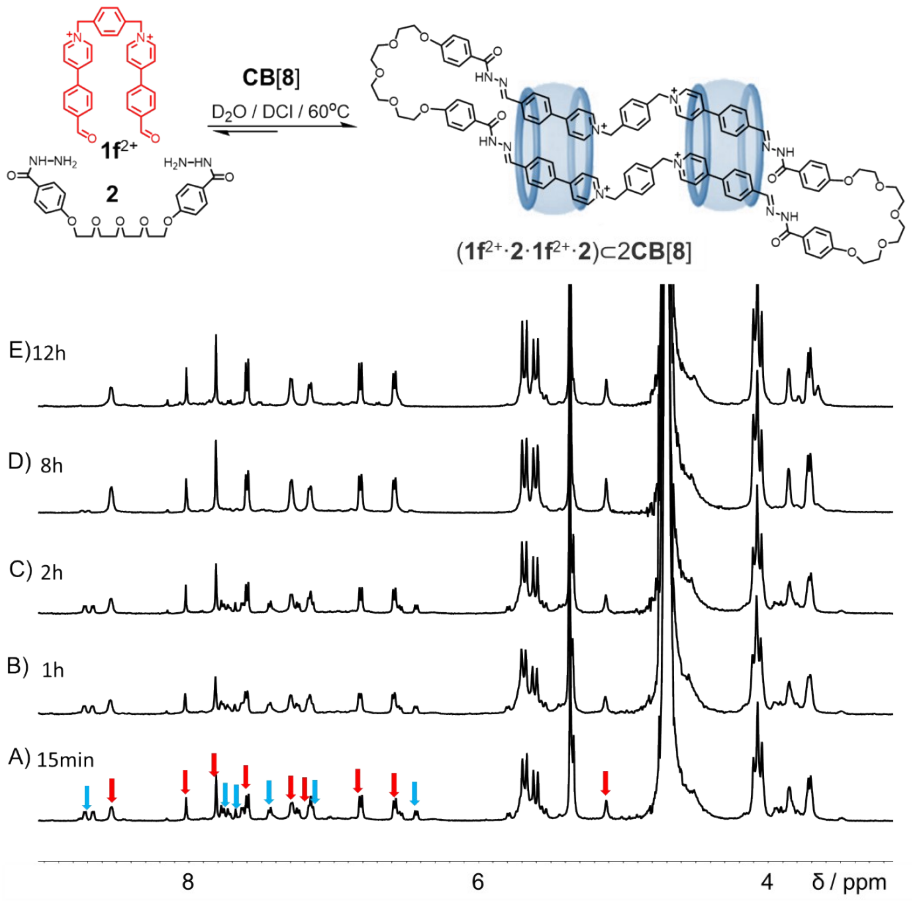

Figure S59. The ^{1}H NMR spectra (500 MHz, D_2O, 298 K) of a 1:1:1 mixture of **1f**$^{2+}$·2Cl^{-}, **2** and **CB[8]**, after mixing the reactants for certain amount of time. The resonances of (**1f**$^{2+}$·**2**)$_2$ and (**1f**$^{2+}$·**2**·**1f**$^{2+}$·**2**)⊂2**CB[8]** are marked with blue arrows and red arrows, respectively.

6. Yields of the condensation of **2** and a series of biscationic dialdehydes

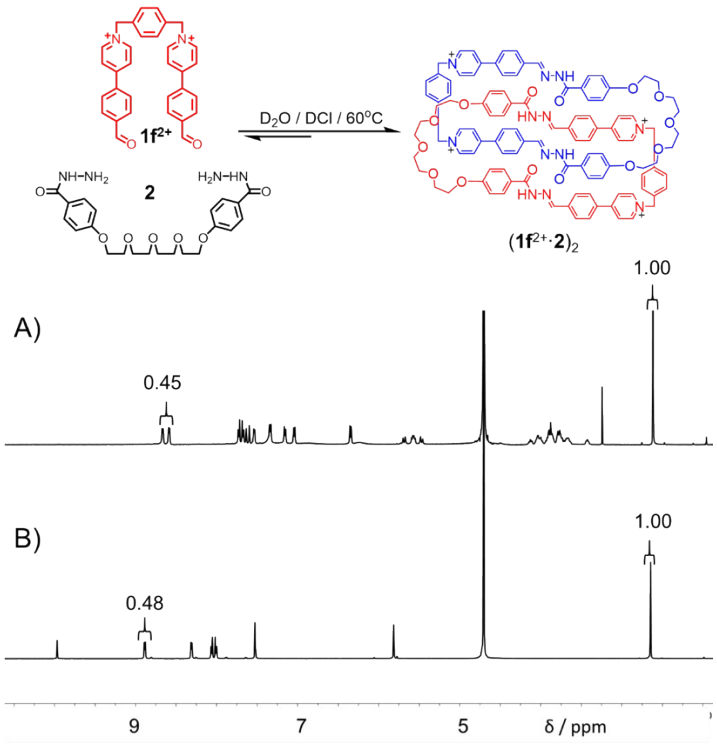

Figure S60. ^{1}H NMR spectra (500 MHz, D_2O, 298 K) of A) $(\mathbf{1f}^{2+}\cdot\mathbf{2})_2$ and B) $\mathbf{1f}^{2+}\cdot 2Cl^-$.

We used ^{1}H NMR spectra to calculate the self-assembly yields by using DMSO with a fixed concentration as the internal standard. The integrated intensity of the resonance of internal standard was normalized to 1, allowing the concentration ratios of the self-assembled products relative to their corresponding aldehyde precursors to be calculated. For example, in the ^{1}H NMR spectra (Figure S60) of $\mathbf{1f}^{2+}\cdot 2Cl^-$ and $(\mathbf{1f}^{2+}\cdot\mathbf{2})_2\cdot 4Cl^-$, whose spectra were recorded before and after adding **2**, the resonances of the hydrogens in pyridine *α* position were integrated as 0.48 and 0.45, respectively, relative to the standard; the yield of $(\mathbf{1f}^{2+}\cdot\mathbf{2})_2\cdot 4Cl^-$ was thus calculated to be 94% (0.45/0.48). The yields mentioned below were all calculated according to this method.

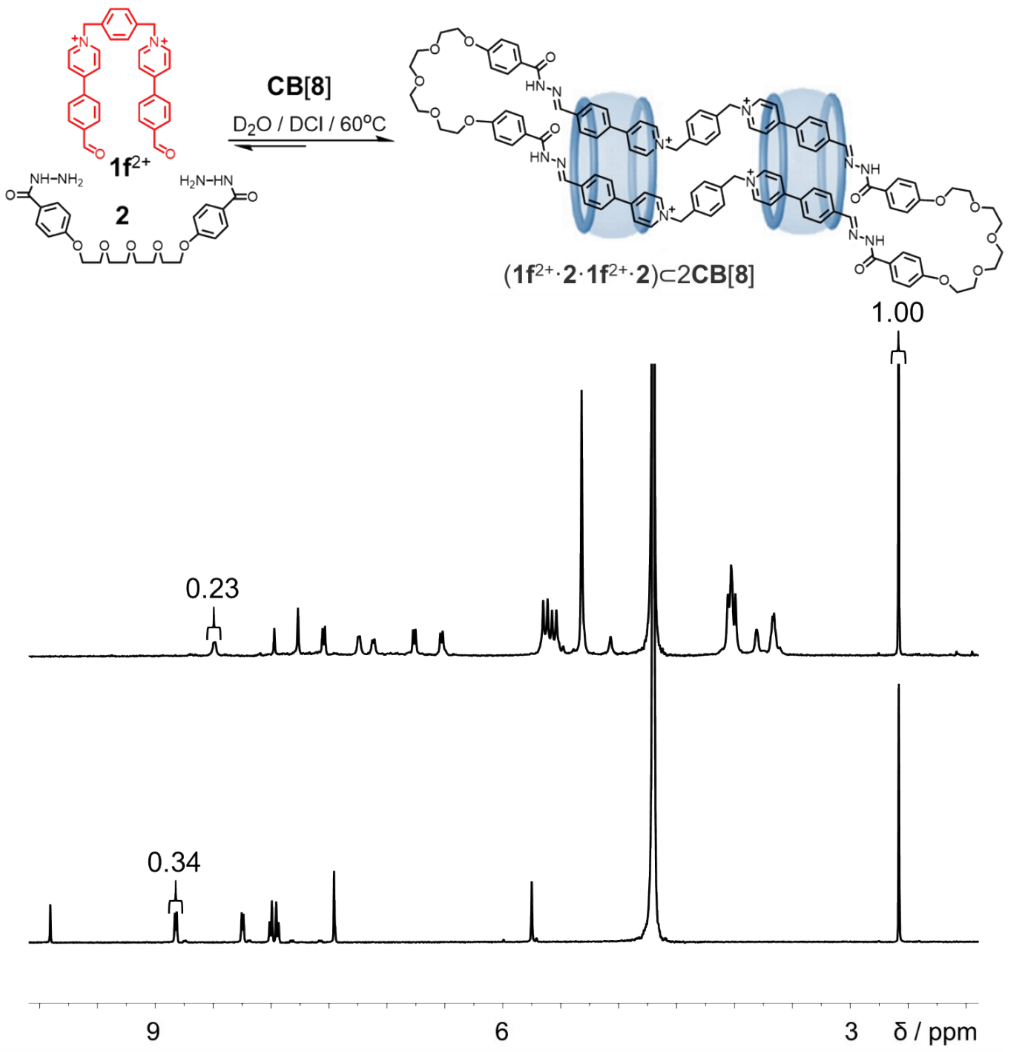

Figure S61. ^{1}H NMR spectra (400 MHz, D_2O, 298 K) of A) (**1f**$^{2+}$·**2**·**1f**$^{2+}$·**2**)⊂2**CB**[**8**], B) **1f**$^{2+}$·2Cl^{-}. The NMR yield of (**1f**$^{2+}$·**2**·**1f**$^{2+}$·**2**)⊂2**CB**[**8**] is 68%.

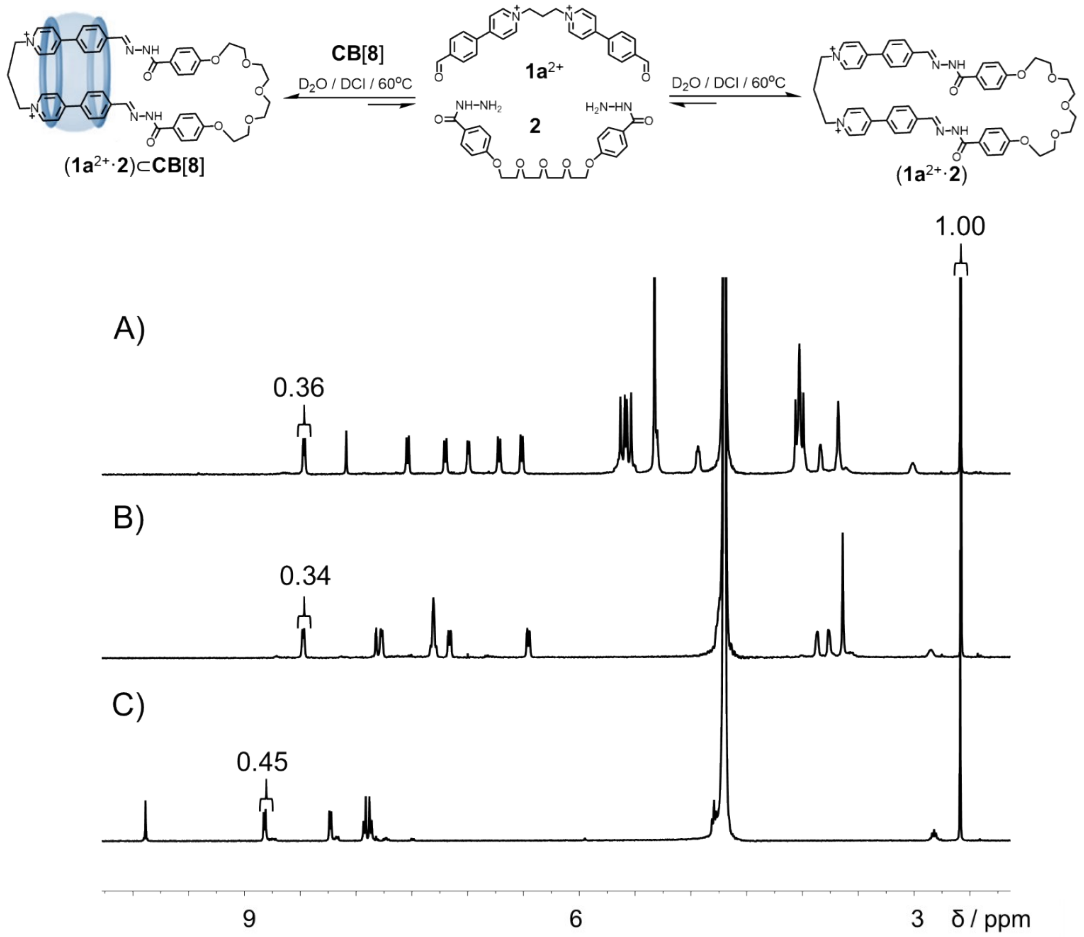

Figure S62. ^{1}H NMR spectra (400 MHz, D_2O, 298 K) of A) (**1a**$^{2+}$·**2**)⊂**CB**[**8**], B) (**1a**$^{2+}$·**2**) and C) **1a**$^{2+}$·2Br^{-}. The NMR yields of (**1a**$^{2+}$·**2**)⊂**CB**[**8**] and (**1a**$^{2+}$·**2**) are 80% and 76%, respectively.

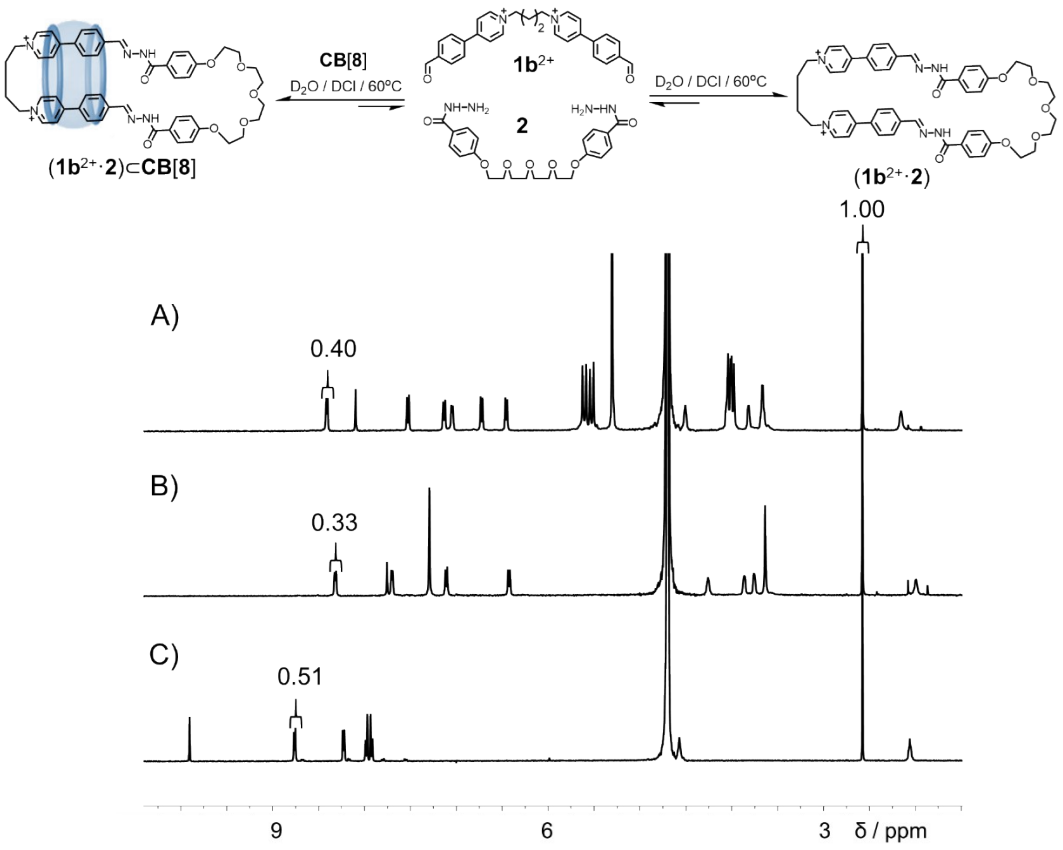

Figure S63. ^{1}H NMR spectra (400 MHz, D_2O, 298 K) of A) (**1b**$^{2+}$·**2**)⊂**CB**[**8**], B) (**1b**$^{2+}$·**2**) and C) **1b**$^{2+}$·2Br^{-}. The NMR yields of (**1b**$^{2+}$·**2**)⊂**CB**[**8**] and (**1b**$^{2+}$·**2**) are 74% and 65%, respectively.

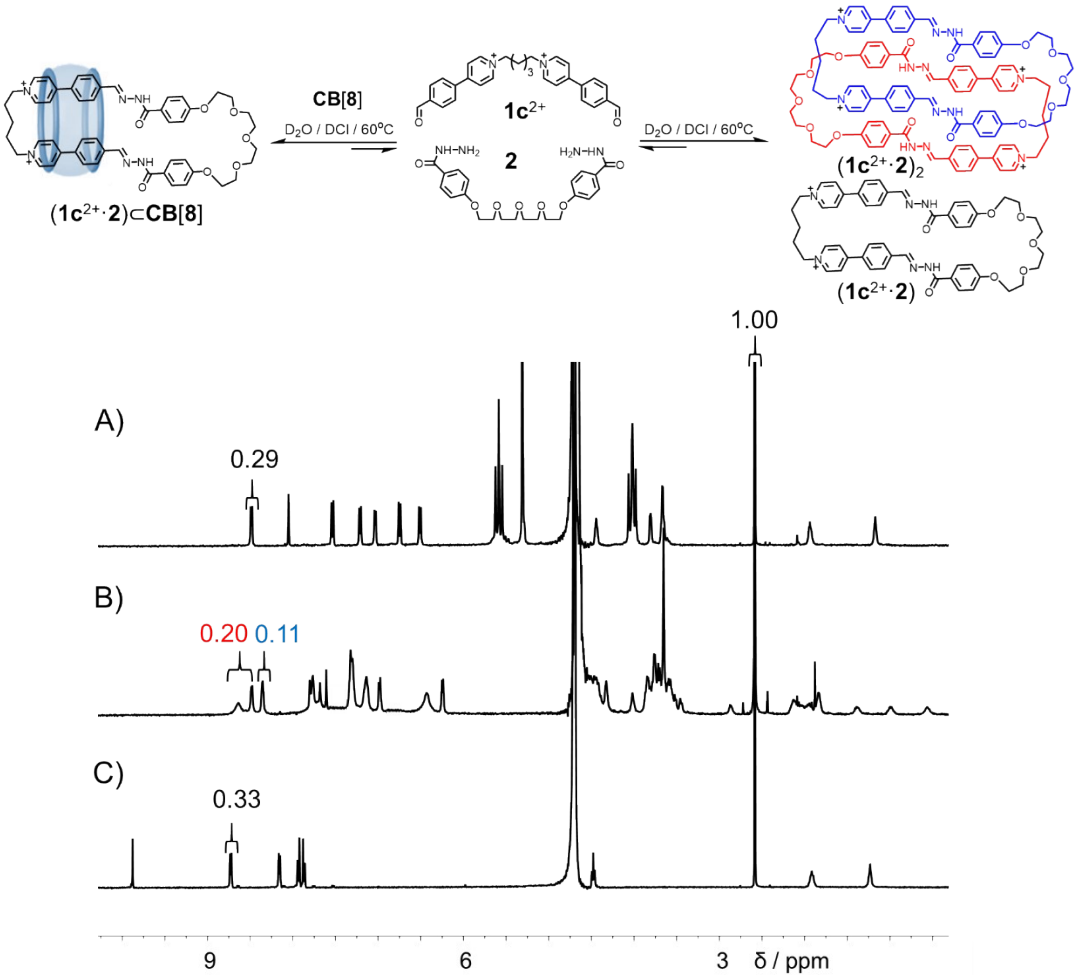

Figure S64. ^{1}H NMR spectra (400 MHz, D_2O, 298 K) of A) (**1c**$^{2+}$·**2**)⊂**CB**[**8**], B) the reaction mixture by condensing a 1:1 mixture of **1c**$^{2+}$2Br$^-$ (2.5 mM) and **2** (2.5 mM) and C) **1c**$^{2+}$·2Br$^-$. The NMR yields of (**1c**$^{2+}$·**2**)⊂**CB**[**8**], (**1c**$^{2+}$·**2**)$_2$ (marked with red colors) and (**1c**$^{2+}$·**2**) (marked with blue colors) are 88%, 61% and 33%, respectively.

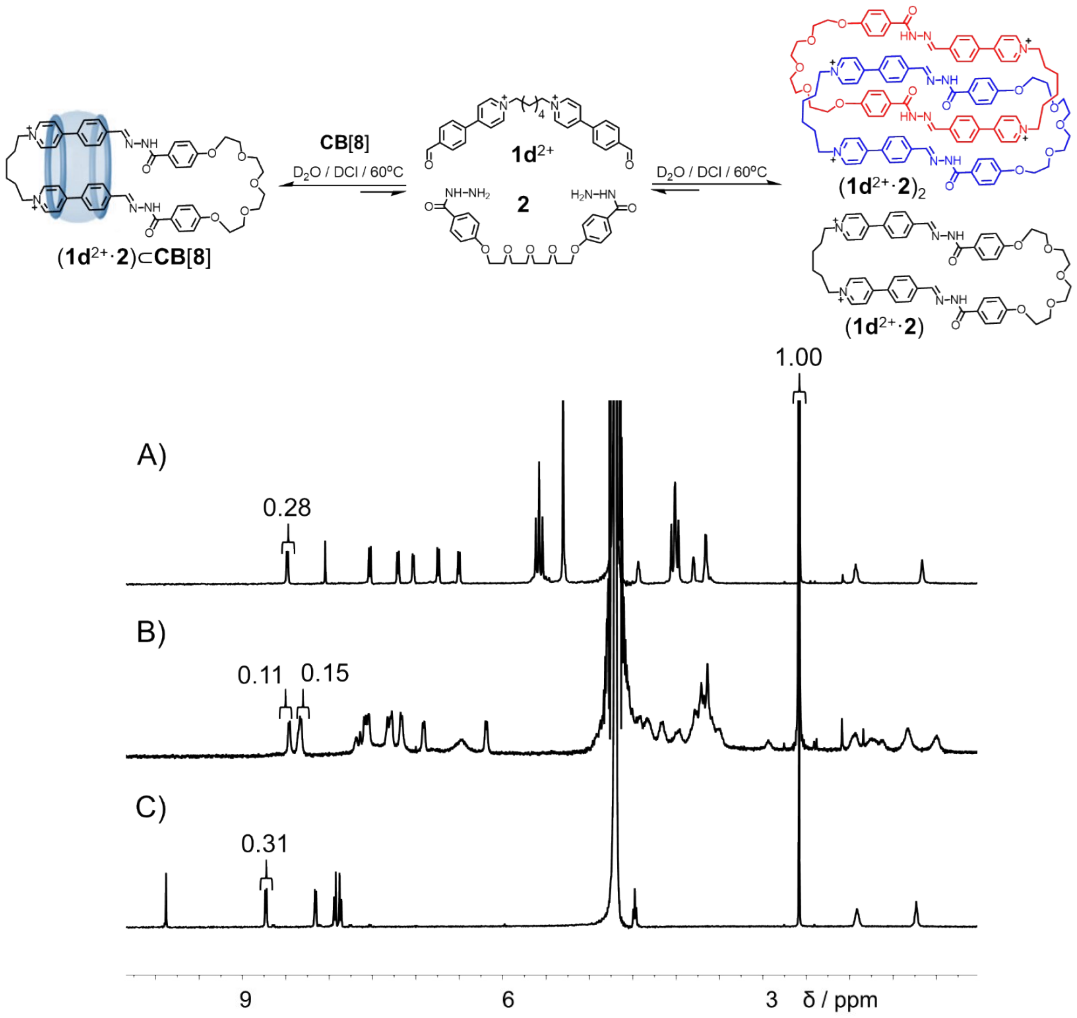

Figure S65. ^{1}H NMR spectra (400 MHz, D_2O, 298 K) of A) (**1d**$^{2+}$·**2**)⊂**CB**[**8**], B) the reaction mixture by condensing a 1:1 mixture of **1d**$^{2+}$2Br$^-$ (2.5 mM) and **2** (2.5 mM) and C) **1d**$^{2+}$·2Br$^-$. The NMR yield of (**1d**$^{2+}$·**2**)⊂**CB**[**8**] is 90%. However, the peaks of the [2]catenane (**1d**$^{2+}$·**2**)$_2$ and the macrocycle (**1d**$^{2+}$·**2**) are overlapped in the spectrum B), so that the NMR yields of them can only be roughly estimated: 71% for (**1d**$^{2+}$·**2**)$_2$ (0.11x2/0.31), 13% for (**1d**$^{2+}$·**2**) {(0.15 − 0.11)/0.31}.

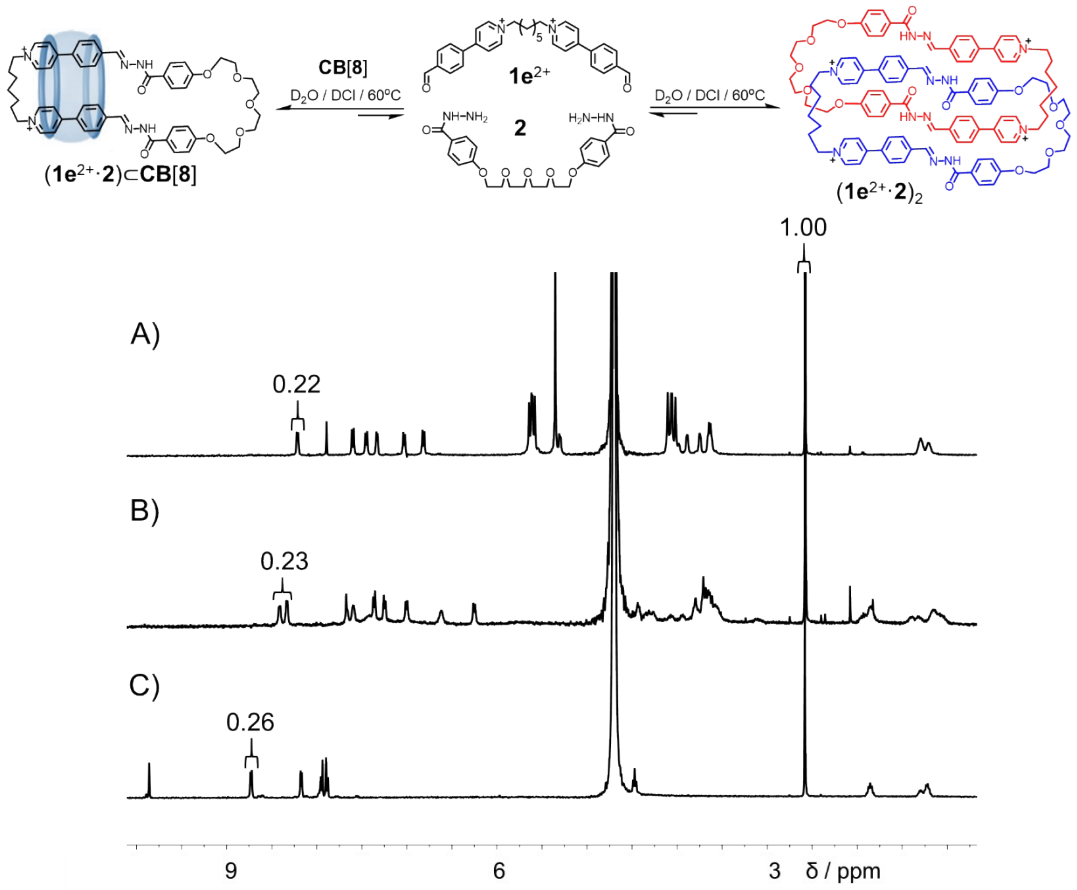

Figure S66. ^{1}H NMR spectra (400 MHz, D_2O, 298 K) of A) (**1e**$^{2+}$·**2**)⊂**CB**[**8**], B) (**1e**$^{2+}$·**2**)$_2$ and C) **1e**$^{2+}$·2Br^{-}. The NMR yields of (**1e**$^{2+}$·**2**)⊂**CB**[**8**] and (**1e**$^{2+}$·**2**)$_2$ are 85% and 88%, respectively.

7. Competitive experiments

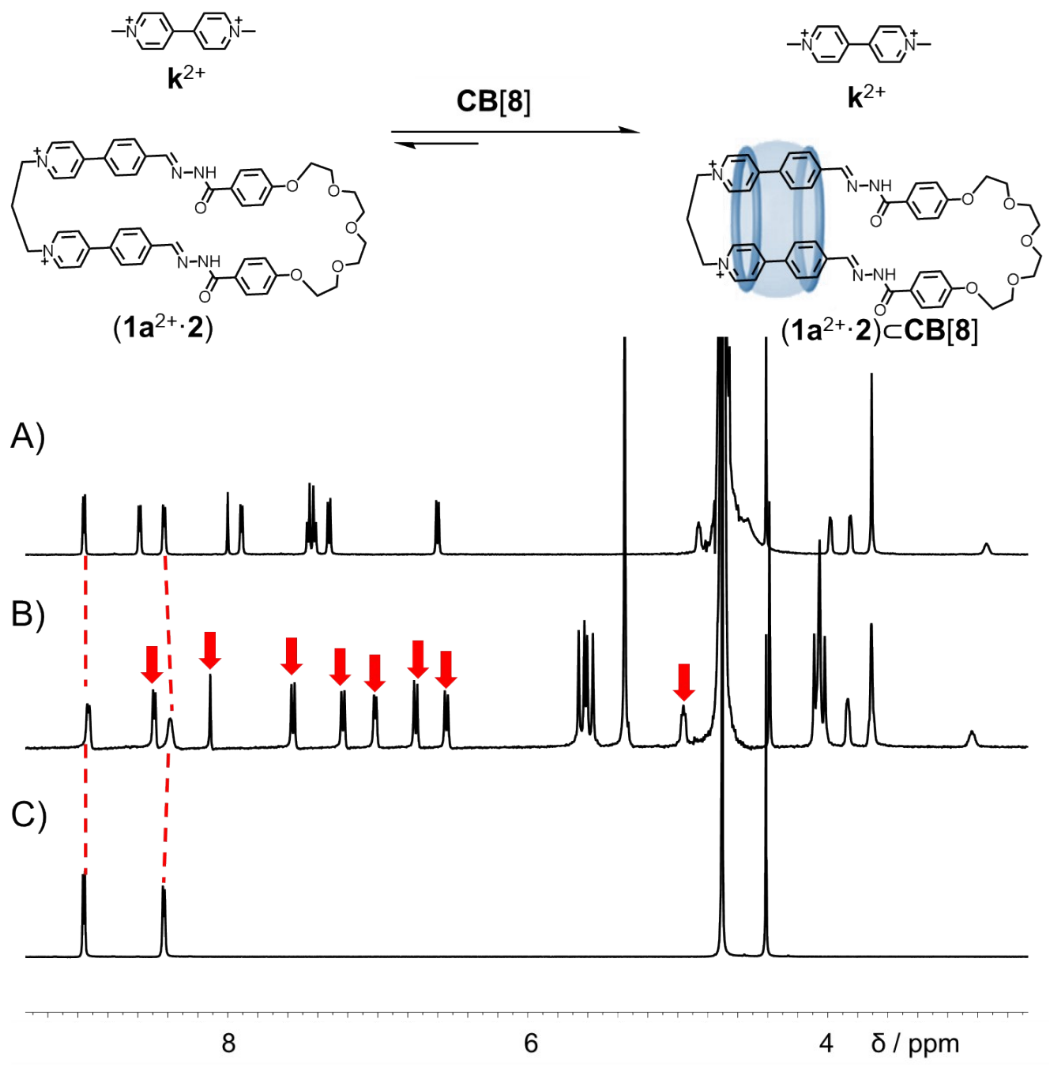

Figure S67. The ^{1}H NMR spectra (500 MHz, D_2O, 298 K) of the 1:1 mixture of the macrocycle (**1a**$^{2+}$·**2**) and paraquat **k**$^{2+}$, A) before and B) after adding 1 equiv. of **CB**[**8**]. C) The ^{1}H NMR spectrum (500 MHz, D_2O, 298 K) of paraquat **k**$^{2+}$. The resonances of (**1a**$^{2+}$·**2**)⊂**CB**[**8**] are marked with red arrows in B).

To a 1:1 mixture of the macrocycle (**1a**$^{2+}$·**2**) and paraquat **k**$^{2+}$, 1 equiv (relative to (**1a**$^{2+}$·**2**)) of **CB**[**8**] was added. After the system reached the equilibrium, the macrocycle (**1a**$^{2+}$·**2**) was recognized within the cavity of **CB[8]**, forming a [2]pseudorotaxane (**1a**$^{2+}$·**2**)⊂**CB**[**8**]. In contrast, the resonances corresponding to paraquat **k**$^{2+}$ barely shifted (Figure S67 B). This experiment indicates that **CB**[**8**] has a stronger binding affinity to recognize (**1a**$^{2+}$·**2**) than **k**$^{2+}$.

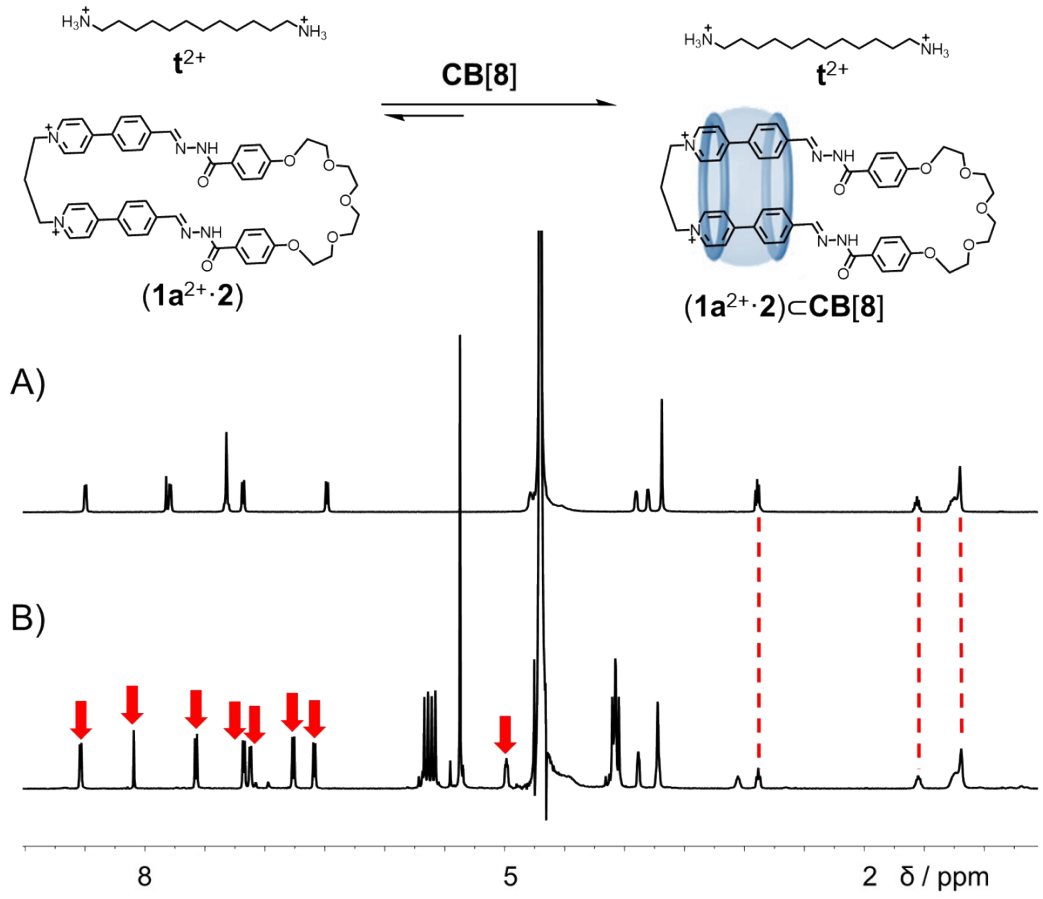

Figure S68. The ^{1}H NMR spectra (500 MHz, D_2O, 298 K) of the 1:1 mixture of the macrocycle (**1a**$^{2+}$·**2**) and **t**$^{2+}$, A) before and B) after adding 1 equiv. of **CB**[**8**]. The resonances of (**1a**$^{2+}$·**2**)⊂**CB**[**8**] are marked with red arrows in B).

To a 1:1 mixture of the macrocycle (**1a**$^{2+}$·**2**) and **t**$^{2+}$, 1 equiv (relative to (**1a**$^{2+}$·**2**)) of **CB**[**8**] was added. After the system reached the equilibrium, the macrocycle (**1a**$^{2+}$·**2**) was recognized within the cavity of **CB**[**8**], forming a [2]pseudorotaxane (**1a**$^{2+}$·**2**)⊂**CB**[**8**]. In contrast, the resonances corresponding to **t**$^{2+}$·2Cl^{-} barely shifted (Figure S68 B). This experiment indicates that **CB**[**8**] has a stronger binding affinity to recognize (**1a**$^{2+}$·**2**) than **t**$^{2+}$.

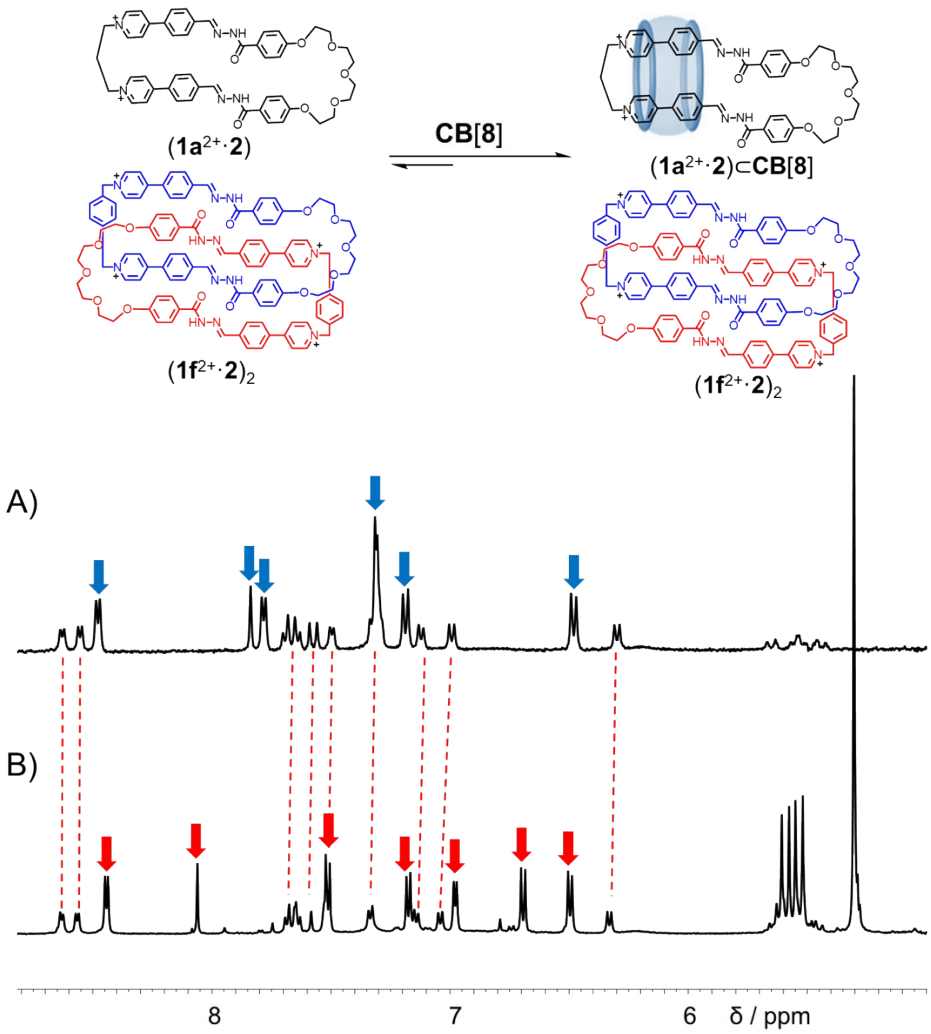

Figure S69. The ^{1}H NMR spectra (500 MHz, D_2O, 298 K) of the 1:0.5 mixture of the macrocycle (**1a**$^{2+}$·**2**) and (**1f**$^{2+}$·**2**)$_2$, A) before and B) after adding 1 equiv. of **CB**[**8**]. The spectrum in B) were recorded after the system reached its equilibrium. The resonances of (**1a**$^{2+}$·**2**) are marked with blue arrows in A) and the resonances of (**1a**$^{2+}$·**2**)⊂**CB**[**8**] are marked with red arrows in B).

To a 1:0.5 mixture of the macrocycle (**1a**$^{2+}$·**2**) and (**1f**$^{2+}$·**2**)$_2$, 1 equiv (relative to (**1a**$^{2+}$·**2**)) of **CB**[**8**] was added. After the system reached the equilibrium, the macrocycle (**1a**$^{2+}$·**2**) was recognized within the cavity of **CB**[**8**], forming a [2]pseudorotaxane (**1a**$^{2+}$·**2**)⊂**CB**[**8**]. In contrast, the resonances corresponding to (**1f**$^{2+}$·**2**)$_2$ barely shifted (Figure S69 B). This experiment indicates that **CB**[**8**] has a stronger binding affinity to recognize (**1a**$^{2+}$·**2**) than (**1f**$^{2+}$·**2**)$_2$.

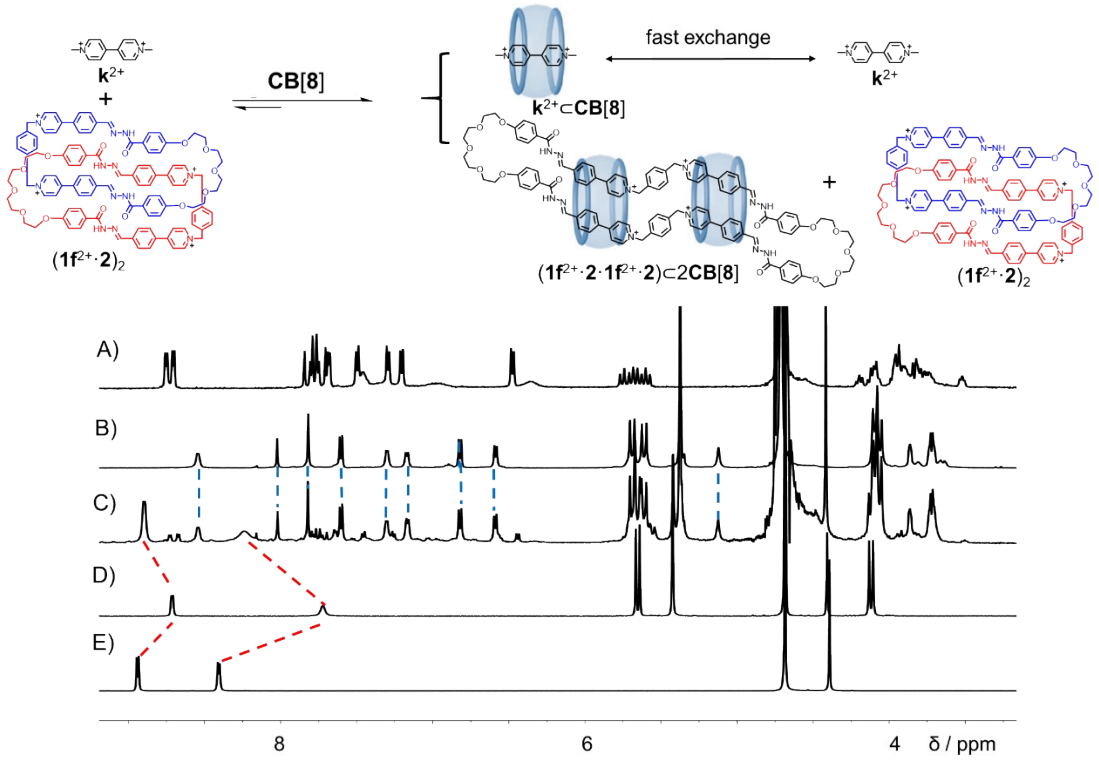

Figure S70. The ^{1}H NMR spectra (500 MHz, D_2O, 298 K) of A) $(\mathbf{1f}^{2+}\cdot\mathbf{2})_2$, B) $(\mathbf{1f}^{2+}\cdot\mathbf{2}\cdot\mathbf{1f}^{2+}\cdot\mathbf{2})\subset 2\mathbf{CB[8]}$, C) the reaction mixture of $(\mathbf{1f}^{2+}\cdot\mathbf{2})_2$, paraquat $\mathbf{k}^{2+}$ and **CB[8]** at the ratio of 0.5:1:1 , D) the reaction mixture of paraquat $\mathbf{k}^{2+}$ and **CB[8]** at the ratio of 1:1 and E) paraquat $\mathbf{k}^{2+}$. All the spectra were recorded after the equilibria were established.

A 0.5:1:1 mixture of the [2]catenane $(\mathbf{1f}^{2+}\cdot\mathbf{2})_2$, paraquat $\mathbf{k}^{2+}$, and **CB[8]** were combined in D_2O. After the system reached the equilibrium, we observed that only small amount of **CB[8]** recognized $\mathbf{k}^{2+}$ to form $\mathbf{k}^{2+}\subset\mathbf{CB[8]}$ (Figure S70 C), as inferred from the observation that the resonances corresponding to $\mathbf{k}^{2+}$ underwent minor upfield shifts, compared to those of the spectrum D). $(\mathbf{1f}^{2+}\cdot\mathbf{2}\cdot\mathbf{1f}^{2+}\cdot\mathbf{2})\subset 2\mathbf{CB[8]}$ (Figure S70 C) were self-assembled as one of the major product, accompanied with the unreacted [2]catenane. This experiment indicates that the binding constants of $(\mathbf{1f}^{2+}\cdot\mathbf{2}\cdot\mathbf{1f}^{2+}\cdot\mathbf{2})\subset 2\mathbf{CB[8]}$ and $\mathbf{k}^{2+}\subset\mathbf{CB[8]}$ might be comparable, the former of which might be slightly larger in a qualitative analysis.

8. UV-Vis Spectroscopic Analysis

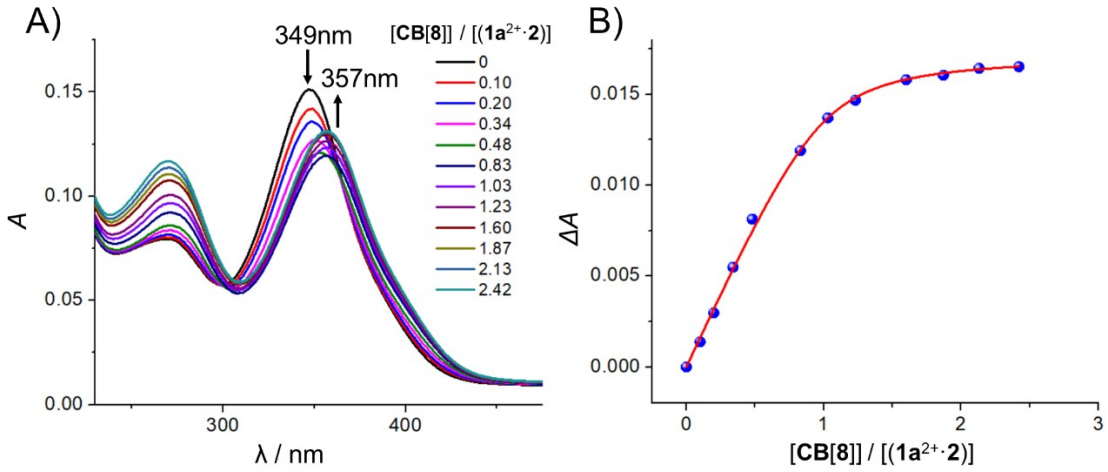

Figure S71. A) UV/Vis absorption spectra of (**1a**$^{2+}$·**2**)·2Cl^{-} after adding different amount of **CB**[**8**] in H_2O at 298 K. B) Plot of the absorbance intensity at λ=400 nm verus [**CB**[**8**]] / [(**1a**$^{2+}$·**2**)]. The concentration of the guest was kept constant for all spectra, namely [(**1a**$^{2+}$·**2**)] = 3.0×10^{-6} M.

UV-Vis spectroscopic studies were performed to investigate the binding affinity of the complex (**1a**$^{2+}$·**2**)·2Cl^{-}⊂**CB**[**8**]. The association constant of complex was determined by probing the charge-transfer band of the complex (Figure S71A) and fitting the change of absorbance with a 1:1 binding curve by using the Benesie-Hildebrand method. The binding constant K_a of (**1a**$^{2+}$·**2**)·2Cl^{-} and **CB**[**8**] was calculated to be around 5.6(±1.1)×10^{6} M^{-1} in D_2O (Figure S71B).

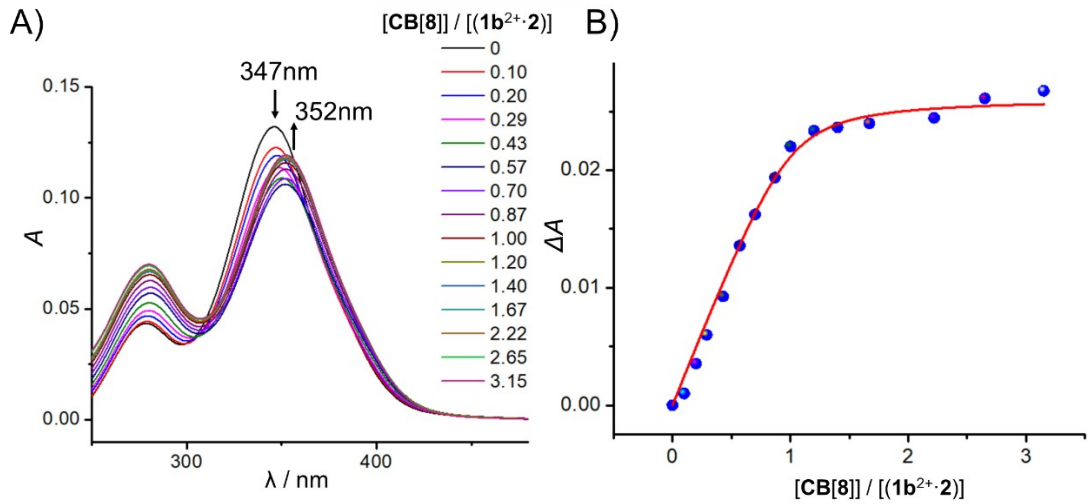

Figure S72. A) UV/Vis absorption spectra of (**1b**$^{2+}$·**2**)·2Cl^{-} after adding different amount of **CB**[**8**] in H_2O at 298 K. B) Plot of the absorbance intensity at λ=400 nm verus [**CB**[**8**]] / [(**1b**$^{2+}$·**2**)]. The concentration of the guest was kept constant for all spectra, namely [(**1b**$^{2+}$·**2**)] = 3.0×10^{-6} M.

UV-Vis spectroscopic studies were performed to investigate the binding affinity of the complex (**1b**$^{2+}$·**2**)·2Cl^{-}⊂**CB**[**8**]. The association constant of complex was determined by probing the charge-transfer band of the complex (Figure S72A) and fitting the change of absorbance with a 1:1 binding curve by using the Benesie-Hildebrand method. The binding constant K_a of (**1b**$^{2+}$·**2**)·2Cl^{-} and **CB**[**8**] was calculated to be around 7.3(±2.9)×10^{6} M^{-1} in D_2O (Figure S72B).

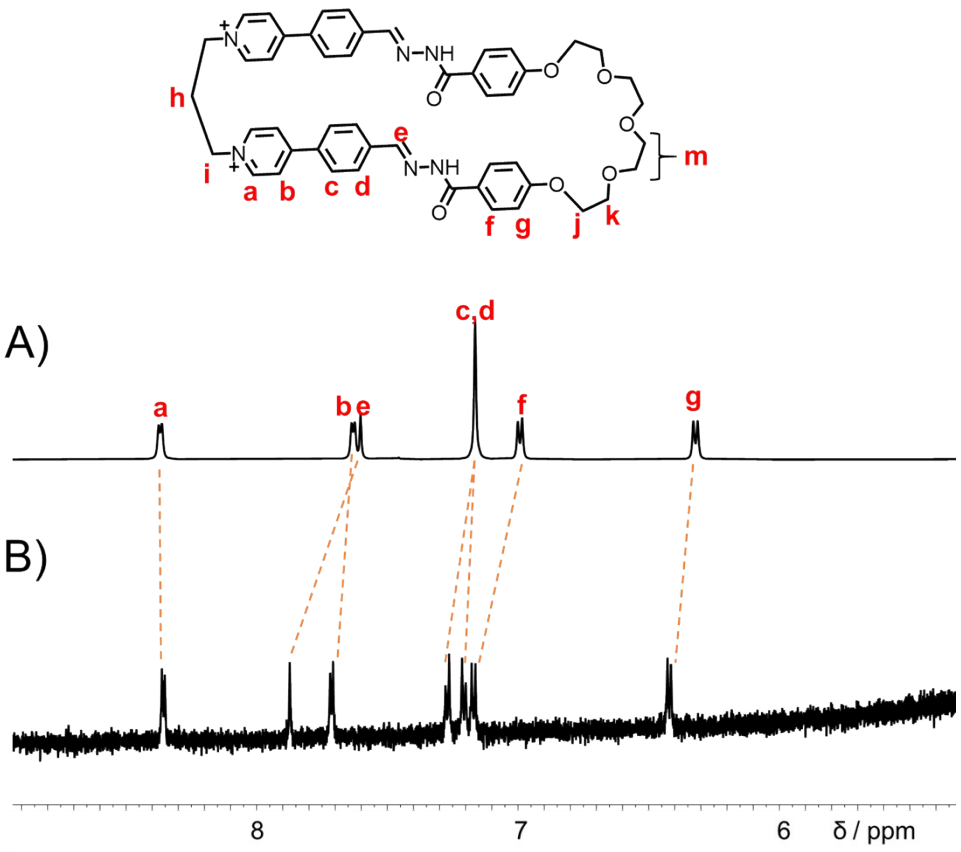

Figure S73. Partial ^{1}H NMR spectrum of (**1a**$^{2+}$·**2**)·2Cl^{-} at different concentrations (600 MHz, D_2O, 298 K), including A) 2.5 mM and B) 3x10^{-3} mM.

9. X-ray Crystallography

1) $(\mathbf{1f}^{2+}\cdot\mathbf{2})_2\cdot 4Cl^-$

1.1) Methods

Single crystals of the [2]catenane $(\mathbf{1f}^{2+}\cdot\mathbf{2})_2\cdot 4Cl^-$ was obtained by slow vapor diffusion of THF into the water solution under room temperature. A suitable crystal was selected on a Bruker D8 Venture diffractometer. The crystal was kept at 170.0 K during data collection. Using Olex2 [1], the structure was solved with the ShelXT [2] structure solution program using Intrinsic Phasing and refined with the ShelXL [3] refinement package using Least Squares minimisation.

1.2) Crystal data

$[C_{108}H_{128}Cl_4N_{12}O_{26}]$ (*M* =2152.02 g/mol): monoclinic, space group $P2_{1/c}$ (no. 14), *a* = 13.6939(9) Å, *b* = 19.0018(12) Å, *c* = 50.945(3) Å, α = 90°, β = 90.412(4)°, γ = 90°, *V* = 13256.0(15) $Å^3$, *Z* = 4, *T* = 170.0 K, μ(GaKα) = 0.876 mm^{-1}, *Dcalc* = 1.078 g/cm^3, 122205 reflections measured (5.614° ≤ 2Θ ≤ 96.354°), 18873 unique (R_{int} = 0.1553, R_{sigma} = 0.1168) which were used in all calculations. The final R_1 was 0.1224 (I > 2σ(I)) and wR_2 was 0.3812 (all data). CCDC number: 2014868.

Table S1 Crystal data and structure refinement for $(\mathbf{1f}^{2+}\cdot\mathbf{2})_2\cdot 4Cl^-$

Empirical formula	$C_{108}H_{128}Cl_4N_{12}O_{26}$
Formula weight	2152.02
Temperature/K	170.0
Crystal system	monoclinic
Space group	$P2_1/c$
a/Å	13.6939(9)
b/Å	19.0018(12)
c/Å	50.945(3)
α/°	90
β/°	90.412(4)

γ/°	90
Volume/Å^3	13256.0(15)
Z	4
ρ_{calc}g/cm^3	1.078
μ/mm^{-1}	0.876
F(000)	4544.0
Crystal size/mm^3	0.05 × 0.02 × 0.015
Radiation	GaKα (λ = 1.34139)
2Θ range for data collection/°	5.614 to 96.354
Index ranges	-15 ≤ h ≤ 15, -21 ≤ k ≤ 21, -56 ≤ l ≤ 49
Reflections collected	122205
Independent reflections	18873 [R_{int} = 0.1553, R_{sigma} = 0.1168]
Data/restraints/parameters	18873/96/1414
Goodness-of-fit on F^2	1.086
Final R indexes [I>=2σ (I)]	R_1 = 0.1224, wR_2 = 0.3055
Final R indexes [all data]	R_1 = 0.2392, wR_2 = 0.3812
Largest diff. peak/hole / e Å^{-3}	1.47/-0.61

1.3) Solid-state structure

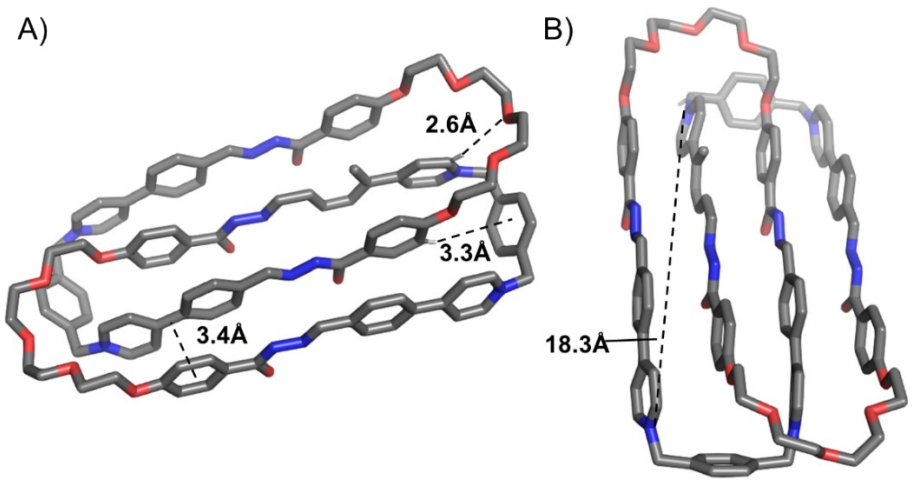

Figure S74. Different views of the solid-state structure of (**1f**$^{2+}$·**2**)$_2$·4Cl$^-$. Counterions and solvent molecules are omitted for the sake of clarity.

2) (**1f**$^{2+}$·**2**·**1f**$^{2+}$·**2**)⊂2**CB**[**8**]

2.1) Methods

Single crystals of the ring in ring complex (**1f**$^{2+}$·**2**·**1f**$^{2+}$·**2**)⊂2**CB**[**8**] was obtained by slow evaporation of the solution of (**1f**$^{2+}$·**2**·**1f**$^{2+}$·**2**)⊂2**CB**[**8**] in water under room temperature. Charges are balanced by chloride counteranions. A suitable crystal was selected on a Bruker D8 Venture diffractometer. The crystal was kept at 170.0 K during data collection. Using Olex2 [1], the structure was solved with the ShelXT [2] structure solution program using Intrinsic Phasing and refined with the ShelXL [3] refinement package using Least Squares minimisation.

2.2) Crystal data

[$C_{102}H_{102}Cl_2N_{38}O_{25}$] (*M* =2331.11 g/mol): Triclinic, space group P-1, *a* = 14.5032(6) Å, *b* = 23.2785(10) Å, *c* = 23.8851(11) Å, α = 107.441(3)°, β = 93.266(3)°, γ = 104.627(3)°, *V* = 7366.6(6) Å^3, *Z* = 2, *T* = 170.02 K, μ(GaKα) = 0.629 mm^{-1}, *Dcalc* =1.051 Mg/m^3, Full-matrix least-squares on F^2 reflections measured (2.845° ≤ 2Θ ≤ 55.148°), 27956 unique (R_{int} = 0.0745) which were used in all calculations. The final R_1 was 0.1686 (I > 2σ(I)) and wR_2 was 0.3908 (all data). CCDC number: 2095808.

Table S2 Crystal data and structure refinement for (**1f**$^{2+}$·**2**·**1f**$^{2+}$·**2**)⊂2**CB**[**8**]

Empirical formula	C_{102} H_{102} Cl_2 N_{38} O_{25}	
Formula weight	2331.11	
Temperature	173.02 K	
Wavelength	1.34139 Å	
Crystal system	Triclinic	
Space group	P-1	
Unit cell dimensions	a = 14.5032(6) Å	a= 107.441(3)°.
	b = 23.2785(10) Å	b= 93.266(3)°.
	c = 23.8851(11) Å	g = 104.627(3)°.
Volume	7366.6(6) Å^3	
Z	2	
Density (calculated)	1.051 Mg/m^3	
Absorption coefficient	0.629 mm^{-1}	

F(000)	2428
Crystal size	0.06 x 0.06 x 0.05 mm^3
Theta range for data collection	2.845 to 55.148°.
Index ranges	-17<=h<=15, -28<=k<=28, -29<=l<=29
Reflections collected	93616
Independent reflections	27956 [R(int) = 0.0745]
Completeness to theta = 53.594°	99.6 %
Absorption correction	Semi-empirical from equivalents
Max. and min. transmission	0.7508 and 0.5498
Refinement method	Full-matrix least-squares on F^2
Data / restraints / parameters	27956 / 76 / 1498
Goodness-of-fit on F^2	1.159
Final R indices [I>2sigma(I)]	R1 = 0.1686, wR2 = 0.3688
R indices (all data)	R1 = 0.2159, wR2 = 0.3908
Extinction coefficient	n/a
Largest diff. peak and hole	1.864 and -0.930 e.$Å^{-3}$

2.3) Solid-state structure

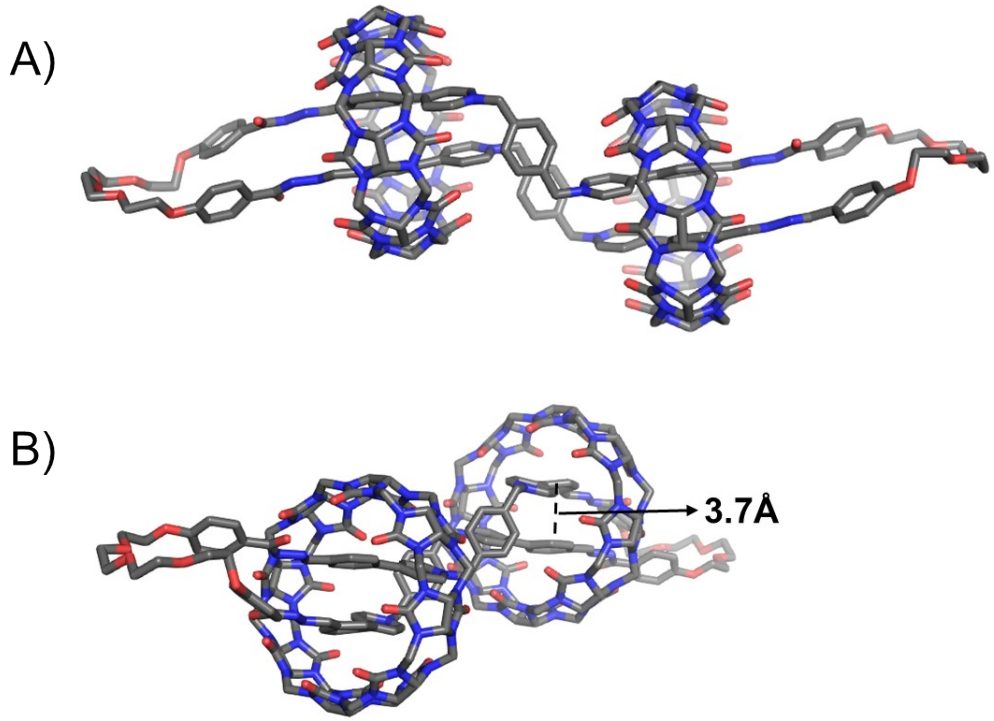

Figure S75. Different views of the solid-state structure of (**1f**$^{2+}$·**2**·**1f**$^{2+}$·**2**)⊂2**CB**[**8**]. Counterions and solvent molecules are omitted for the sake of clarity.

3) (**1a**$^{2+}$·**2**)·2Cl^{-}

3.1) Methods

Single crystals of the macrocycle (**1a**$^{2+}$·**2**)·2Cl^{-} was obtained by slow vapor diffusion of acetone into the water solution under room temperature. A suitable crystal was selected on a Bruker D8 Venture diffractometer. The crystal was kept at 170.0 K during data collection. Using Olex2 [1], the structure was solved with the ShelXT [2] structure solution program using Intrinsic Phasing and refined with the ShelXL [3] refinement package using Least Squares minimisation.

3.2) Crystal data

[$C_{49}H_{51}Cl_2N_6O_{11.5}$] (*M* =984.9 g/mol): Triclinic, space group P-1, *a* = 10.3120(12) Å, *b* = 20.687(2) Å, *c* = 26.395(3) Å, α = 74.272(7)°, β = 81.268(8)°, γ = 78.693(8)°, *V* = 5285.7(10) Å^3, *Z* = 4, *T* = 183.95 K, μ(GaKα) = 1.054 mm^{-1}, *Dcalc* =1.238 Mg/m^3, Full-matrix least-squares on F^2 reflections measured (3.182° ≤ 2Θ ≤ 55.148°), 19978 unique (R_{int} = 0.1519) which were used in all calculations. The final R_1 was 0.1263 (I > 2σ(I)) and wR_2 was 0.4007 (all data). CCDC number: 2096625

Table S3 Crystal data and structure refinement for (**1a**$^{2+}$·**2**)·2Cl^{-}

Empirical formula	$C_{49}\ H_{57}\ Cl_2\ N_6\ O_{11.50}$	
Formula weight	984.90	
Temperature	183.95 K	
Wavelength	1.34139 Å	
Crystal system	Triclinic	
Space group	P-1	
Unit cell dimensions	a = 10.3120(12) Å	a= 74.272(7)°.
	b = 20.687(2) Å	b= 81.268(8)°.
	c = 26.395(3) Å	g = 78.693(8)°.
Volume	5285.7(10) Å^3	
Z	4	
Density (calculated)	1.238 Mg/m^3	
Absorption coefficient	1.054 mm^{-1}	
F(000)	2076	
Crystal size	0.05 x 0.03 x 0.02 mm^3	
Theta range for data collection	3.182 to 55.148°.	

Index ranges	-12<=h<=11, -25<=k<=25, -32<=l<=32
Reflections collected	66904
Independent reflections	19978 [R(int) = 0.1519]
Completeness to theta = 53.594°	99.7 %
Absorption correction	Semi-empirical from equivalents
Max. and min. transmission	0.7508 and 0.3544
Refinement method	Full-matrix-block least-squares on F^2
Data / restraints / parameters	19978 / 0 / 1267
Goodness-of-fit on F^2	1.036
Final R indices [I>2sigma(I)]	R1 = 0.1263, wR2 = 0.3271
R indices (all data)	R1 = 0.2236, wR2 = 0.4007
Extinction coefficient	n/a
Largest diff. peak and hole	1.685 and -0.474 e.Å^{-3}

3.3) Solid-state structure

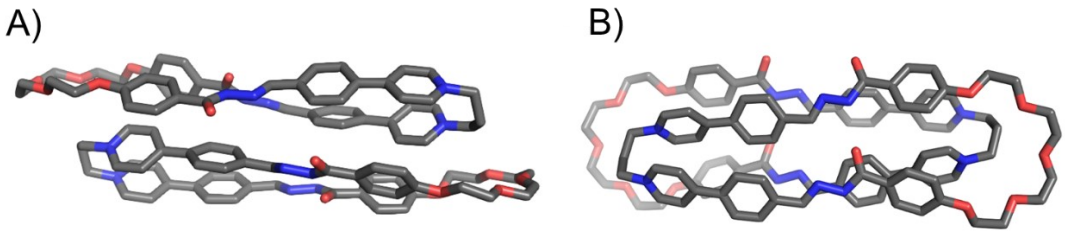

Figure S76. Different views of the solid-state structure of (**1a**$^{2+}$·**2**)·2Cl$^-$. Counterions and solvent molecules are omitted for the sake of clarity.

4) (**1b**$^{2+}$·**2**)·2PF_6^-

4.1) Methods

Single crystals of the [2]catenane (**1b**$^{2+}$·**2**)·2PF_6^- was obtained by slow vapor diffusion of isopropyl ether into the acetonitrile solution under room temperature. A suitable crystal was selected on a Bruker D8 Venture diffractometer. The crystal was kept at 170.0 K during data collection. Using Olex2 [1], the structure was solved with the ShelXT [2] structure solution program using Intrinsic Phasing and refined with the ShelXL [3] refinement package using Least Squares minimisation.

4.2) Crystal data

[$C_{50}H_{52}F_{12}N_6O_7P_2$] (*M* =1138.91 g/mol): Triclinic, space group P-1, *a* = 9.22(2) Å, *b* = 19.51(5) Å, *c* = 20.82(5) Å, α = 62.99(5)°, β = 86.96(6)°, γ = 78.01(5)°, *V* = 3260(14) Å^3, *Z* = 2, *T* = 174.82 K, μ(GaKα) = 0.847 mm^{-1}, *Dcalc* =1.160 Mg/m^3, Goodness-of-fit on F^2

reflections measured (3.698° ≤ 2Θ ≤ 49.650°), 10023 unique (R_{int} = 0.2692) which were used in all calculations. The final R_1 was 0.1221 (I > 2σ(I)) and wR_2 was 0.4298 (all data).

CCDC number: 2096626

Table S4 Crystal data and structure refinement for $(\mathbf{1b}^{2+}\cdot\mathbf{2})\cdot 2PF_6^-$

Empirical formula	$C_{50}\ H_{52}\ F_{12}\ N_6\ O_7\ P_2$	
Formula weight	1138.91	
Temperature	174.82 K	
Wavelength	1.34139 Å	
Crystal system	Triclinic	
Space group	P-1	
Unit cell dimensions	a = 9.22(2) Å	a= 62.99(5)°.
	b = 19.51(5) Å	b= 86.96(6)°.
	c = 20.82(5) Å	g = 78.01(5)°.
Volume	3260(14) $Å^3$	
Z	2	
Density (calculated)	1.160 Mg/m^3	
Absorption coefficient	0.847 mm^{-1}	
F(000)	1176	
Crystal size	0.08 x 0.02 x 0.01 mm^3	
Theta range for data collection	3.698 to 49.650°.	
Index ranges	-10<=h<=10, -22<=k<=22, -23<=l<=23	
Reflections collected	63457	
Independent reflections	10023 [R(int) = 0.2692]	
Completeness to theta = 49.650°	100.0 %	
Absorption correction	Semi-empirical from equivalents	
Max. and min. transmission	0.7508 and 0.5004	
Refinement method	Full-matrix least-squares on F^2	
Data / restraints / parameters	10023 / 22 / 694	
Goodness-of-fit on F^2	0.935	
Final R indices [I>2sigma(I)]	R1 = 0.1221, wR2 = 0.3225	
R indices (all data)	R1 = 0.2840, wR2 = 0.4298	
Extinction coefficient	n/a	
Largest diff. peak and hole	0.457 and -0.345 e.$Å^{-3}$	

4.3) Solid-state structure

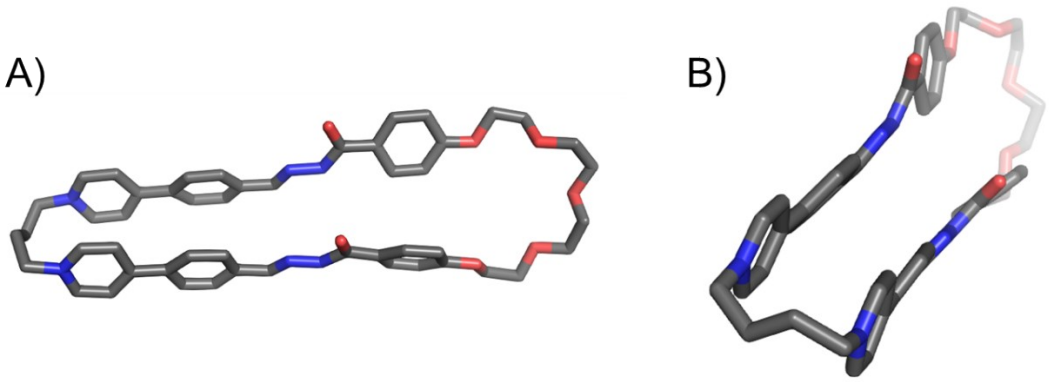

Figure S77. Different views of the solid-state structure of (**1b**$^{2+}$·**2**)·2PF_6^-. Counterions and solvent molecules are omitted for the sake of clarity.

10. References

1. D. Benito-Alifonso, B. Richichi, V. Baldoneschi, M. Berry, M. Fragai, G. Salerno, M. C. Galan, C. Nativi. *ACS Omega* 2018, **3**, 9822−9826.